INITIAL MAPPING OF THE EARTH'S BOW SHOCK, MAGNETOSHEATH AND MAGNETIC TAIL BY EXPLORER 33*

by

Kenneth Wayne Behannon

Thesis submitted to the Graduate Faculty of the
Virginia Polytechnic Institute
in candidacy for the degree of
MASTER OF SCIENCE
in
Physics

APPROVED:

Chairman, Dr. A. Keith Furr

Dr. James A. Jacobs

Dr. Ray F. Tipsword

Dr. Clayton D. Williams

May, 1967

Blacksburg, Virginia

*Supported by the National Aeronautics and Space Administration

CONTENTS

		Page
I.	INTRODUCTION	8
II.	HISTORICAL BACKGROUND	22
III.	EXPERIMENT INSTRUMENTATION	35
IV.	EXPERIMENTAL DATA REDUCTION AND ANALYSIS	43
V.	RESULTS AND CONCLUSIONS	58
	A. GENERAL TOPOLOGY	58
	B. THE BOW SHOCK	75
	C. THE MAGNETOSHEATH	81
	D. THE GEOMAGNETIC TAIL	87
VI.	SUMMARY OF RESULTS	115
VII.	ACKNOWLEDGEMENTS	118
VIII.	BIBLIOGRAPHY	119
IX.	VITA	132
APPENDIX A – LEAST SQUARES FIT ROUTINE		133
APPENDIX B – DATA TRANSFORMATIONS		135
APPENDIX C – ERROR ANALYSIS		139
APPENDIX D – MULTIPLE AND PARTIAL CORRELATION COEFFICIENTS		146

LIST OF FIGURES

Figure		Page
1	Explorer 33 spacecraft in flight configuration with booms and solar paddles fully deployed	9
2	Solar ecliptic reference frame and associated parameter nomenclature and definitions	11
3	Summary of trajectories of ten spacecraft that have investigated the outer magnetosphere	12
4	Variation of Explorer 33 spin rate and spin axis and orbit orientation parameters	14
5	Ecliptic plane view of first eight orbits of Explorer 33	15
6	Variation of Explorer 33 solar ecliptic apogee position	17
7	Illustration of the variation of the apogee position relative to the ecliptic plane	19
8	Magnetometer sensor frequency response and instrumental phase shift	38
9	Block diagram of GSFC magnetic field experiment	41
10	Orientation of magnetometer sensors relative to spacecraft spin axis before and after reorientation	48
11	Example of magnetometer sensor in-flight sensitivity calibration results	53

Figure		Page
12	Magnetic field data from July 13, 1966 illustrating traversals of the earth's bow shock and magnetopause	61
13	Magnetic field data from August 14, 1966 illustrating multiple traversals of dawn flank of bow shock	65
14	Magnetic field data from October 4. 1966 illustrating multiple traversals of dusk flank of bow shock	66
15	Magnetic field data from October 19, 1966 illustrating magneto-sheath fields and multiple traversals of the tail magnetopause . .	68
16	Summary of Explorer 33 bow shock and magnetopause traversals (rotated into ecliptic plane)	69
17	View from the earth of the downstream segments of orbits 1-8 and the cross section of a cylindrical magnetic tail	71
18	Explorer 33 bow shock and magnetopause traversals in solar magnetospheric coordinates revealing the noncylindrical shape of the magnetic tail	73
19	Average vector magnetic field topology in the geomagnetic tail during July-November 1966	74
20	Detailed magnetic field data from July 21, 1966 illustrating a traversal of the bow shock at a geocentric distance of 75.7 R_E . .	76
21	Magnetic field data from October 18, 1966 illustrating a quiet magnetosheath	82

Figure		Page
22	Magnetic field data from November 5, 1966 illustrating moderately disturbed magnetosheath	83
23	Magnetic field data from October 5, 1966 illustrating a highly disturbed magnetosheath	85
24	Regular-run magnetic observatory horizontal component magnetograms for August 30, 1966 sudden commencement storm period	86
25	Magnetic field data illustrating commencement of August 30, 1966 magnetic storm in magnetosheath	88
26	Magnetic field data from October 21, 1966 illustrating steady character of undisturbed magnetic tail field	89
27	Regular-run magnetic observatory horizontal component magnetograms for September 14, 1966 sudden commencement storm period	91
28	Solar ecliptic and midnight meridian plane views of orbit 5	93
29	Magnetic field data from September 14, 1966 illustrating commencement of September 14, 1966 magnetic storm in the geomagnetic tail	94
30	Magnetic field data from September 15, 1966 illustrating recovery phase in tail following geomagnetic storm	96

Figure		Page
31	Magnetic field data from August 22, 1966 illustrating a traversal of the geomagnetic tail neutral sheet at 78.0 R_E	99
32	Detailed magnetic field data from August 23, 1966 illustrating a thin neutral sheet	101
33	Magnetic field data illustrating the variations in SM field components during the August 23 neutral sheet traversal	102
34	Detailed magnetic field data from August 24, 1966 illustrating an inflated neutral sheet	103
35	Magnetic field data illustrating the variations in SM field components during the August 24 neutral sheet traversal	104
36	Distribution of undisturbed average magnetic tail field magnitudes as a function of geocentric distance down the tail	107

LIST OF TABLES

Table		Page
1	MAGNETIC FIELD CHARACTERISTICS AT THE BOW SHOCK	80
2	NEUTRAL SHEET EQUIVALENT CURRENT DENSITIES	106
3	MULTIPLE CORRELATION AND REGRESSION COEFFICIENTS FOR MAGNETIC TAIL FIELD MAGNITUDE VARIATIONS . . .	109

I. INTRODUCTION

The Explorer 33 spacecraft was launched from the Eastern Test Range, Cape Kennedy, Florida on July 1, 1966 at 1602:25.375 Universal Time. The 57.1 kilogram satellite shown in Fig. 1 was the first of the Anchored Interplanetary Monitoring Platform (AIMP) series and had as its primary mission to be placed into a captive orbit about the moon. Thus anchored in the lunar gravitational field, the spacecraft would be able to investigate the magnetic field, plasma and energetic particle environment of the moon, both in interplanetary space and for approximately 3.5 days every 29.5 days in the magnetic tail of the earth.

Explorer 33 was boosted into a transfer orbit by a three-stage Thrust Augmented Improved Delta launch vehicle. Subsequent real time analysis of tracking data showed that the injection velocity following third stage burnout was 0.2% above nominal. This excess velocity was sufficient to make it impossible to achieve a stable lunar orbit since the spacecraft had no attitude control capability. The decision was made at 2100 UT to abort the primary mission and switch to the alternate mission. The alternate mission was planned in advance for the small number of possible lunar transfer trajectories in which a successful lunar orbit could not be achieved.

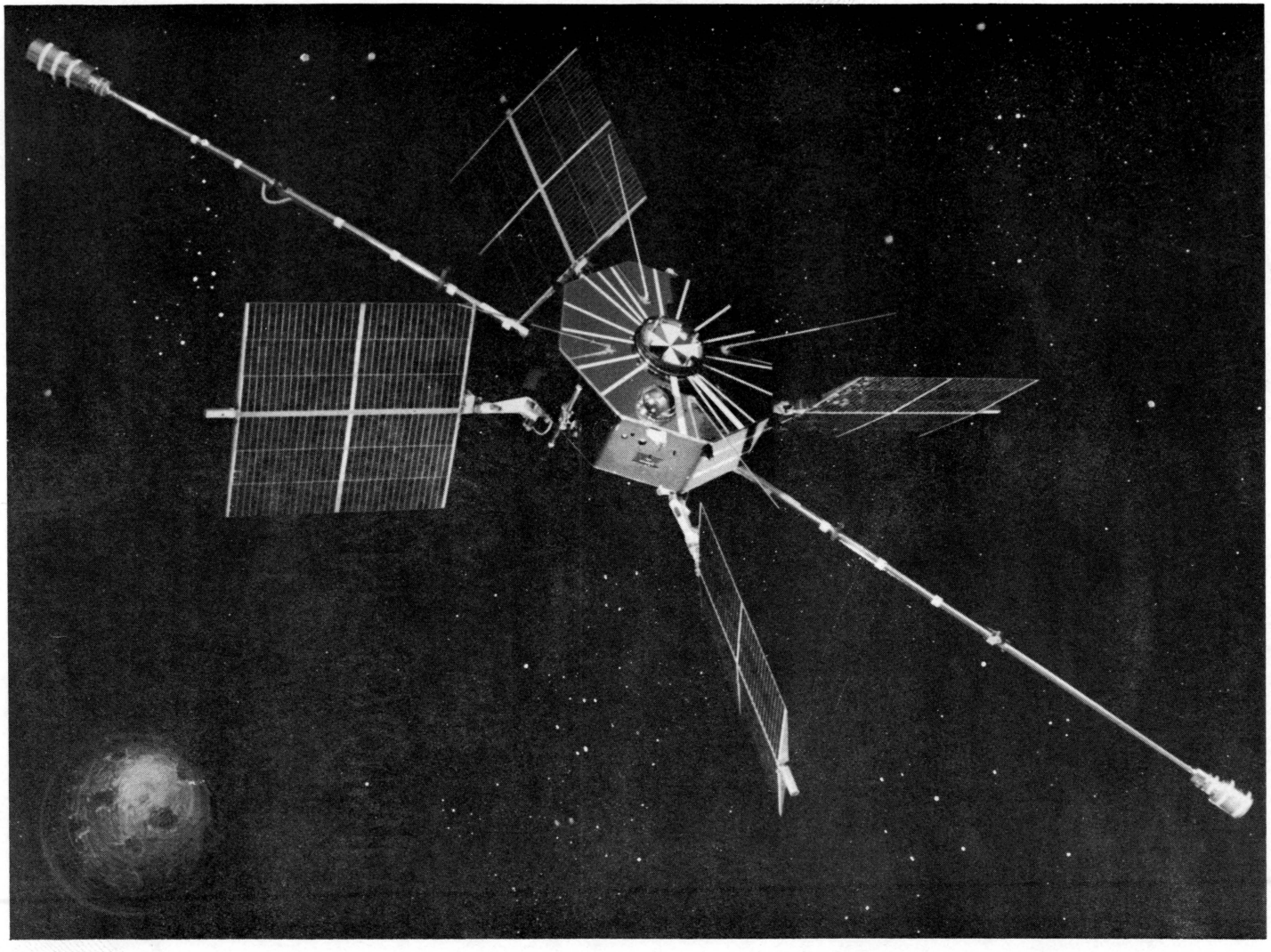

Figure 1–Explorer 33 spacecraft in flight configuration with booms and solar paddles fully deployed.

By firing the fourth stage retrorocket at 2233 UT, a highly elliptical earth orbit was selected which would carry the satellite to a predicted apogee of approximately 450,000 km, well beyond the lunar orbital distance. The line of apsides of this initial orbit would have a geocentric solar ecliptic longitude ϕ_{SE} of approximately 240°. The geocentric solar ecliptic coordinate system, shown in Fig. 2, is oriented so that the X_{SE} axis points from the earth to the sun, the Z_{SE} axis is normal to the solar ecliptic plane, and Y_{SE} is chosen to form a right-handed coordinate system. Geocentric solar ecliptic longitude ϕ_{SE} is measured counterclockwise from the X_{SE} axis in the ecliptic plane and θ_{SE} is the corresponding latitude or angular distance above or below the ecliptic plane.

With the line of apsides initially 120° west of the sun, the earth's orbital motion about the sun would sweep the orbit of Explorer 33 across the magnetic tail of the earth during the first six months after launch. This would extend the investigation of that region of the geomagnetic field to beyond the orbital distance of the moon.

The actual initial apogee was reached on July 7 at a geocentric distance of 440,300 km and solar ecliptic longitude and latitude of $\phi_{SE} = 242°$ and $\theta_{SE} = -1°$, respectively. Fig. 3 shows the projection of the first orbit onto the ecliptic plane. For comparison, the apogee distances of a number of previous high orbit satellites are shown, as well as the initial trajectories of three interplanetary probes.

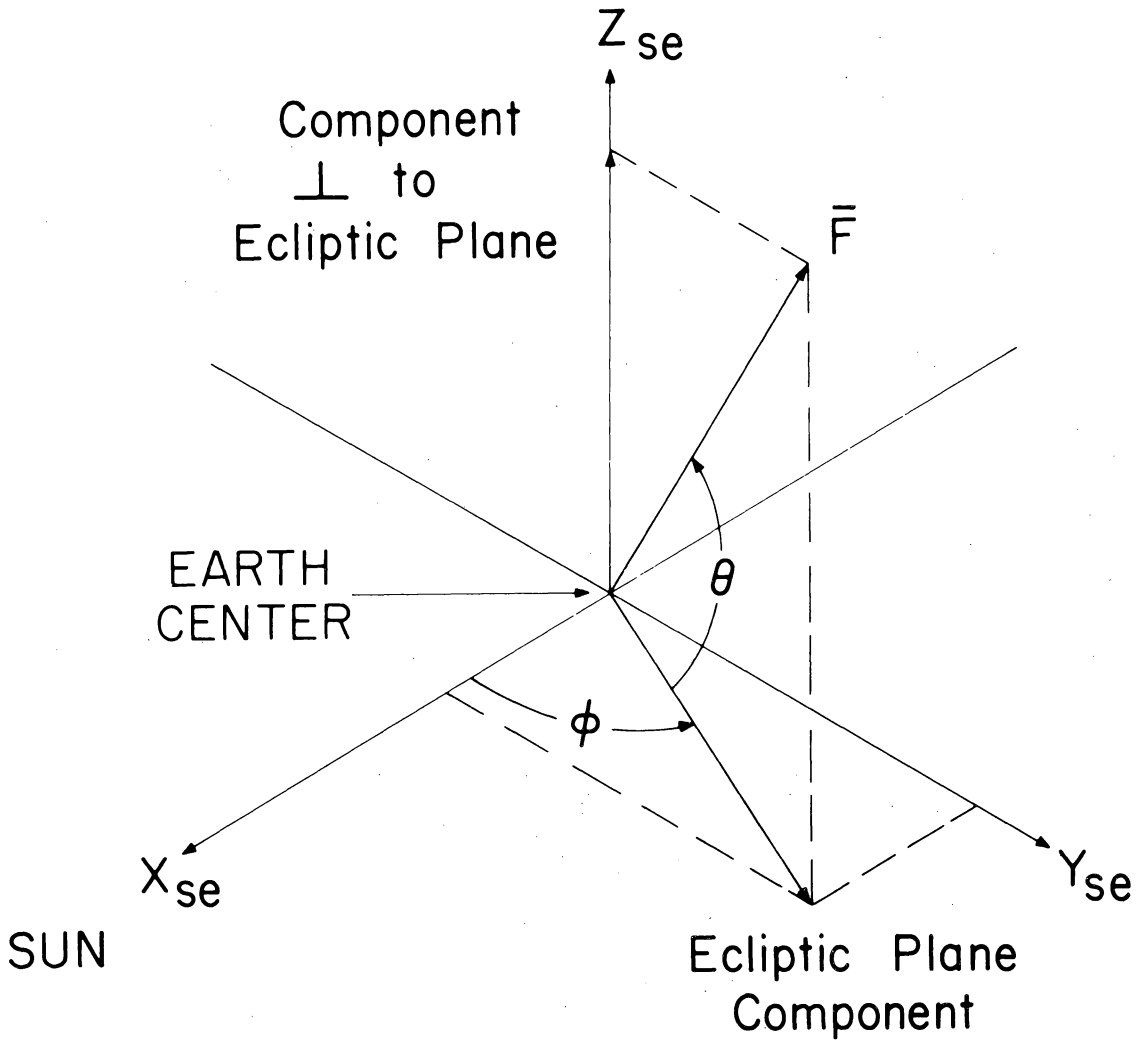

Figure 2–Solar ecliptic reference frame and associated parameter nomenclature and definitions.

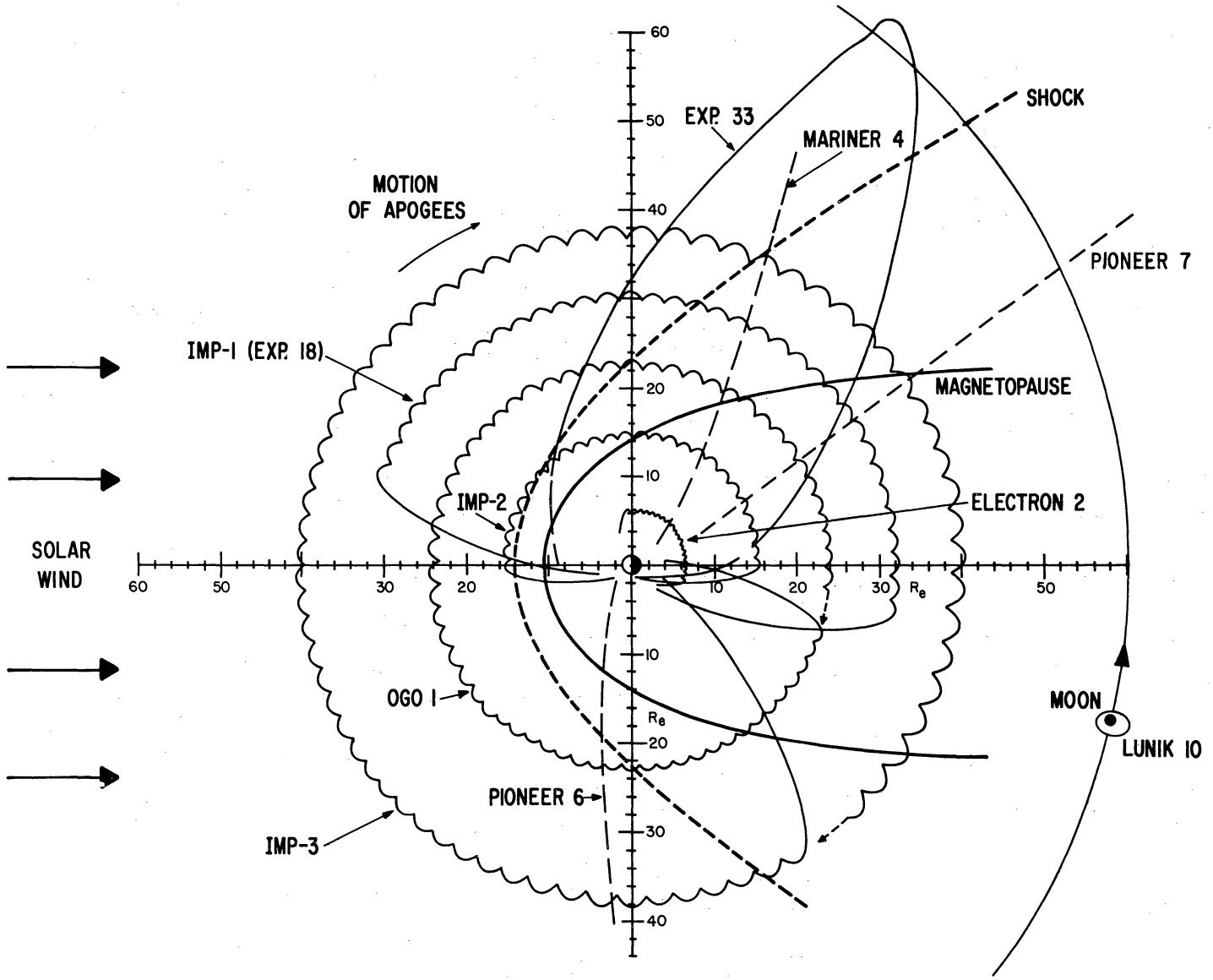

Figure 3–Summary of trajectories of ten spacecraft that have investigated the outer magnetosphere.

The Explorer 33 spacecraft was spin stabilized at an initial rate of 26.5 rpm with a spin axis orientation of $\phi_{SE} = 129°$ and $\theta_{SE} = -4°$. The initial angle between the spin axis and a line from the satellite to the sun was approximately 118°. The torque effects associated with solar radiation pressure on the spinning spacecraft and its solar paddles produced a subsequent precession of the spin axis in an inertial frame of reference and a continuous change in spin rate. Fig. 4 shows the variations in spin rate, spin axis-sun angle and apogee-earth-sun angle during the first five months in orbit. As can be seen the spin rate increased until the spin axis-sun angle decreased to below 90° on August 10. The spin rate then decreased for the remainder of this period of solar aspect between 0° and 90°. The orientation of the spin axis in solar ecliptic coordinates at the end of November was $\phi_{SE} = 339°$ and $\theta_{SE} = -5°$. It is to be noted then that the spacecraft spin axis was nearly parallel to the plane of the ecliptic throughout the period under discussion. It will remain so during the spacecraft lifetime.

During the first 19 weeks of the lifetime of Explorer 33, the satellite completed eight orbits about the earth, with a mean orbital period of 16.6 days. In Fig. 5 is shown the projection of the initial eight orbits on the solar ecliptic plane. Also sketched in for reference are the collisionless magnetohydrodynamic bow shock wave and the magnetosphere boundary or magnetopause. The bow shock is defined as the surface separating the interplanetary region, where the properties of the interplanetary medium are undisturbed by the presence of the

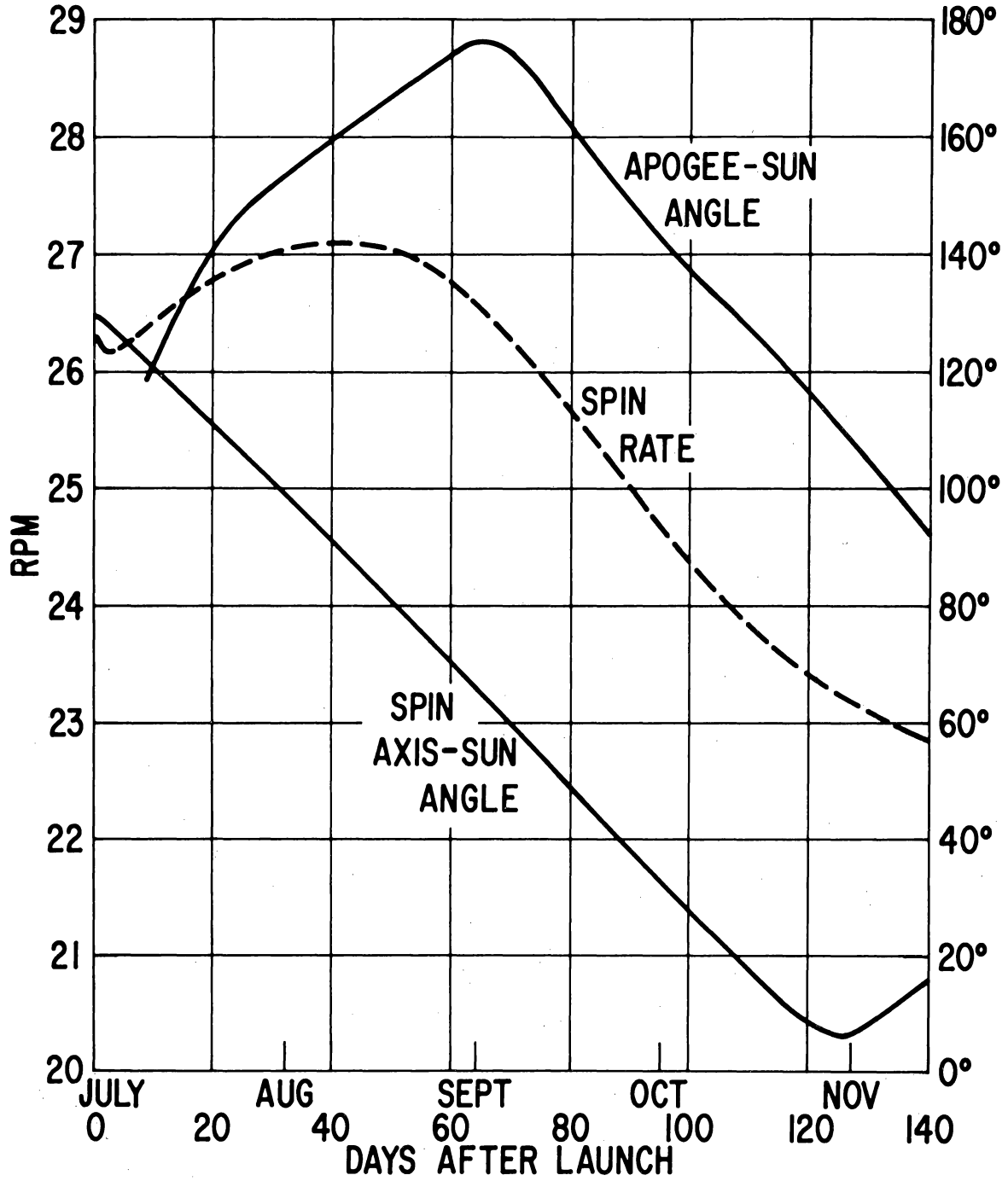

Figure 4–Variation of Explorer 33 spin rate and spin axis and orbit orientation parameters.

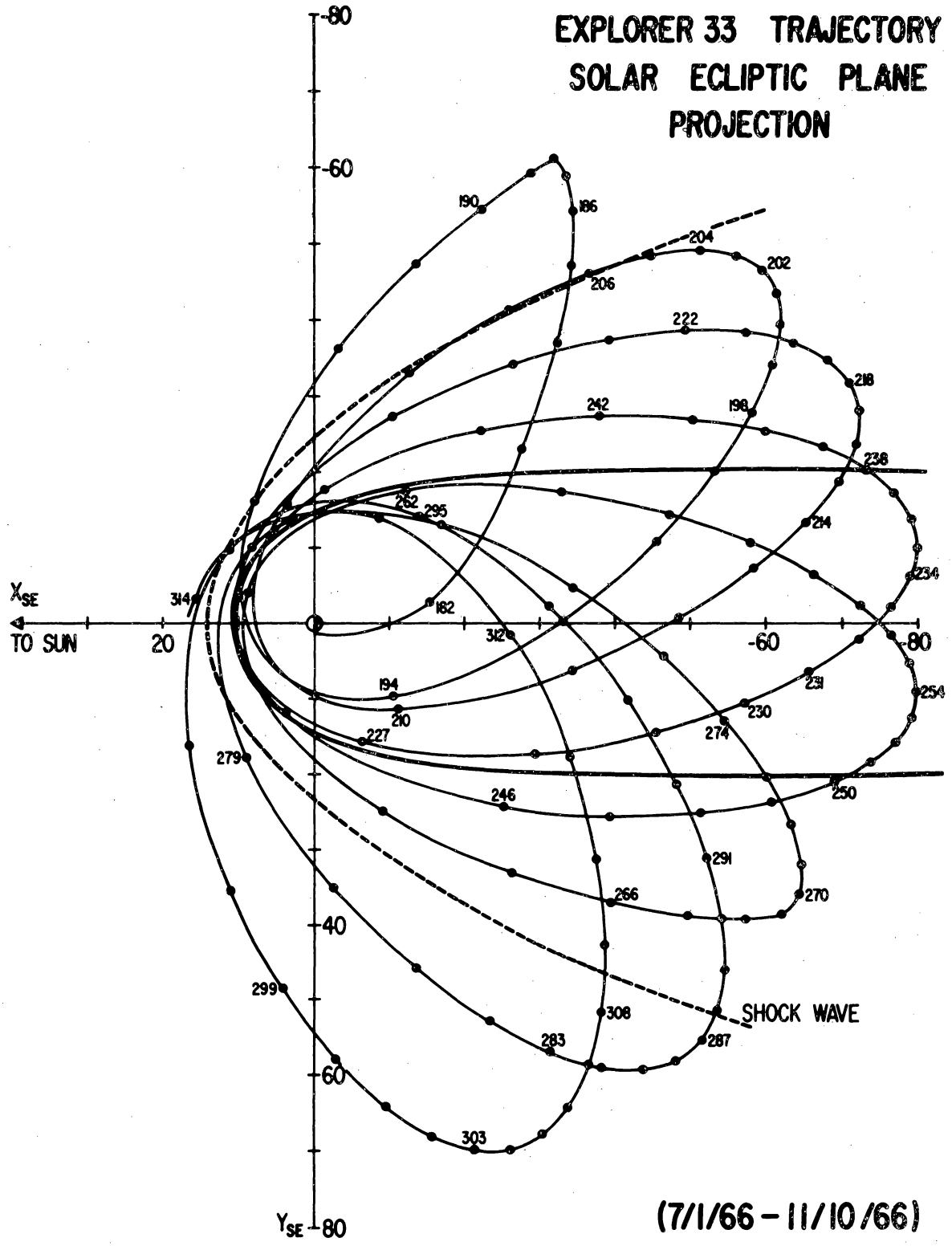

Figure 5–Ecliptic plane view of first eight orbits of Explorer 33.

geomagnetic field, from the magnetosheath or transition region. The magnetopause separates the magnetosheath from the magnetosphere, or region of space containing the geomagnetic field. The magnetosheath is hence a boundary region formed by interaction between the streaming solar wind and the geomagnetic field. One consequence of this interaction is a deformation of the magnetosphere such as to produce a geomagnetic tail that extends away from the sun.

The bow shock and magnetopause shown in Fig. 5 are approximate boundaries for the case of cylindrical symmetry about the earth-sun line. The boundary topology actually observed by Explorer 33 is discussed in Section V. As can be seen in Fig. 5, the apparent precession of the Explorer 33 orbit by an average angle of 19° per orbit carried the spacecraft apogee across the magnetic tail from the western flank of the earth's bow shock to the eastern flank. The day numbers used in the figure are decimal-day-of-the-year numbers. In this system January 1 is day 0 and July 1 is day 181. Distances are in units of earth radii (1 R_E = 6378.2 km).

In Fig. 6 are shown the variations in ϕ_A, the solar ecliptic longitude of the apogee of the orbit, and in θ_A, the corresponding solar ecliptic latitude, during the first four months in orbit. Because of its high apogee the Explorer 33 orbit is highly sensitive to the gravitational attraction of the moon. The orbital motion of the satellite was strongly perturbed near apogee of the first orbit when the moon passed within 36,000 km of the spacecraft on July 8. This first lunar

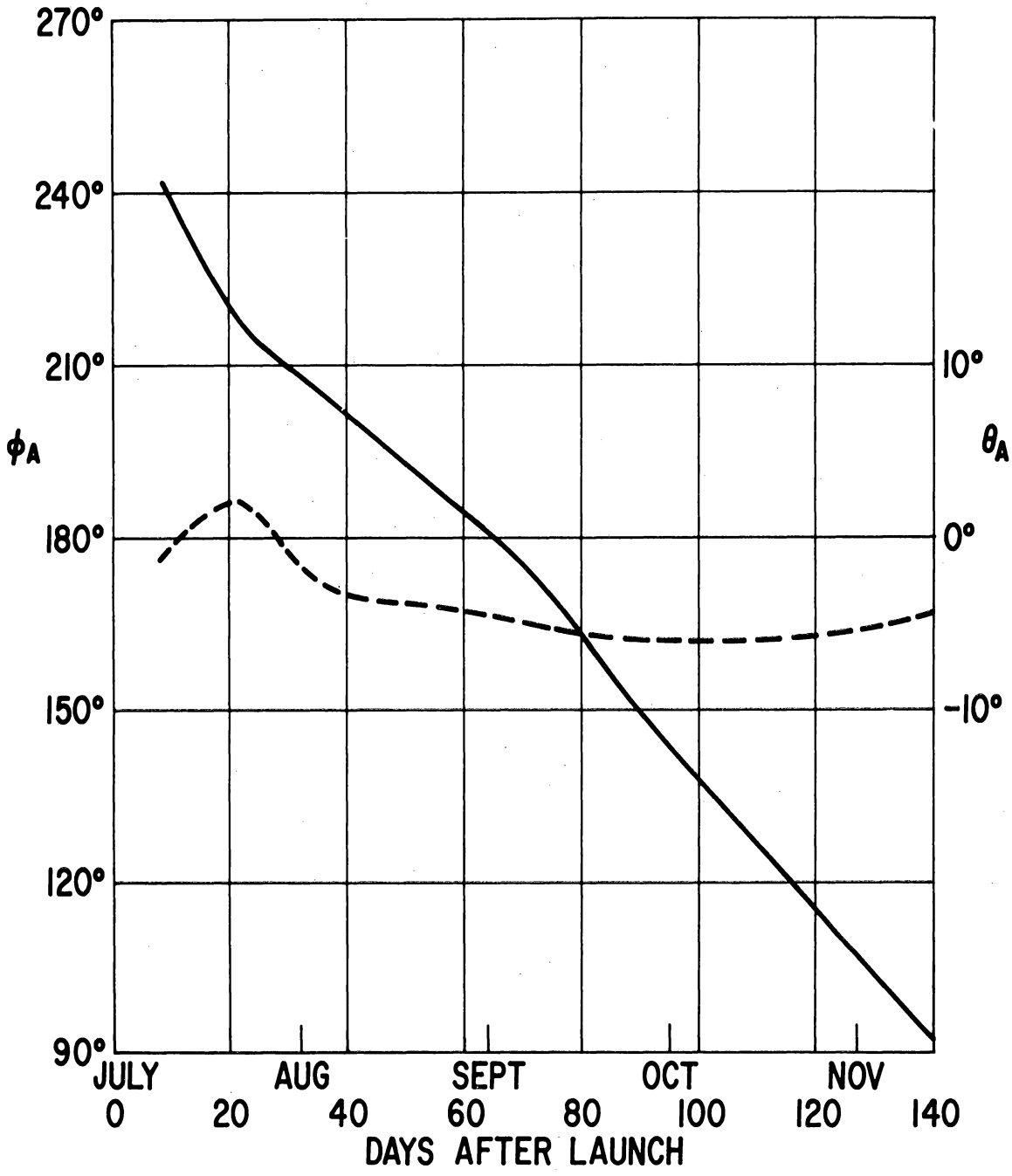

Figure 6–Variation of Explorer 33 solar ecliptic apogee position.

encounter was the closest approach of the satellite to the moon that occurred during the first ten months in orbit.

The line of apsides was rotated upward across the ecliptic plane, moving the apogee of the orbit to $\theta_{SE} = 2°$ for the second orbit. Fig. 7 shows the projection of the initial four orbits on the noon-midnight meridian (X_{SE}, Z_{SE}) plane. The effects of the lunar perturbation on July 8 are clearly seen. Less drastic orbital changes occurred when Explorer 33 was within 91,500 km of the moon on August 2 (orbit 3 – decimal day 213) and within 60,000 km of the moon on September 27 (orbit 6 – decimal day 269).

As can be seen in Fig. 6, the line of apsides moved downward after orbit 2, shifting the apogee latitude θ_A southward to a minimum of -6° in orbit 7. On orbits 4 and 5 the apogee distance increased to 514,000 km, or greater than 80 R_E. During the first eight orbits the perigee distance was a minimum of 50,000 km on July 13 (day 193) and a maximum of 96,500 km on October 23 (day 295).

The Explorer 33 spacecraft was in interplanetary space 29 days out of the first 133 days in orbit. Solar-associated events monitored by the satellite during the interplanetary phases of the initial eight orbits included the passage of a shock wave on July 8 propagating outward from a solar flare (Van Allen and Ness, 1967). Because of the extensive coverage of the geomagnetosphere and magnetosheath provided by the unique Explorer 33 orbit, much of the general topology of the outer magnetosphere during the period July 1 – November 10, 1966, may be deduced from the observations made by this satellite. It is the

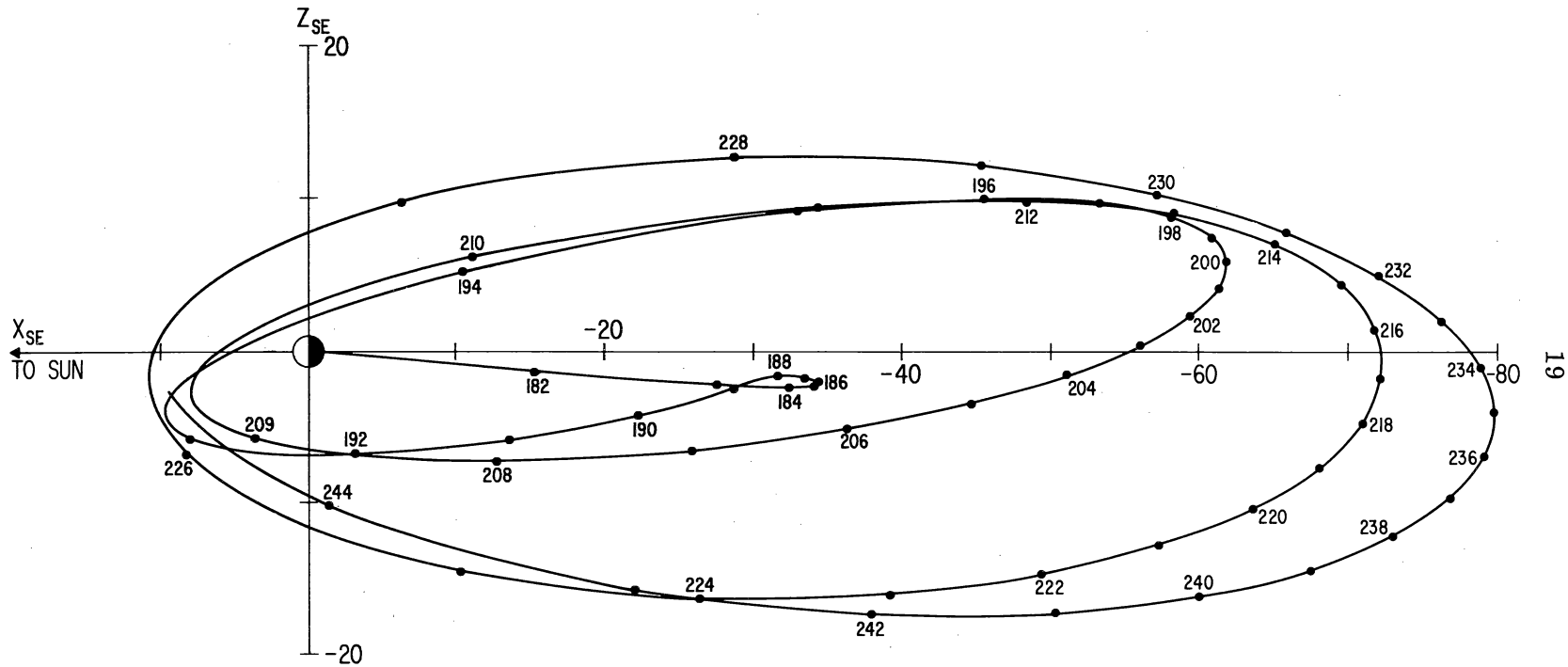

EXPLORER 33 ORBITS 1-4 MIDNIGHT MERIDIAN PLANE PROJECTION

Figure 7–Illustration of the variation of the apogee position relative to the ecliptic plane.

purpose of this thesis to discuss the initial results from the magnetosphere and magnetosheath measurements made by the Goddard Space Flight Center (GSFC) magnetic field experiment on board Explorer 33 during that time period.

A review of previous investigations of the outer magnetosphere, magnetosheath, and bow shock is presented in Section II. The instrumentation of the Explorer 33 magnetic experiment is described in Section III, and the data reduction and analysis are discussed in Section IV. Initial experimental results for orbits 1-8 are presented in Section V. In addition to a general description of the topology of the outer magnetosphere and collisionless shock wave, magnetopause and bow shock traversals are discussed in detail.

Detailed results from measurements in the geomagnetic tail are also presented. Magnetic measurements by Explorer 33 have demonstrated that the earth's magnetic tail extends beyond the orbital distance of the moon (Ness et. al., 1967a). Moreover, the topology of the tail at that distance is similar to that found previously at half the lunar distance by IMP 1 (Ness, 1965). The neutral sheet-associated variations observed in the tail by Explorer 33 are discussed in detail.

The gross geometry of the magnetic tail is described and significant spatial and temporal variations of the magnetic field in the tail are discussed. Magnetic disturbance or storm variations observed both in the magnetic tail and in the magnetosheath are correlated with variations seen in the horizontal component of the geomagnetic field at the surface of the earth and with the planetary

magnetic activity index K_p. These include the observation of a magnetic storm during orbit 5 when Explorer 33 was near the midnight meridian plane in the tail beyond the lunar orbital distance.

This thesis will follow the practice common in geophysics of using 1 gamma $= 10^{-5}$ oersted as the basic unit of magnetic intensity.

II. HISTORICAL BACKGROUND

A confined geomagnetic field was postulated more than 30 years ago (Chapman and Ferraro, 1931-32) in an attempt to account for certain observed features of terrestrial magnetic disturbances. It was proposed that a transient ejection of solar plasma would confine the geomagnetic field temporarily and electric currents would develop on the boundary surface, producing magnetic fields that would perturb the geomagnetic field.

Twenty years later in an effort to explain observed characteristics of Type I comet tails, Biermann (1951) suggested that there must be a corpuscular flux of substantial intensity continuously flowing away from the sun. On this basis Parker (1958) developed the theory of the solar wind and concluded that a continual confinement of the geomagnetic field would exist. It was further asserted that the geomagnetic field would form an obstacle in the path of the streaming solar wind. In the interaction between the solar wind and the geomagnetic field a boundary layer would be created. The solar plasma would be "thermalized" in this layer and would flow downstream around the confined geomagnetic field, compressing it on the sunlit side and carrying away the outermost lines of force in the antisolar direction.

The formation of the geomagnetic tail was anticipated theoretically by Piddington (1960). Geomagnetic field line interconnection with the interplanetary field as a mechanism for extending the geomagnetic lines of force into the earth's tail was introduced by Dungey (1961, 1963). More definitive theoretical studies of the interaction between the solar wind and the geomagnetosphere and the formation of the magnetic tail have been conducted by Beard (1960 a, b, 1962), Axford and Hines (1961), Levy, et. al., (1964), Axford (1964, 1966), Dessler and Walters (1964), Axford et. al., (1965), Piddington (1965), and Dessler and Juday (1965).

In considering the steady-state existence of a geomagnetic tail, Axford et. al., (1965) concluded that a magnetically neutral sheet centered in a region of hot plasma would be required to maintain a separation between the antisolar directed lines of magnetic flux extended into the tail from the south polar region of the earth and the oppositely directed lines connected to the north polar region. They deduced that the thickness of the sheet would be of the order of a few earth radii.

Theoretical computations of the shape of the magnetospheric boundary have been carried out by a number of authors (reviewed by Beard, 1964). In addition, Spreiter and Jones (1963) computed the shape of a detached bow shock wave on the sunward side of the magnetosphere in the solar plasma, which is supersonic in the magnetohydrodynamic sense. From the classical gas dynamics analogy Zhigulev (1959), Kellogg (1962), Gold (1962), Axford (1962) and Rossi (1963)

all concluded that a standing shock wave must exist in the interplanetary medium a short distance upstream of the magnetosphere.

An ionized gas is called a plasma if the Debye or shielding length is small compared with other physical dimensions of interest in the system. For the solar wind the Debye length is of the order of 10 meters (Levy et. al., 1964), which is small compared with significant dimensions in interplanetary space. Because of the extremely low density of the solar plasma (generally on the order of 10 protons/cm^3) one would expect that an individual particle treatment would have to be used to describe the plasma dynamics. The condition for a fluid flow or mass transport treatment is that the mean free path be small compared to relevant lengths of importance in the system. The mean free path of a proton in the solar wind is of the order of 10^6 km. Parker (1958) pointed out that this is 10 times the radius of the magnetosphere at the earth. He concluded that many strictly hydrodynamical properties of the solar wind in the large would not be applicable to the details of flow past the magnetosphere.

Levy et. al., (1964) justify the continuum treatment in the case of a rarified plasma on the basis of several mechanisms involving electric and magnetic fields which are not available in a flowing neutral gas but which can give rise to coherent phenomena in a plasma. There cannot be appreciable differences between the electron and ion densities over distances larger than the Debye length, which for the solar wind is very small compared to the radius of the magnetosphere. Further, it is known that several linear wave propagation

modes can exist in a collision-free plasma, evidence for the interdependence of particle motions.

Over a period of approximately 2-1/2 months in 1963-64 an average interplanetary magnetic field magnitude of 5.1 gammas (Ness et. al., 1966a) and an average solar wind velocity of 378 km/sec (Wolfe et. al., 1966) were observed by the IMP 1 satellite. These values yield a proton cyclotron radius of 774 km, which is small compared to the radius of the magnetosphere. A more appropriate cyclotron radius in the context of the interaction between the solar plasma and an obstruction in the flow stream would be obtained using the thermal velocity component. Since the thermal velocity is small compared with the streaming velocity, an even smaller gyroradius results. If the Larmor radius can be considered as an "effective" mean free path, then a fluid continuum approximation can be used in treating the interaction between the solar wind and the magnetosphere.

According to Levy et. al., (1964), as long as flow properties only change by small amounts in a distance of the order of the gyroradius, detailed consideration of the particle orbits does in fact lead to the isentropic continuum magnetohydrodynamic equations. These are the fundamental equations for the fluid dynamical treatment of a plasma (Pai, 1962). They are based on conservation laws of mass, momentum, energy and charge and neglect any dissipative effects. At least until thicknesses of the order of the gyroradius are reached, a compression pulse will steepen to form a discontinuity or shock wave. The result

is that any object larger than a few ion gyroradii will create a magnetohydrodynamic shock wave when immersed in the solar wind. However, the tenuous nature of the plasma necessarily requires that the shock wave be of the collision-free type in which the required randomization of particles is produced by non-linear interactions of waves and particles rather than by particle-particle interactions. Detailed theoretical studies of the structure and properties of such collisionless shocks have been conducted by De Hoffman and Teller (1950), Fishman, et. al., (1960), Auer et. al., (1961, 1962), Petchek (1961), Morawitz (1961, 1962), Wilson (1962), Noerdlinger (1964), Corday (1965) and Tidman (1967 a, b).

Direct measurements of magnetic fields in space have been performed by satellites and deep space probes since 1958. A number of such measurements have verified the continuous existence of the solar wind and that the geomagnetic field is always to be found in a confined and distorted state. Measurements on Pioneers 1 and 5 (Sonett, 1960; Sonett et. al., 1960 a, b; Coleman et. al., 1960; Coleman, 1964) suggested termination of the geomagnetic field but no continuous traversal of the boundary was achieved because of intermittent satellite data transmission. In 1961 data from the Explorer 10 satellite, which transmitted useful information out to apogee on its first orbit, revealed the large scale distortion of the geomagnetic field on the night-time side of the earth (Heppner et. al., 1963; Bonetti et. al., 1963). In addition this spacecraft provided the first detection of the magnetopause or magnetosphere boundary.

It was also in 1961 that the first measurements of trapped particles, fields and plasmas were made at the magnetopause by Explorer 12 (Cahill and Amazeen, 1963; Freeman et. al., 1963; Freeman, 1964). These data indicated a termination of the compressed geomagnetic field on the sunlit side of the earth coincident with a termination of the trapping region of energetic particles as well as the onset of thermalized solar plasma. Evidence was later found in the magnetometer data that the earth's bow shock had been traversed on at least three orbits (Kaufmann, 1966).

With an apogee of 13.1 R_E, Explorer 12 was ideally suited for observing the day-side distortion of the geomagnetosphere by the solar wind (Mead and Cahill, 1966). The results of magnetic measurements by Explorer 12 were further used to compute the vector normal to the magnetopause and hence to deduce the attitude of the magnetospheric boundary at the traversal points (Sonnerup and Cahill, 1967). In 1962-63 the Explorer 14 satellite also provided measurements of both particle and magnetic field phenomena, in this case out to a geocentric distance of 16.5 R_E (Frank, 1965; Cahill, 1964, 1966).

The first comprehensive survey of the confined geomagnetic field, including its boundary and bow shock on the sunward side and its magnetic tail in the antisolar direction, was performed in 1963-64 by the IMP 1 (Explorer 18) satellite (Ness et. al., 1964, 1966a). The corresponding energetic particle and plasma observations have been described by Bridge et. al., (1965), Anderson et. al., (1965), Fan et. al., (1966), Wolfe et. al., (1966), and Serbu (1965). The region

of space mapped during the six months of continuous operation by IMP 1 was shown in Fig. 3. IMP 1 provided the first highly accurate measurements of the interplanetary magnetic field and the collisionless bow shock wave.

Measurements performed in the earth's magnetic tail out to 30 R_E by IMP 1 established that the tail is a permanent appendage of the geomagnetosphere (Ness, 1965). An average tail field magnitude of 16 gammas was found. These measurements further provided the first experimental detection of the neutral sheet in the geomagnetic tail (Ness, 1965; Speiser and Ness, 1967). In a second inspection of Explorer 14 measurements in the magnetic tail, Cahill (1966) also found examples of field reversal undoubtedly associated with the neutral sheet. A broad region of low magnetic field magnitude rather than a sharp transition was generally found. Since the Explorer 14 measurements were made nearer to the earth than the IMP 1 observations, they suggested that the field reversal region becomes thinner with increasing geocentric distance, approaching a physically real "neutral sheet" at great distances.

Large temporal field variations or "magnetic storms" were observed in the earth's tail by IMP 1 and were correlated with the corresponding disturbance variations recorded by magnetic observatories at the earth's surface (Behannon and Ness, 1966). A positive correlation was found between the tail field magnitude and the planetary magnetic activity or three-hour-range index K_p. The K_p index is basically a summary of worldwide magnetic activity as measured by the range of fluctuations shown in individual observatory magnetograms. At a

single magnetic observatory the measure of the intensity of magnetic disturbance for a three-hour interval is the individual K index (see IGY Annals, 4, 227-236). For 11 high latitude observatories widely distributed in longitude these indices are standardized to eliminate local effects. K_p is the average of the 11 standardized K indices. There are 28 grades of K_p on an intensity scale of 0 to 9. A K_p of 4 or greater is considered to be indicative of magnetically stormy conditions.

A correlation of IMP 1 magnetic storm observations with measurements performed at an altitude of 1100 km by the APL satellite 1963 38C demonstrated the collapse of the outer trapping boundary to lower latitudes following the onset of a magnetic disturbance (Ness and Williams, 1966). Other satellite observations of the geomagnetic field during magnetic storms have been described by Smith and Sonett (1962), Smith et. al. (1964) and Cahill and Bailey (1967).

In analyzing the IMP 1 interplanetary measurements, Wilcox and Ness (1965) found that through three solar rotations the observed directions of the magnetic field in the interplanetary medium fell into a systematic pattern of quasi-stationary sectors that corotated with the sun. Within each sector the field direction was generally near the ecliptic plane but predominantly either toward or away from the sun along the spiral angle inclined at approximately 45° to the earth-sun line. The spiral interplanetary field configuration results from the magnetic lines of force remaining attached to the rotating sun as they are extended outward by the radially streaming solar plasma.

The interplanetary magnetic field direction was observed to reverse at each sector boundary. Within each sector a systematic behavior of field magnitude and solar wind flux was apparent. There was a pronounced tendency for both the interplanetary field magnitude and the solar wind flux to be enhanced near the leading edge of each corotating sector. These occurrences of enhanced fields and plasmas in the sectors were found to correlate well with the occurrences of high terrestrial magnetic activity index K_p and with the onset of geomagnetic disturbances. An extrapolation of the sector boundaries to the later period of IMP 1 magnetic tail observations was in close agreement with the pattern of recurrent magnetic disturbances observed in the tail and at the earth's surface (Behannon and Ness, 1966). Such magnetic storms recurring in the magnetosphere with the 27-day solar rotation period over several to many solar rotations have been studied for many years (Bartels, 1932; Allen, 1944; Saemundssen, 1962; Dessler and Fejer, 1963; Mustel, 1964 and others).

Anderson (1965) found from IMP 1 particle data that energetic particles (mostly electrons > 30 keV) characteristically occur in the geomagnetic tail as isolated bursts with flux buildup times of the order of a few minutes or less and much longer decay times. To account for these observations, mechanisms involving local acceleration of the particles or impulsive injection from outside the tail were suggested. Sharp decreases in the magnetic field magnitude were found to accompany these electron events (Anderson and Ness, 1966). Measurements by the Explorer 14 satellite (Frank, 1965) had earlier revealed the formation

of an "electron tail" on the night side of the earth. Gringauz et. al. (1960), Freeman (1964), McDiarmid and Burrows (1965), Singer et. al., (1965) and Montgomery et. al., (1965) all have found enhanced particle fluxes in the anti-solar region of the magnetosphere, and the plasma sheet associated with the magnetically neutral sheet has been detected (Bame et. al., 1966, 1967).

During 1964-66 continued mapping of the magnetopause and bow shock positions were provided by the Vela 2 satellites (Gosling et. al., 1967), IMP 2 (Fairfield and Ness, 1966; Serbu and Maier, 1966), and OGO 1 (Heppner, et. al., 1965; Heppner, 1965; Holzer, et. al., 1966). The Vela satellites extended measurements of the boundary positions to solar ecliptic latitudes of ±60°. The measured positions were found to be highly variable in time. The IMP 2 measurements showed that both the shock front and the magnetopause frequently moved back and forth past the satellites. Boundary motion also has been observed by Explorer 10, IMP 1, OGO 1 and other spacecraft.

Definitive mapping on the dawn side of the magnetosphere by IMP 2 demonstrated the distortion of magnetic field lines in that region and the gradual formation of the magnetic tail. The high field sampling rate of OGO 1 permitted the identification of large amplitude rapid magnetic field oscillations near the bow shock in both the magnetosheath and in the interplanetary medium. Such magnetic fluctuations also were observed by Mariner 4 on its outbound pass (Siscoe et. al., 1967).

Some investigators have questioned the continuous existence of a feature that can properly be defined as a magnetohydrodynamic bow shock wave, Bernstein et. al., (1964), Fredricks et. al. (1965) and Scarf et. al., (1965) all have argued that only a broad disordered region exists upstream of the magnetosphere. However, both the frequently repeated observations of the shock on a long term basis by a number of the earth orbiting satellites and single pass traversals by interplanetary probes such as Pioneer 6 (Ness et. al., 1966b) and Mariner 4 (Siscoe et. al., 1967) have found what must be called a well-defined shock on the basis of sudden discontinuous changes in the character of both the plasma and the magnetic field as this thin layer upstream from the magnetosphere is traversed. These many observations of the bow shock have indicated that its thickness is on the order of tens of kilometers. Its distance from the center of the earth has been found on the average to be approximately 13 R_E along the earth-sun line. The average geocentric magnetopause distance along the earth-sun line, or stagnation point distance, has been established as approximately 10.5 R_E .

An east-west asymmetry of the magnetopause and the bow shock about the earth-sun line was anticipated theoretically on the basis of both the small (2° - 5°) aberration of the solar wind direction caused by the earth's motion about the sun and the effect of the oblique interplanetary magnetic field (Walters, 1964). The existence of an asymmetry of both the magnetopause and the bow shock has been experimentally verified by the Vela 2 measurements (Bame et. al., 1964;

Coon, 1966; Gosling et. al., 1967) and by OGO 1 (Heppner, 1965; Holzer et. al., 1966) and IMP 3 (Ness, 1966a). The center of symmetry was observed to lie approximately 2-4° west of the earth-sun line.

The three-dimensional shape of the magnetopause has not yet been completely determined by space measurements. Some theories of the shape of the magnetosphere indicate that it should be slightly flattened toward the poles near the bow of the magnetosphere and perhaps elongated in a north-south direction further downstream (Beard, 1964). Although the Vela observations have extended measurements to much higher latitudes than reached by previous experiments, those results only have permitted a conservative limit to be set on the amount of flattening of the day-side magnetopause at high latitudes (Gosling, et. al., 1967).

Widely different estimates have been advanced concerning the length of the earth's magnetic tail. Dessler (1964) has calculated that the shortest possible length for the magnetospheric tail would be of the order of 100 R_E. He has argued, however, that hydromagnetic wave radiation pressure will keep the tail open to a distance as great as 20-50 astronomical units. On the basis of the length of time that terrestrial lines of force being swept back into the tail will remain attached to interplanetary field lines, Dungey (1965) has estimated a much more conservative geomagnetic tail length of approximately 1000 R_E.

The first opportunity to detect the tail far downstream in the solar wind experimentally was provided by Mariner 4, which spent seven days of flight within a geocentric angle between 1° and 5° from the presumed center line of

the tail at a radial distance of approximately 3300 R_E (Van Allen, 1965). The Geiger tube detectors on board failed to detect any effects of a magnetospheric tail during that week of favorable trajectory orientation. The Pioneer 7 spacecraft passed through the downstream region of solar wind interaction with the geomagnetic field at a geocentric distance of approximately 1000 R_E in September 1966. Detailed magnetic field measurements by Pioneer 7 (Ness et. al., 1967b) suggest that magnetic lines of force connecting to the earth through the geomagnetic tail were observed. However, this preliminary inspection of the data did not reveal a coherent, well-defined tail at that distance.

III. EXPERIMENT INSTRUMENTATION

The GSFC magnetic field experiment on board Explorer 33 utilizes a tri-axial fluxgate magnetometer to detect the ambient magnetic field. In general in a fluxgate or saturable core magnetometer a sample of magnetic core material is driven alternately positive and negative through saturation magnetization by an AC input signal which is applied to a primary winding about the core. When the hysteresis curve is symmetrical, the waveforms of the positive and negative half-cycles are identical. The flux variation, therefore, contains only odd harmonics. This is because in this case the hysteresis function is an anti-symmetric function satisfying the condition

$$f\left(t \pm \frac{T}{2}\right) = - f(t) \tag{1}$$

where T is the period of the function. The Fourier series for a function of this kind contains only odd-harmonic components. This fact can be proved by showing that the odd harmonic components satisfy equation (1) but the even harmonic components do not and hence cannot exist if the function itself satisfies the equation (M.I.T. Electrical Engineering Staff, 1943).

A shift of the center position of the hysteresis curve such as would be caused by the instrument being immersed in an external magnetic field in addition to the flux generated by the AC input signal will result in the addition of even harmonic components into the spectrum. The mechanical configuration of the GSFC fluxgate instrument is such that only the even harmonics are detected. The second harmonic is much larger in amplitude than the other even harmonics. For this reason a relatively broad band filter will effectively pass only the second harmonic component.

The second harmonic saturable core magnetometer is designed to be linear over the desired operating range. Within the selected range of applied magnetic field magnitudes a change in field strength parallel to the core axis produces a proportional change in the magnitude of the second harmonic output voltage. Thus with calibration the output of the secondary coil provides a measurement of the instantaneous ambient magnetic field along the axis of the instrument. By using a triaxial magnetometer, in which three separate fluxgate sensors are arranged in an orthogonal configuration, an unambiguous measurement of the instantaneous vector magnetic field can be obtained. In Explorer 33 the three sensors are mounted together as a single physical unit.

The fluxgates used in this instrument were designed for maximum stability and minimum permanent field retention. Partial feedback of the secondary output contributes to the stability of the sensors. Each sensor is cyclically saturated at approximately 10 KC. There is a maximum frequency at which

the core material can be driven without generating significantly large eddy currents. This constraint together with the need to use the smallest possible electronic components is the determining factor in the selection of the AC input signal.

The sensor solenoids must respond to field changes produced by the spin of the spacecraft at frequencies comparable to the spin rate. A spin rate of 24 rpm modulates the ambient magnetic field at a frequency of 0.4 cps. The bandpass of the electronics was chosen so that a frequency between 0 and approximately 5 cps is passed without attenuation and all frequencies beyond are attenuated at a rate of approximately 20 db per decade. The upper limit is above major frequencies to be expected for significant physical phenomena in interplanetary space and interaction of the solar wind with the geomagnetic field (Ness, 1966b).

The frequency response out to 10 cps and the phase shift are shown in Fig. 8 for one of the Explorer 33 fluxgates. The corresponding characteristics of the other two sensors are almost identical. As can be seen the response of the sensors is essentially flat over the passband containing the frequencies of physical interest. Since the phase shift is not entirely negligible at the spin frequency, it is compensated for in the analysis (see Section IV).

The fluxgate sensing elements can present zero scale offsets associated with sensor drift which must be determined in-flight. The unique way in which the sensors are mounted and reoriented aboard the spin-stabilized spacecraft

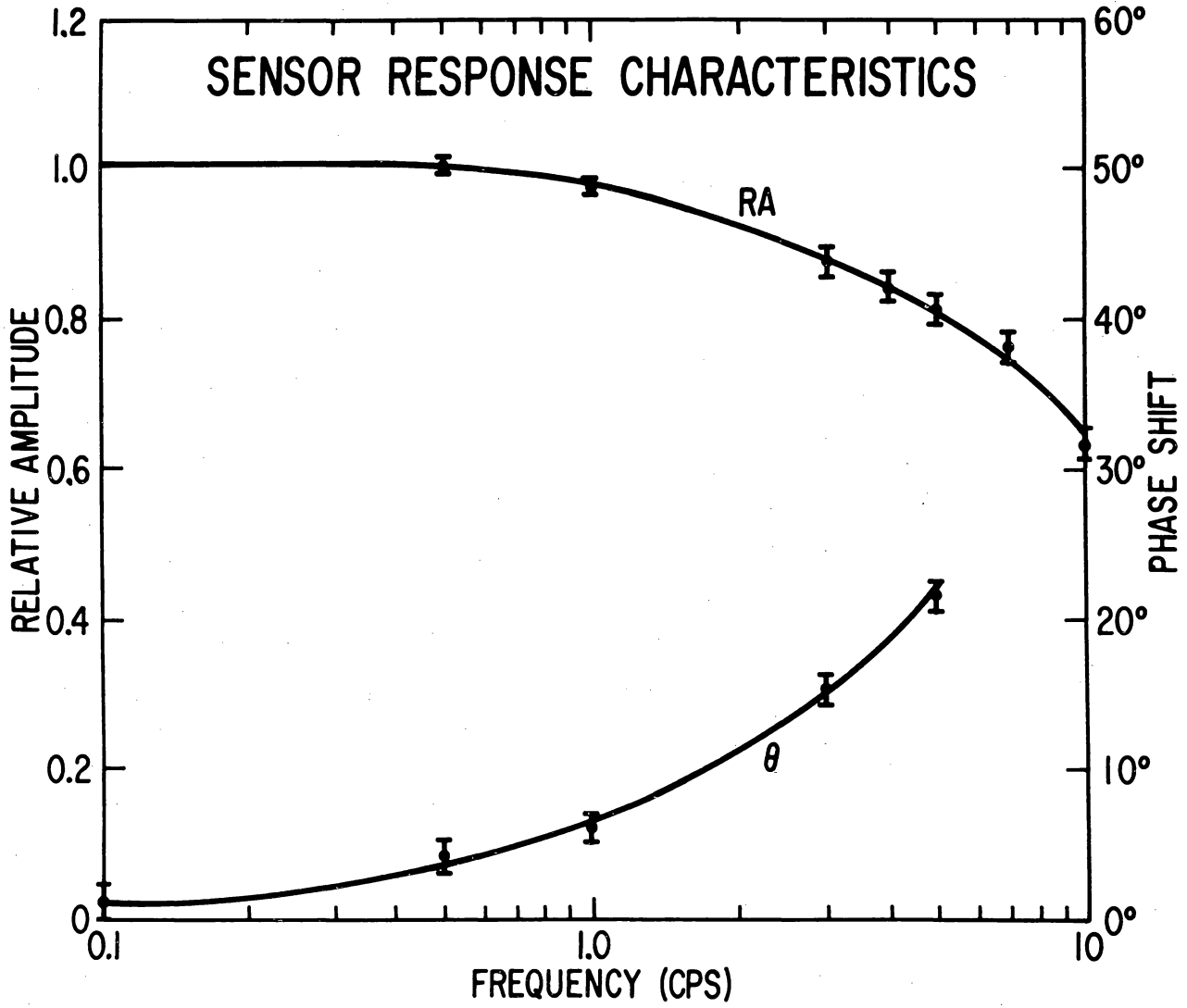

Figure 8–Magnetometer sensor frequency response and instrumental phase shift.

solves this problem. In order to determine the zero level of a sensing element, it is necessary to reverse its directional sense by exactly 180° while the ambient field is stationary. This experiment takes advantage of the spin stabilization of the spacecraft by mounting two of the sensors perpendicular to the spin axis as well as perpendicular to each other. Thus the basic rotation of the spacecraft reorients and thereby calibrates the zero level for two of the three axes without additional equipment.

A 90° rotation of the sensor system about an axis through one of the sensors normal to the spin axis is equivalent to a 180° rotation of the spin axis sensor because it interchanges the sensor initially parallel to the spin axis with one of the sensors initially in the equatorial plane of the satellite. Thus a thermo-mechanical "flipper" device which reorients the triaxial sensor set by 90° provides periodic reversal of the spin axis sensor. This permits continuous monitoring and calibration of the zero level along that axis over the lifetime of the spacecraft. On Explorer 33 this reorientation is commanded once each 24 hours by the spacecraft encoder.

Stationary spacecraft magnetic fields perpendicular to the spin axis are cancelled out in the determination of the zero level shift of the two sensors which are normal to the spin axis. Thus the final accuracy of the experimental measurements are limited only by time-varying spacecraft magnetic fields for the field component perpendicular to the spin axis. However, any spacecraft field parallel to the spin axis is not cancelled out in the calibration of that sensor's

zero level since the spacecraft is not inverted 180° by the flipper. The only solution to this final limitation on the accuracy of the experiment is to place the sensors at a remote distance from the spacecraft on a boom support. In Fig. 1 the booms and instrument canisters are shown deployed. On Explorer 33 the triaxial sensor set is 2.1 meters from the spin axis. Since this spacecraft is extremely clean magnetically already, the contamination field at the position of the sensors is reduced to the noise level of the magnetometer ($\leq 1/4$ gamma) (Harris, 1966).

A block diagram of the experiment is shown in Fig. 9. The three sensor data channels are sequentially gated to an analog-to-digital converter. By means of voltage comparison the 0-5 volt analog output of each of the three sensors is digitized. Following the conversion, each of the three resulting 8 bit words is stored in a 32 bit buffer register which also stores an 8 bit status or housekeeping word. The contents of the register are commutated to the output lines during readout period. The three axes are sampled, digitized and buffer stored in less than 15 milliseconds (10 ms for the two sensors in the plane of rotation, which corresponds to 1.2° of spacecraft rotation for a spin period of 3 seconds). These stored values (24 bits for all three axes) are read out four bits at a time by the telemetry data system at the scheduled times in the 81.808 second telemetry sequence.

For reasons of format simplification the magnetic field sampling was chosen to be synchronous with the telemetry rate rather than with the spin rate

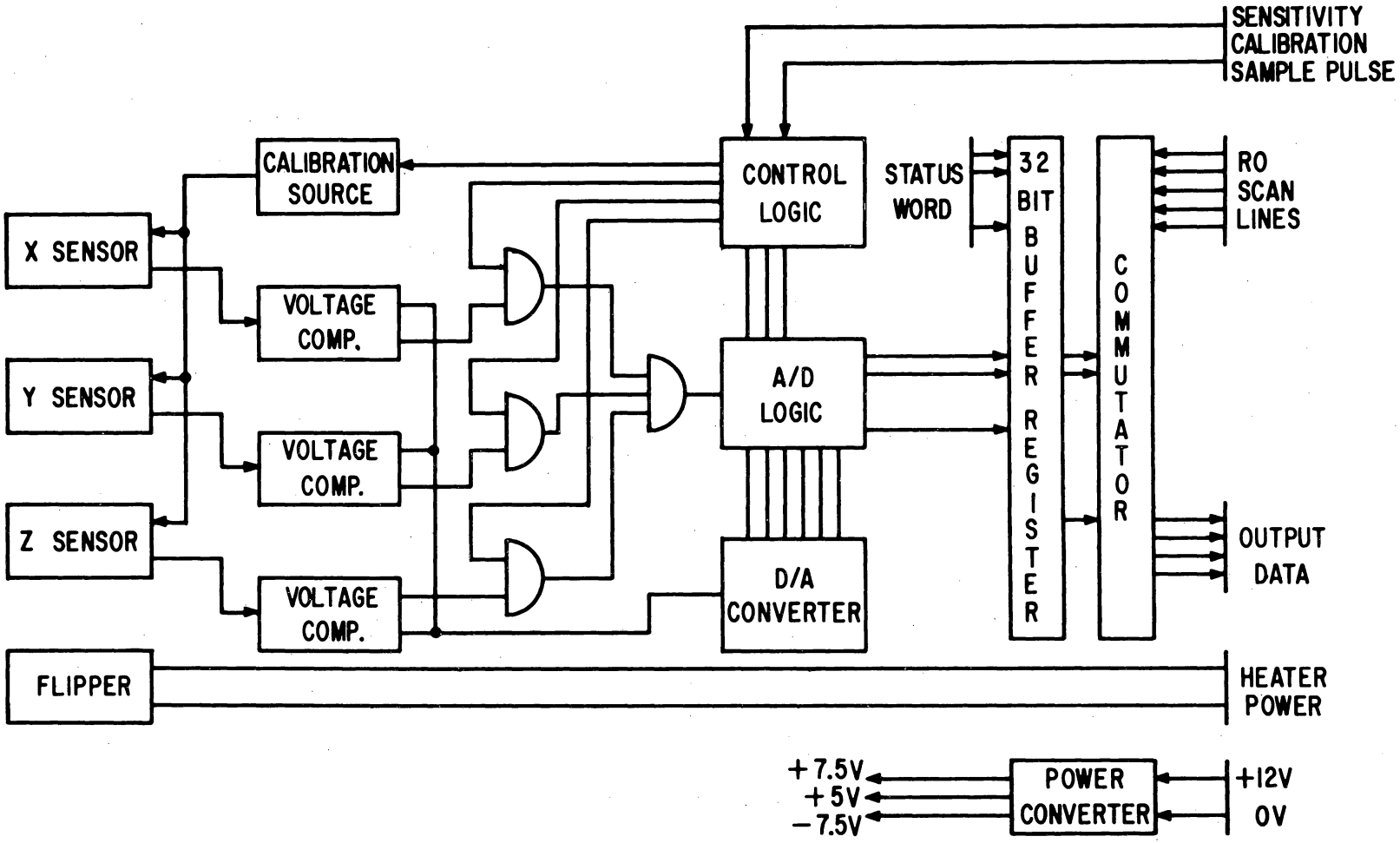

Figure 9–Block diagram of GSFC magnetic field experiment.

of the spacecraft. Because of this a measurement of the vector field is performed once every 5.11 seconds (16 measurements per telemetry sequence). This gives a sampling frequency of 0.195 cps, or for spectral analysis considerations a folding frequency of 0.0975 cps. A comparison with a typical spin modulation frequency of 0.4 cps shows that the sampling rate is less than the spin rate, so that if there are zero level errors aliasing of the spin frequency is possible, along with any other frequency between 0.0975 and 10 cps. The effects of aliasing in the data will be investigated further in Section IV.

For this experiment the sensitivity level of the instrument was matched with the noise level of the quantization error. Extensive investigations have shown the noise level to be less than ±1/4 gamma. There is a maximum precision of 8 bits per axis in the analog-to-digital conversion. Since decimal numbers from 0 to 255 can be represented by 8 binary digits, the maximum possible number of magnetic field steps is 256. With ±1/4 gamma per step the resulting dynamic range of the instrument is ±64 gammas along each axis.

The sensitivity and linearity of each axis is checked each 12 hours by the addition of a known magnetic field parallel to the sensor axis. A special solenoidal coil carrying an accurately known current provides the field for the sensitivity checks. The performance of the magnetic field experiment for the first five months of operation was completely consistent with preflight calibrations of accuracy and precision.

IV. EXPERIMENTAL DATA REDUCTION AND ANALYSIS

The Explorer 33 spacecraft employs a pulse frequency modulation (PFM) telemetry system (Rochelle, 1962) to transmit experimental data back to earth. In this system the outputs from the various experiments on the satellite are commutated to the appropriate oscillator, depending on whether the output is digital or analog, for conversion to a pulse frequency output. A pulsed digital oscillator accepts four bits of information at a time from the magnetic field experiment and encodes this as one of 16 discrete frequencies. The oscillator output phase modulates the transmitter carrier wave.

The continuous telemetry stream is built up of individual telemetry sequences. A telemetry sequence is in general the smallest segment of telemetry output which is uniquely identified and which contains data readouts from all the experiments on the spacecraft. These readouts are commutated and time multiplexed according to a specific repetitive sequence format.

In the telemetry stream unique identification of each telemetry sequence to modulo 2^{16} is provided by the spacecraft clock, which is a 16 bit accumulator that is updated once each sequence. Besides identification, this serves as a stable, independent clock against which ground station time can be compared.

Acquisition of the data from the satellite is accomplished through a world-wide system of Satellite Tracking and Data Acquisition Network (STADAN) stations. Telemetry data signals and time data are recorded on separate tracks on analog magnetic tapes, which are subsequently shipped to the Information Processing Division (IPD) at Goddard Space Flight Center (GSFC). Range and range rate tracking data are also returned to GSFC for use in computation of spacecraft orbital parameters.

Within the IPD facility the telemetry data signals are decoded into digital form. The output raw digital data tapes are then processed through the AIMP Edit Program, the Time and Statistical Analysis Program, and the Decommutation Program (Mish and Haney, 1966) on an IBM 1410 computer. These passes generate diagnostic information on data quality, tag each telemetry sequence uniquely for the life the spacecraft, smooth and correct the ground time data using the satellite sequence clock, and generate individual experimenter tapes. The time smoothing and correction process corrects the Universal Time of each sequence recorded at the tracking stations for propagation delay time between WWV and the stations and then uses the corrected times and the sequence clock counts to generate a linear smoothing equation. The resulting adjusted time is written on the experimenter tapes.

The experimenter tapes provide each experimenter with the measurements performed by his experiment on board Explorer 33 as a function of Universal Time, as well as solar aspect and spin period data, data quality indicators or

flags, and experiment housekeeping information. Separate trajectory tapes are generated from the tracking data and are also provided to the experimenters. These contain spacecraft position and orientation as functions of Universal Time at five minute intervals.

Upon receipt from the IPD the GSFC magnetic field experimenter tapes are initially subjected to a calibration analysis. A data tape is scanned for calibration and sensor reorientation (flip) events. These occur at uniform multiples of telemetry sequence clock counts. Calibrations occur at intervals of 512 sequences (twice daily) and reorientation or flips at intervals of 1024 sequences (once daily). Around these events the 16 data values in each telemetry sequence from each of the sensors in the plane of rotation are fitted by a least squares technique, and the DC level, amplitude and phase of the fitted cosine wave as well as the root-mean-square error of the best fit are obtained. This technique is described in detail in Appendix A.

The DC levels for each sensor are averaged to provide a daily zero level for that sensor. This information is used in the subsequent analysis of the magnetic field data. The zero levels determined in this manner are accurate to within ±0.2 gammas.

The least squares method breaks down when the sampling period is an integral multiple of the spin period of the satellite. During the week of October 22-28 the spin period passed through a value of 2.5566 seconds which is exactly half the sampling period. The least squares fit results were completely

spurious for that week and for the week on each side the RMS deviations of the fit were on the average greater than those computed prior to that three week interval by as much as an order of magnitude. Interpolated zero levels were used for those three weeks. The zero levels changed by no more than 0.2 gamma across that interval.

A check on the sensitivities of the sensors is obtained from the fit to the data around the time when the calibration currents are on at the sensors. The difference in the DC level when the current is on provides an incremental magnetic field and hence a measure of the sensitivity.

Both the magnetic field experimenter tapes and the trajectory tapes are inputs to the Phase I Data Analysis Program (PDAP) which runs on the IBM 7040/7094 Direct Coupled System (DCS) at the GSFC. This program performs the following operations on the data:

(1) The zero levels and the slopes of the calibration curves for each sensor are used to convert the data from engineering units to magnetic field units (gammas).

(2) Magnetic field magnitudes are computed from each of the set of outputs (D_1, D_2, D_3) from the three sensors using

$$F = \sqrt{D_1^2 + D_2^2 + D_3^2} \ .$$

(3) The field component data are transformed from the triaxial sensor frame of reference to a reference frame $(X, Y, Z)_A$ that rotates with the spacecraft but is stationary with respect to sensor reorientation (see Fig. 10).

(4) The data are further transformed from the rotating frame of reference to a fixed, payload reference frame $(X, Y, Z)_p$. The payload frame is a right-handed coordinate system defined such that the Z_p axis is colinear with the spin axis of the satellite and positive above the spacecraft. The mutually perpendicular X_p and Y_p axes lie in the equatorial plane of the spacecraft, with the X_p axis always in the plane defined by the satellite-sun vector and the spin axis.

(5) The next transformation rotates the data from the payload reference frame into the previously defined (see Fig. 2) solar ecliptic frame, which is the most meaningful coordinate system for studying interplanetary phenomena.

(6) The payload field components are also rotated into the solar magnetospheric coordinate system, which is useful in studies of the geomagnetic tail. This earth-centered right-handed system of coordinates is defined such that the X_{SM} axis always points toward the sun, the Z_{SM} axis is directed so that the $X_{SM} Z_{SM}$-plane always contains the geomagnetic dipole axis, and thus Y_{SM} is always orthogonal to both the earth-sun line and the geomagnetic dipole axis.

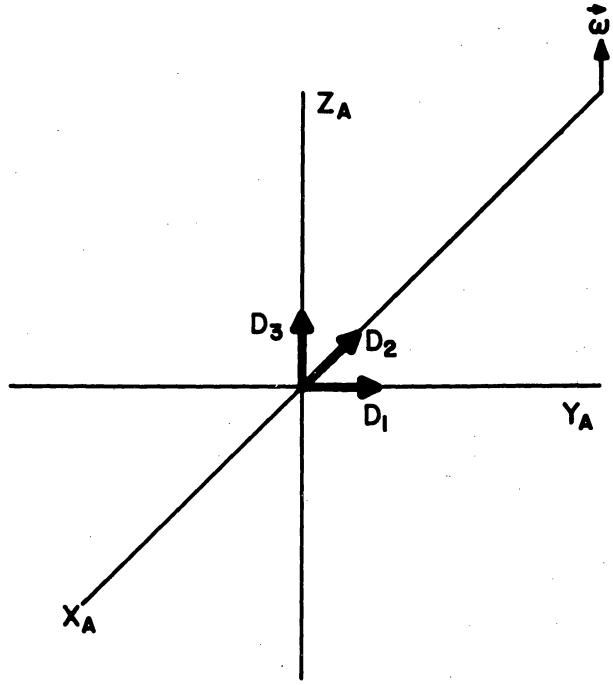

NORMAL POSITION

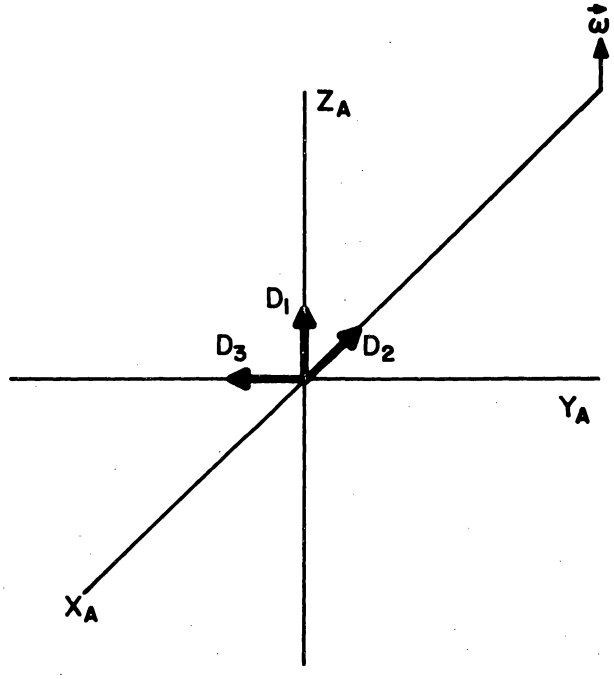

FLIPPED POSITION

TRIAXIAL SENSOR REORIENTATION

Figure 10–Orientation of magnetometer sensors relative to spacecraft spin axis before and after reorientation.

The rotation matrices utilized in each of the above transformations are given in Appendix B. The computation of the angle of rotation from spinning to fixed coordinates is also described, including the compensation for phaseshift (see Fig. 8).

The PDAP further computes sequence averages of the magnetic field magnitude and of the vector components in each of the reference frames. These are linear averages over the 16 or less individual magnitude or component values present in each 81.808 second telemetry sequence. Occasionally data values are missing because of telemetry signal noise. These are replaced by 9999 on the experimenter tape. For each average value that is computed for the total field or field component, the corresponding root-mean-square deviation over the telemetry sequence period is also computed, using the average and the N good data values, according to the relation

$$\mathrm{BRMS} = \sqrt{\frac{1}{N} \sum_{i=1}^{N} (B_i - \bar{B})^2} \ .$$

These deviations are measures of the high frequency fluctuations of the field.

Other diagnostic quantities which are computed are:

(1) Total field ratio,

$$\mathrm{FRATIO} = \frac{\text{sequence total field RMS deviation}}{\text{sequence average total field magnitude}} ;$$

(2) Component ratio,

$$\text{CRATIO} = \frac{\text{BRMS}(X_{SE}) + \text{BRMS}(Y_{SE}) + \text{BRMS}(Z_{SE})}{3\sqrt{\overline{BX}_{SE}^{\,2} + \overline{BY}_{SE}^{\,2} + \overline{BZ}_{SE}^{\,2}}} .$$

$\overline{BX}_{SE}$ is the sequence average of the solar ecliptic X component of the field and $\text{BRMS}(X_{SE})$ is the corresponding sequence root-mean-square deviation. More will be said about these ratios in the discussion of experimental results.

The sequence average solar ecliptic field components are also used to compute the orientation of the magnetic field vector in terms of the solar ecliptic azimuthal and latitudinal angles ϕ_{SE} and θ_{SE}. These are given by

$$\phi_{SE} = \tan^{-1}\left(\frac{\overline{BY}_{SE}}{\overline{BX}_{SE}}\right),$$

$$\theta = \tan^{-1}\left(\frac{\overline{BZ}_{SE}}{\sqrt{\overline{BX}_{SE}^{\,2} + \overline{BY}_{SE}^{\,2}}}\right) .$$

The Explorer 33 trajectory tapes include spacecraft positions in both solar ecliptic and solar magnetospheric coordinates at five minute intervals. The PDAP linearly interpolates between these five minute positions to obtain the corresponding position of the satellite for each set of sequence average data.

The final function of the program is to generate binary summary tapes containing all of the computed 5.11 second and sequence average data. These tapes

then serve as inputs to all other analysis programs as well as to plot programs which write tapes for E.A.I., Gerber and Calcomp Automatic Data Plotters.

An error analysis has been performed to investigate the propagation of errors through the series of transformations used in the PDAP. The details of this analysis are presented in Appendix C. As stated in Section III, the quantization error of measurement of the field is ±0.25 gamma on each axis. This is the initial error in each component in the rotating frame of reference.

It is found that, on the average, the error in the field magnitude is no greater than that in each individual component (±0.25 gamma). When the data are rotated into the fixed payload reference frame, the errors in the equatorial plane components then also include the effect of the small uncertainty in the rotation angle and in addition are directly proportional to the field strengths being measured. For the range of magnetic field magnitudes observed by Explorer 33, from less than one gamma on each axis to nearly 64 gammas on each axis, the errors in the payload equatorial plane components BX_p and BY_p range from ±0.25 gamma to ±0.40 gamma. Because it is not effected by the transformation, the error in the spin axis component BZ_p remains a constant ±0.25 gamma.

It is further found in the error analysis that the additional transformation into solar ecliptic or solar magnetospheric coordinates does not introduce any significantly large additional errors if the spin axis orientation angles in those reference frames are accurate to within ±0.1 degree. Then the errors in the solar ecliptic components $(BX, BY, BZ)_{SE}$ are approximately equal to the errors

in the BX_p and BY_p components over the observed range of field intensities, and hence for initial component errors of ±0.25 gamma the solar ecliptic and solar magnetospheric field components are accurate to within ±0.5 gamma, even in the strongest fields encountered by Explorer 33.

Up to this point it has been assumed that no errors are introduced into the data in the conversion from engineering units to magnetic field units. For the ith component this conversion has the form

$$B_i \text{ (gammas)} = [B_i \text{ (e.u.)} - Z_i]\, S_i ,$$

where Z_i is the zero level for the ith component in engineering units and S_i is the slope of the linear part of the calibration curve for that sensor (which is valid over the range of field magnitudes being measured).

As can be seen an error in the slope would produce an error in the converted data which is directly proportional to the component magnitude being converted. An example of the generally good agreement between the results of the in-flight calibration checks and the laboratory and test coil facility calibration of the sensors is shown in Fig. 11. The difference between the output of one of the sensors when the calibration current is on and when it is off is shown as a function of the component of the field being measured. In this case it is the component parallel to the spin axis. The component magnitudes are in units of counts (engineering units) and are sequence averages. The constant value of the difference over the range of observed field strengths is seen to justify the assumption of a linear sensitivity.

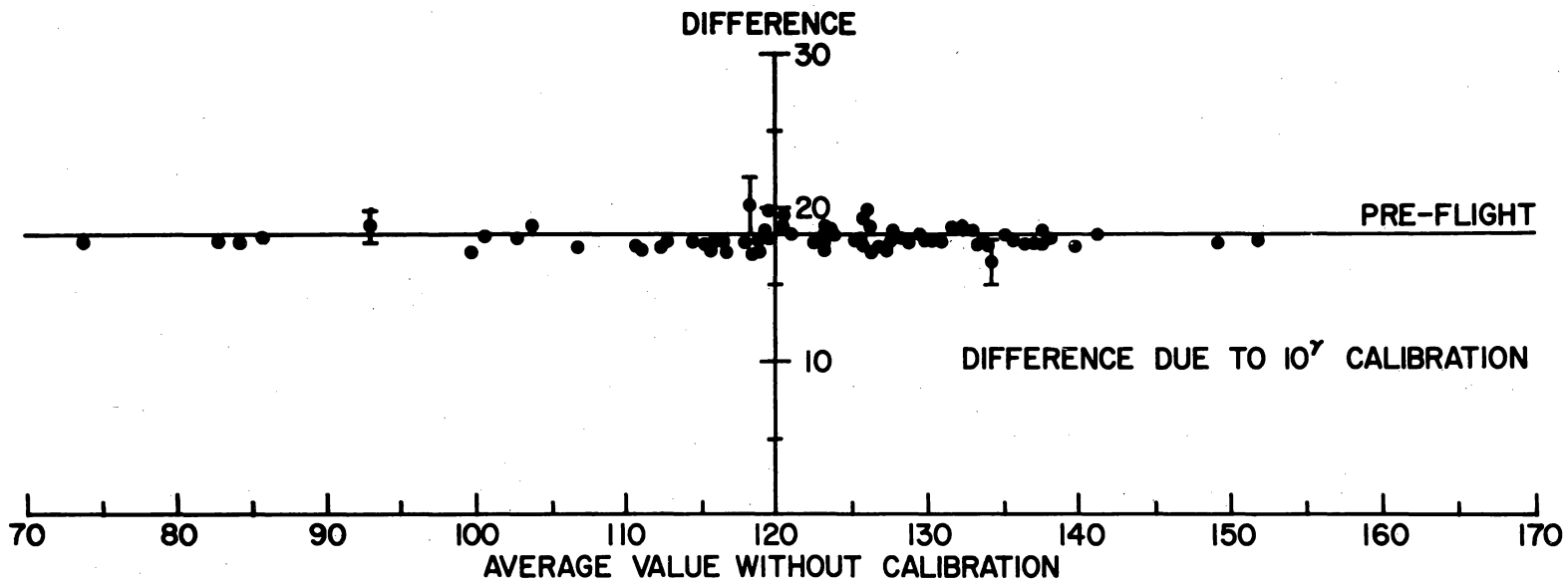

Figure 11–Example of magnetometer sensor in-flight sensitivity calibration results.

For a 10 gamma calibration field the pre-flight difference measured was 18.2 counts for the spin axis sensor. The average difference for 86 in-flight calibration events was 17.9 ±0.7 counts. This leads to an error in slope of ±0.022 gammas/count. Similar results are obtained for the other two sensors. It can be seen that the pre-flight difference falls well within the in-flight difference limits. The pre-flight slopes have been used in the conversion of all of the measurements performed during the period discussed by this thesis.

An uncertainty in the zero levels of ±0.2 gamma has been stated previously. The zero level and slope errors combine to produce a resultant error of conversion that ranges from ±0.3 gamma to ±2.8 gammas for fields ranging from 6 gammas to 64 gammas. The errors in the payload components and hence also in the solar ecliptic components are then determined almost entirely by the ±5% conversion uncertainty and will increase as the ambient field magnitude increases. However, since Explorer 33 spends better than 90% of its time measuring magnetic fields of total magnitude ≤ 15 gammas, the errors in the solar ecliptic and solar magnetospheric components generally will be within ±0.5 gamma for at least 90% of the data.

An error in zero level results in not being able to remove all of the spin modulation from the data values after the conversion. This may be seen as follows:

Let $B_\perp$ be the component of the ambient magnetic field in the equatorial plane of the satellite, separated from the X_p axis by an angle Ψ. Then if

at a given time t there is an angle ωt between the $(X, Y)_p$ axes and the rotating $(X, Y)_A$ axes and there are small errors δx and δy in the zero levels of the sensors in the plane of rotation, then the transformation to the payload reference frame has the following result:

$$\begin{bmatrix} BX \\ BY \end{bmatrix}_p = \begin{bmatrix} \cos \omega t & -\sin \omega t \\ \sin \omega t & \cos \omega t \end{bmatrix} \begin{bmatrix} BX \\ BY \end{bmatrix}_A$$

$$= \begin{bmatrix} \cos \omega t & -\sin \omega t \\ \sin \omega t & \cos \omega t \end{bmatrix} \begin{bmatrix} B_\perp \cos (\Psi - \omega t) + \delta x \\ B_\perp \sin (\Psi - \omega t) + \delta y \end{bmatrix},$$

or

$$BX_p = B_\perp \cos \Psi + \delta x \cos \omega t - \delta y \sin \omega t$$

$$BY_p = B_\perp \sin \Psi + \delta x \sin \omega t + \delta y \cos \omega t.$$

This demonstrates that time-varying components may exist in the payload and other fixed magnetic field components if either or both of δx and δy are non-zero. Further, this variation will be at the spin frequency of the satellite.

The sampling theorem of information theory (Goldman, 1953) states that if a function G(t) contains no frequencies higher than W cycles per second, then it is completely determined by giving its ordinates at a series of points spaced $1/_{2W}$ seconds apart, the series extending throughout the entire time domain. Conversely any frequencies in data sampled at a given rate that are greater than half the sampling frequency will produce a stroboscopic phenomenon referred to

in digital data sampling as aliasing. Hence any periodic variation in the field measurements beyond the cutoff or Nyquist frequency, defined by

$$F_c = F_{s/2} = 1/2\Delta T,$$

will be aliased down into the portion of the spectrum below the cutoff frequency.

The zero levels can be determined to better than ±0.2 gamma. This is below the digitization noise level of ±0.25 gamma and hence in the time domain this nonrandom oscillation in the data is not detectable. If frequency spectra are computed using these data, then even with a very minute amount of energy in this oscillation it may produce a peak above the noise. For example, a spectral peak of width (3 spectral estimates) (.01 cps) = 0.03 cps produced by a total zero level error of 0.1 gamma would reach a power level of

$$\frac{(.1)^2}{.03} = .33 \frac{\text{gamma}^2}{\text{cps}},$$

which is well above the noise level of between 10^{-2} and 10^{-3} $\text{gamma}^2/\text{cps}$ to be expected in these spectra.

During the first 19 weeks that Explorer 33 was in orbit the spin period ranged from 2.29 seconds to 2.58 seconds. The corresponding aliased frequencies were computed from the relation

$$F_k = 2k\, F_c \pm F_0,$$

where for a cutoff frequency of F_c, F_0 is the alias ($0 \leq F_0 < F_c$) of all higher frequencies F_k, k ranging over all positive integers. These aliased frequencies ranged from 0.0455 cps down to zero in week 18 and back up to 0.0036 cps five months after launch. Thus at least during the early weeks when the aliased frequency was closest to the cutoff frequency, spectra computed from the magnetic field data will provide a sensitive measure of any small errors in the sensor zero levels.

V. RESULTS AND CONCLUSIONS

A. GENERAL TOPOLOGY

As stated in Section I, it is the purpose of this thesis to present an analysis of the initial results from magnetic field measurements performed by Explorer 33 as it repeatedly traversed the earth's bow shock wave, magnetosheath, and magnetic tail during the five month period after launch. Specifically, the results will be concerned with the topological and temporal characteristics of the magnetic fields observed in those regions. Investigations of such details as internal shock structure and frequency spectra in the different regions are still in progress and will not be discussed.

Fig. 5 has shown that the extensive coverage of the regions of interest by Explorer 33, out to geocentric distances of greater than 80 R_E, make it well suited for investigating the topology of the geomagnetosphere and bow shock wave at large distances. This spacecraft has demonstrated that the geomagnetic tail remains well defined at geocentric distances of greater than 80 R_E downstream in the solar wind (Ness et. al., 1967). In addition it has been revealed that the earth's bow shock wave remains a well-defined surface far downstream, at least to geocentric distances as great as 75 R_E. One such distant shock wave traversal will subsequently be discussed in detail.

A shock wave is characterized by a discontinuity of plasma density and by the fact that the plasma moves through the discontinuity (neither of the plasma velocity components $\vec{v}_{n1}$ and $\vec{v}_{n2}$ normal to the shock surface on each side of the surface are zero) (Landau and Lifshitz, 1960). No change in the normal component of the magnetic field would be expected with any approximately planar discontinuity. The radius of curvature of the bow shock surface is large so that any small region of the surface is approximately planar. The theory of hydromagnetic shock fronts further requires no change in the field direction in the plane of discontinuity.

If $\vec{B}_1$ and $\vec{B}_2$ are the total vector fields on each side of the shock and $\vec{n}$ is the normal to the surface, then the tangential components $\vec{B}_{t1}$ and $\vec{B}_{t2}$ are parallel and thus the three vectors $\vec{B}_1$, $\vec{B}_2$ and $\vec{n}$ are coplanar. One would expect to observe a discontinuous change in both the total field magnitude and direction across the shock surface.

Identification of the bow shock in the magnetic field data is based principally on the observation of the discontinuity in field magnitude and an increase in higher frequency fluctuations. This change in magnitude generally occurs over an interval of time of between two and three telemetry sequences (on the order of 150-250 seconds). This traversal time reflects the combined effects of the thickness of the shock layer and the component of relative velocity (between spacecraft and shock) normal to the shock surface.

It will be shown that the shock and magnetopause boundaries move in and out due to variations in solar wind characteristics. Thus the relative velocity is determined by both the satellite velocity and the boundary velocity. The mean velocity of the boundaries in their in and out motions is greater than the normal component of spacecraft velocity, and hence multiple traversals are observed when the satellite is in the vicinity of either surface. The fluctuations always seen in the magnetic field near the shock indicate that it is a source of high frequency waves.

Fig. 12 illustrates multiple traversals of both the bow shock and the magnetopause near the bow of the magnetosphere on day 193 (July 13). The AIMP D designation in Fig. 12 is an alternate designation for Explorer 33. This figure consists of a full day of sequence average data. The two top panels show the solar ecliptic field orientation angles θ_{SE} and ϕ_{SE}. As previously defined, they are the angle between the field vector and the ecliptic plane and the azimuthal angle in the ecliptic plane, respectively.

In the lower two panels F is the 82 second sequence average field magnitude in gammas and RMS is the root-mean-square deviation of the total field magnitude over each 82 second sequence period. The magnitude scale in Fig. 12 has three ranges: 0-32 gammas, 32-64 gammas and 64-96 gammas. Universal Time (UT) is given under each panel. At the bottom of the figure the position of the spacecraft in solar ecliptic coordinates is given in units of earth radii.

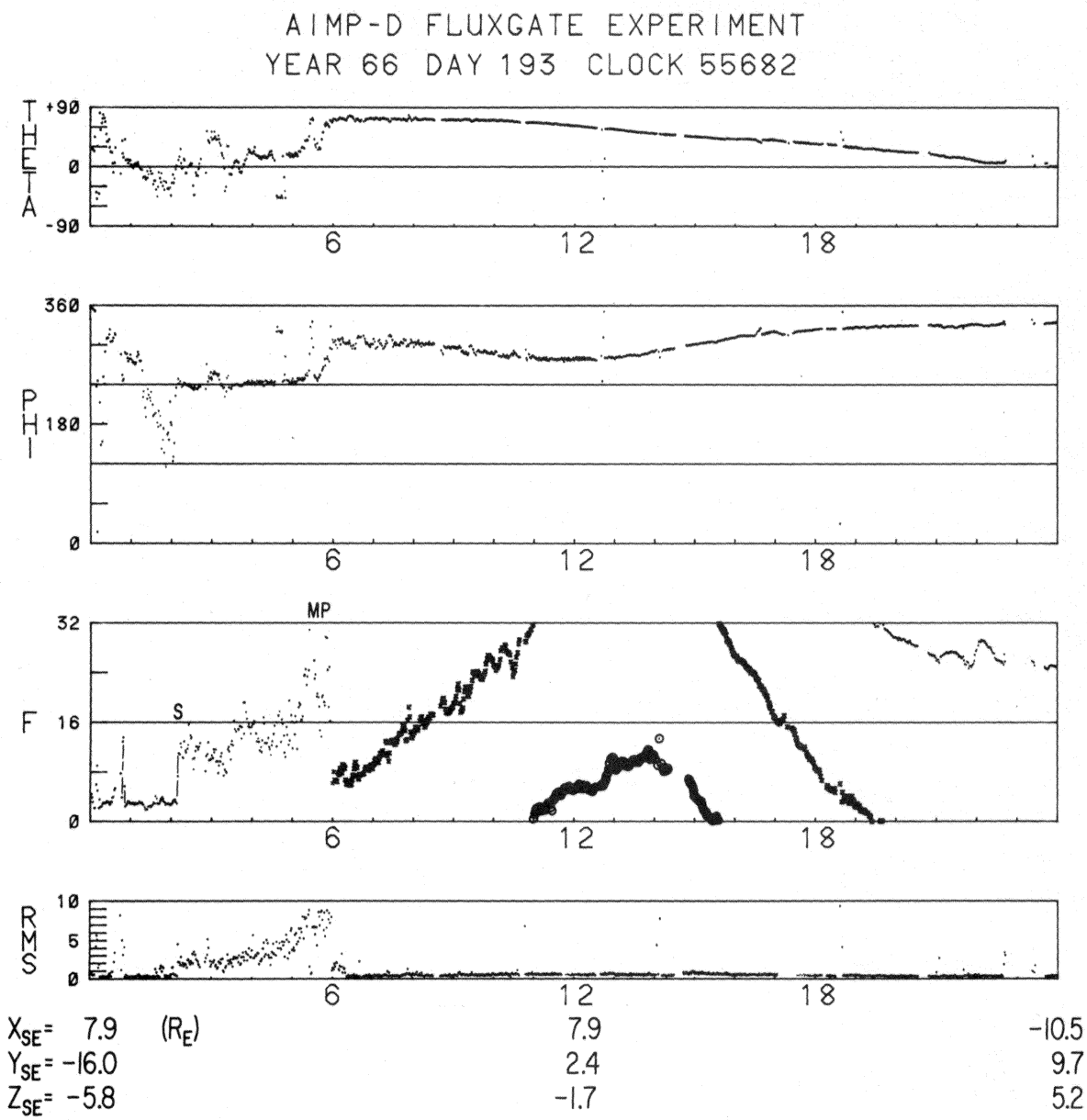

Figure 12–Magnetic field data from July 13, 1966 illustrating traversals of the earth's bow shock and magnetopause.

Dashes have been sketched in to delineate the field magnitude discontinuity at the shock, indicated by S.

The bow shock was traversed three times on day 193 and six times on the previous day. A magnitude jump of 9 gammas is seen at the final shock crossing. The azimuthal field orientation angle ϕ_{SE} is seen to become steadily aligned along a direction of 240° inside the shock. In a statistical investigation of IMP 2 magnetosheath data Fairfield (1967) has found that there is a decided preference west of the noon meridian plane for ϕ_{SE} values near 50° and 230°. This corresponds to field alignment tangent to the magnetopause as the incoming lines of force become draped around the bow of the magnetosphere. The orientation of 230° corresponds to field lines that were directed toward the sun along the spiral angle (negative sector) when in the interplanetary medium. The interplanetary magnetic field direction observed ahead of the bow shock by Explorer 33 on day 192 was that corresponding to a negative sector. Thus in this one case the observations are consistent with the IMP 2 results.

The field magnitude in the bow magnetosheath is seen to increase as the magnetopause is approached, accompanied by a steady increase in the RMS deviation of the magnitude, indicative of increasing high frequency fluctuation. The field magnitude ratio FRATIO, defined in Section IV, also increased across the magnetosheath, which means that the magnitude RMS increased at a faster rate than did the total field magnitude. The component ratio CRATIO remained relatively steady throughout the pass, however. CRATIO characterizes the level of vector field component, and hence directional, fluctuation.

Because of its motion the magnetopause was observed once briefly for approximately seven minutes some 20 minutes before the final traversal occurred. At the magnetopause the field magnitude is seen in Fig. 12 to increase to a magnitude that is approximately twice the theoretical magnitude of the undistorted geomagnetic field just inside the boundary. As can be seen the field magnitude folded over into the second magnitude range as it jumped to approximately 40 gammas at the magnetopause.

Inside the magnetopause the magnitude RMS and both ratios dropped sharply in one sequence. Then for the next 16 sequences an intermediate region was observed in which the RMS deviations and the ratios gradually decreased down to their low and steady magnetospheric levels. This is interpreted as being a region in which high frequency fluctuations inside the magnetopause are being damped out.

Large amplitude magnitude oscillations of approximately 20 minute periodicity are seen during the five hours following magnetopause traversal. This suggests that long period hydromagnetic waves were being observed in the outermost region of the dayside magnetosphere. The largest total field magnitude observed on this pass was 76.8 gammas. Although the upper limit on each sensor is 64 gammas, none of the sensors became saturated during the pass because the field was oriented at an angle of 133° to the spin axis. After traversal of the magnetopause, θ_{SE} and ϕ_{SE} show the characteristic orientation of the magnetospheric field at the position of the spacecraft for the remainder of the day.

Figure 13 illustrates multiple shock traversals observed by Explorer 33 on day 225 (August 14) along the western flank of the bow shock. Once again the characteristic sharpness of magnitude change is seen, accompanied by an increase in the root-mean-square deviation of the magnitude at the shock surface. The intervals of interplanetary data marked I correlate precisely with intervals during which solar wind plasma was observed by the Massachusetts Institute of Technology (MIT) plasma detector onboard Explorer 33 (Bridge and Binsack, 1967).

The large scale variations seen in the field orientation angles correlate with angular variations observed in the interplanetary field at this time by IMP 3. This was also found on other similar passes. Thus the general directional characteristics of the magnetosheath field near the flanks of the bow shock are determined by the interplanetary field orientation.

Multiple shock traversals along the eastern flank of the bow shock on day 307 (October 4) are shown in Fig. 14. As can be seen the spacecraft was more than 26 R_E further downstream and was further below the ecliptic plane than in the case shown in Fig. 13. The total field magnitude in the magnetosheath is approximately 4 gamms lower than that seen in Fig. 13, although on the average the interplanetary field is only approximately 2 gammas lower than the interplanetary field in Fig. 13. In addition the RMS deviation of the magnitude is at a low level in the magnetosheath except near the shock.

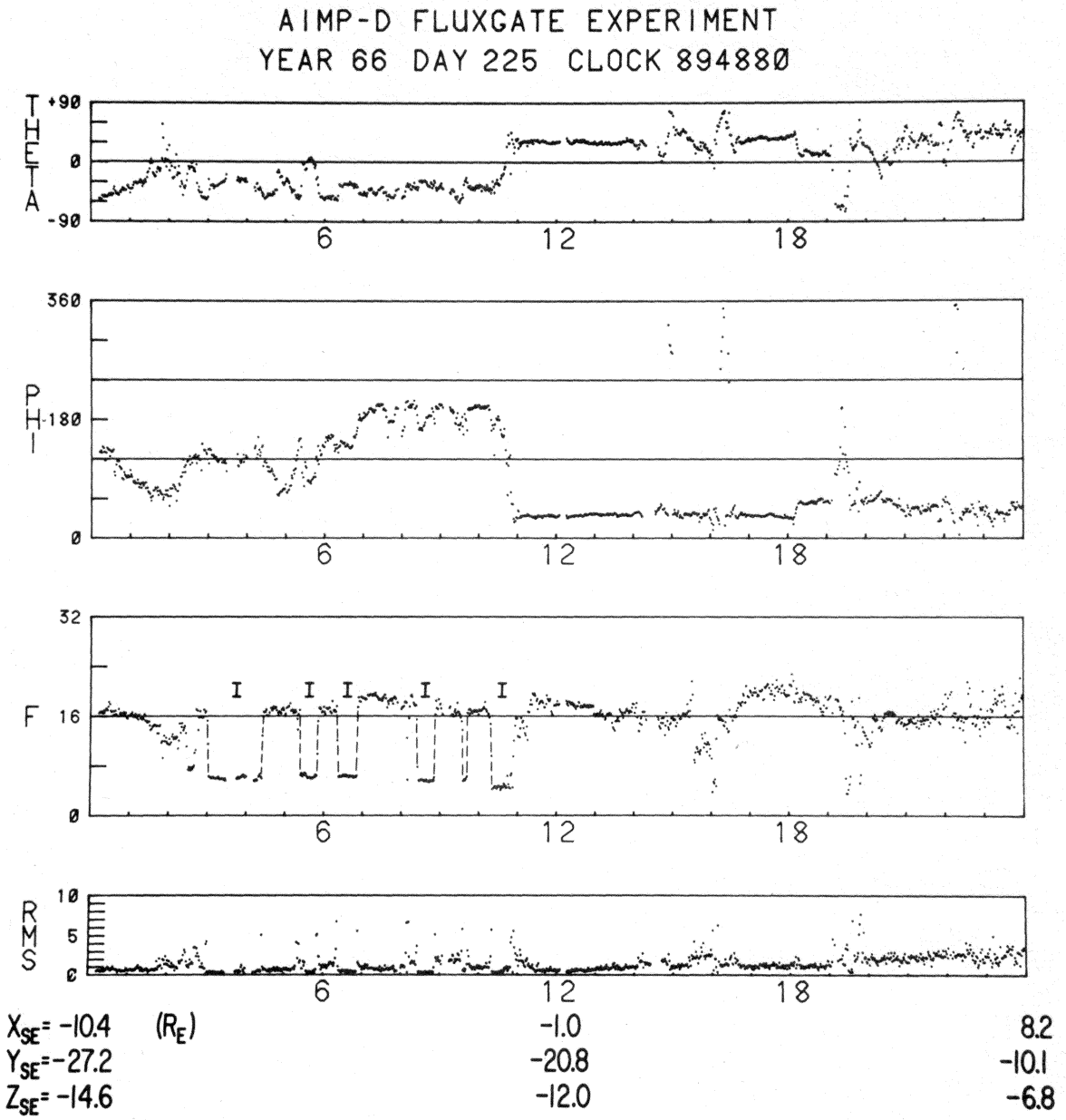

Figure 13–Magnetic field data from August 14, 1966 illustrating multiple traversals of dawn flank of bow shock.

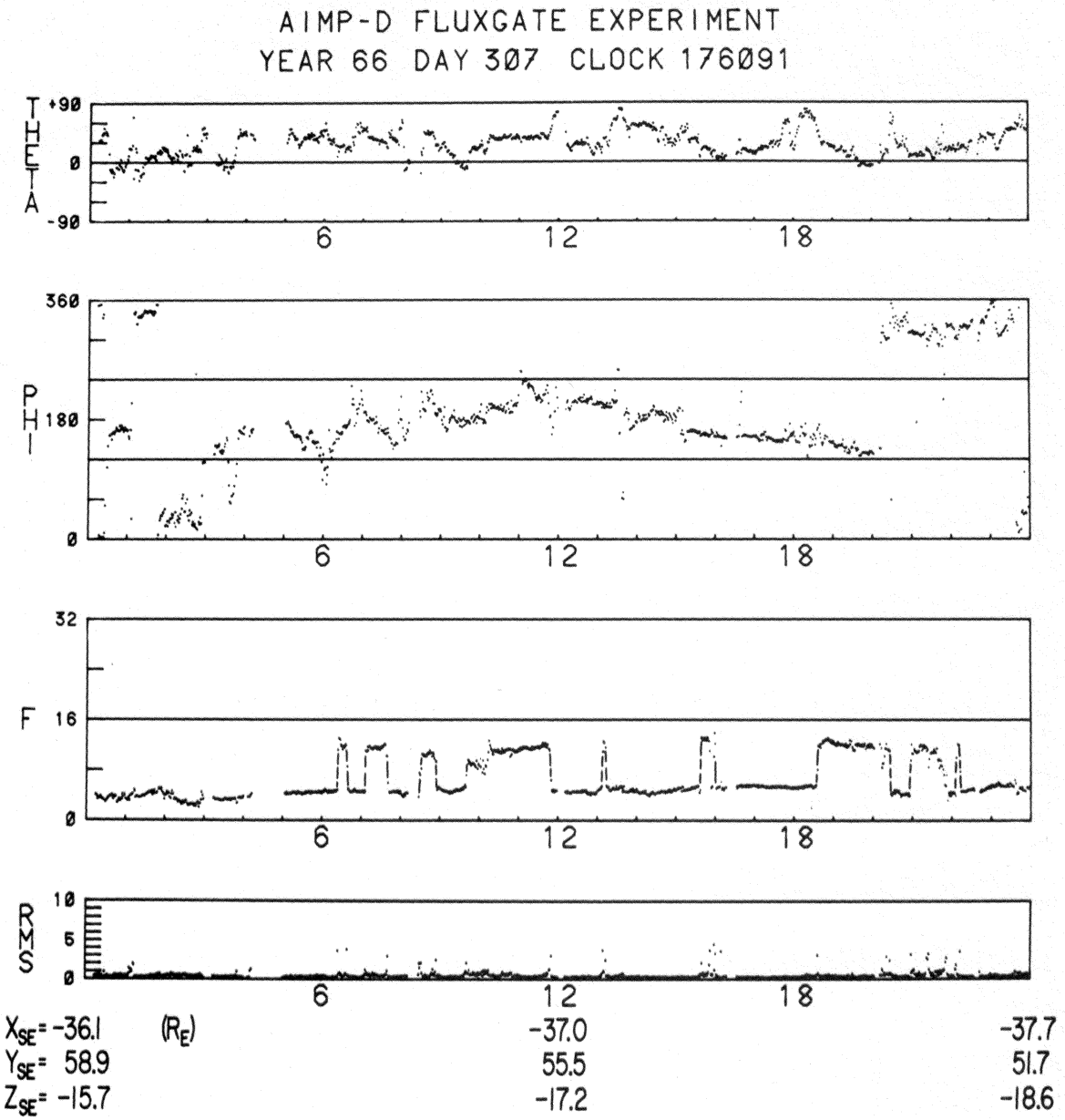

Figure 14—Magnetic field data from October 4, 1966 illustrating multiple traversals of dusk flank of bow shock.

Figure 15 shows predominantly magnetosheath data for day 291 (October 19). The spacecraft was even further downstream than in Fig. 14 and was more than 20 R_E below the ecliptic plane. During the first half of the day it was more than 25 R_E east of the noon-midnight meridian plane. The magnetosheath field is seen to be generally characterized by θ_{SE} large and negative and ϕ_{SE} roughly parallel to the interplanetary field azimuthal angle of 330° (negative sector).

Embedded in these magnetosheath data are intervals of from 1/2 hour to 2 hours of geomagnetic tail data. Thus Fig. 15 illustrates multiple magnetopause traversals along the earth's magnetic tail. As can be seen, the direction of the magnetic field vector changes relatively sharply at the magnetopause to the below-the-neutral sheet orientation of θ_{SE} approximately 0° and ϕ_{SE} approximately 180°. The field magnitude is seen to be approximately 5 gammas larger inside the tail.

Altogether 195 bow shock traversals and 136 magnetopause traversals similar to those shown in Figs. 12-15 have been found in the Explorer 33 magnetic field data between day 181 and day 342. The positions of as many of those traversals as could be plotted are summarized in Fig. 16. The traversal positions have been rotated into the ecliptic plane, and average boundary positions have been sketched in. At the bow, west of the earth-sun line, these boundaries coincide with the average IMP 1 boundary positions. Pioneer 6 and 7 traversal positions are also shown. Magnetopause traversals occurring during times when the boundary is compressed by an enhanced solar wind are marked. On the eastern flank of

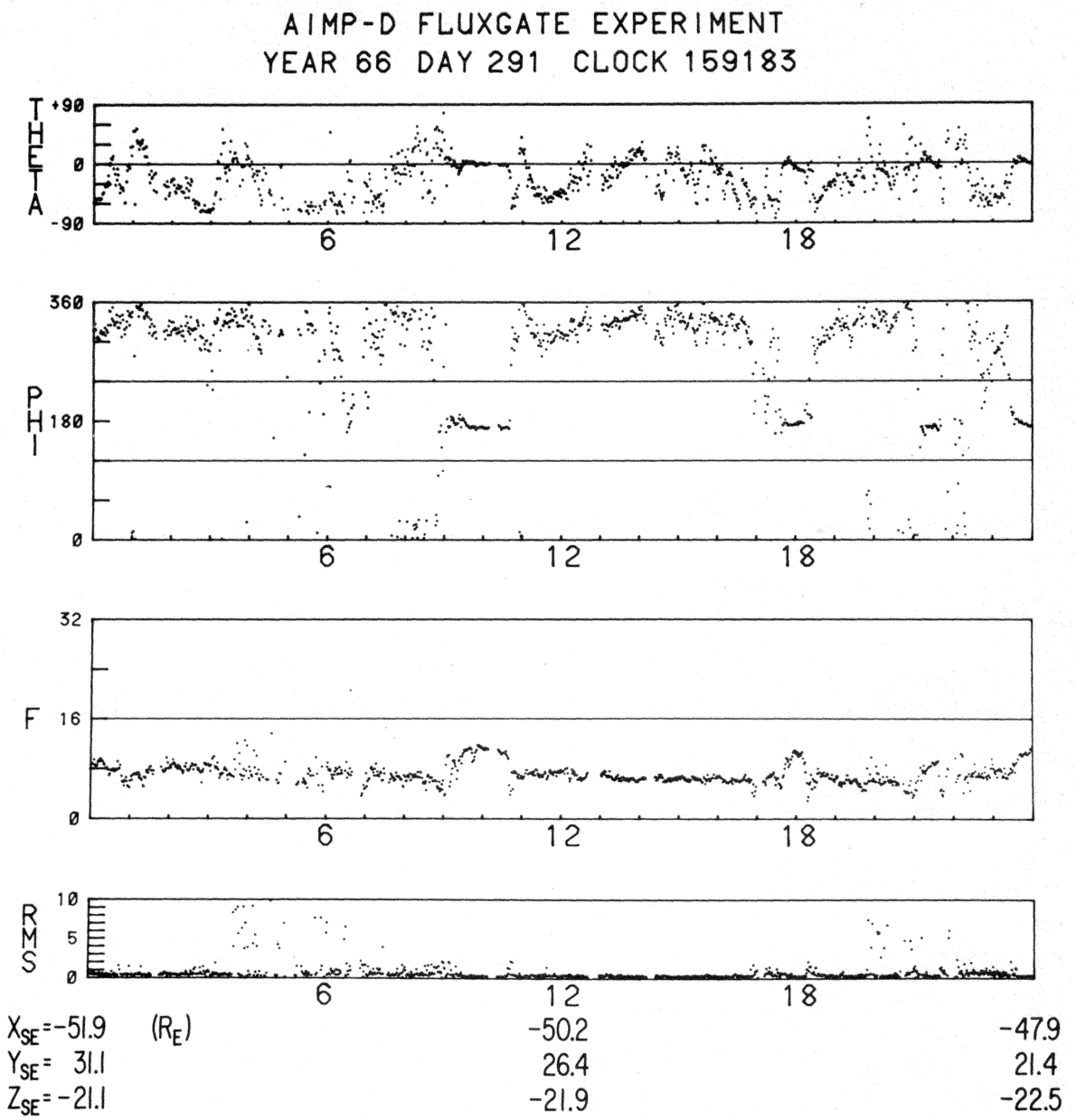

Figure 15–Magnetic field data from October 19, 1966 illustrating magnetosheath fields and multiple traversals of the tail magnetopause.

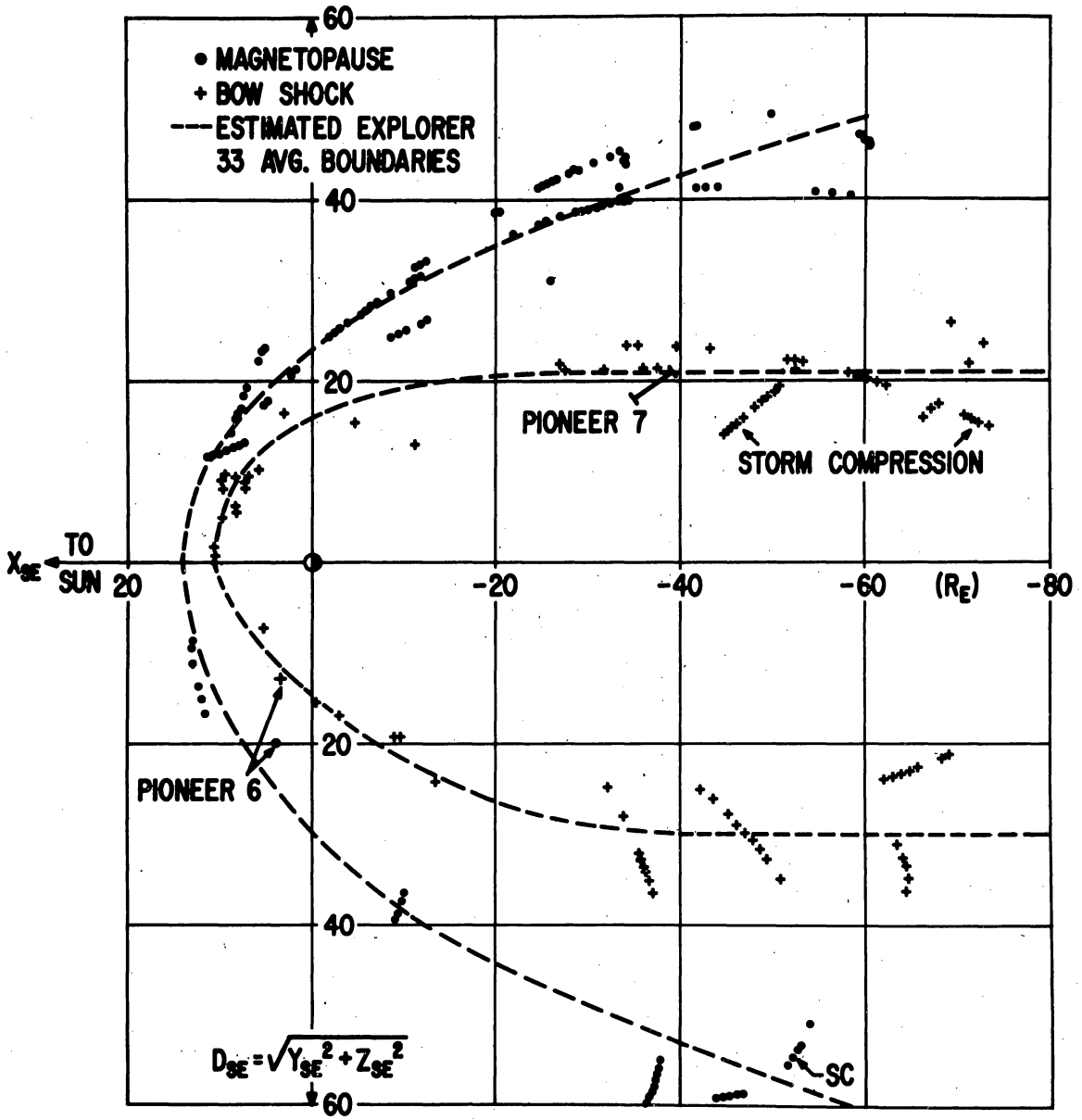

Figure 16–Summary of Explorer 33 bow shock and magnetopause traversals (rotated into ecliptic plane).

the bow shock (lower edge of the figure) an interplanetary shock wave passage that correlates with a storm sudden commencement at the earth's surface has been labeled SC.

It is immediately apparent from Fig. 16 that a much larger asymmetry of the boundaries is suggested by these data than has been found previously by other spacecraft with much more restricted coverage (Ness, 1966a). However, it must be taken into consideration that many of the eastern flank traversals were made near the time of the maximum inclination of the geomagnetic dipole axis to the noon-midnight meridian plane (autumnal equinox), as well as at increasingly greater distances below the ecliptic plane.

Viewing the geomagnetic tail from the earth, the segments of orbits 1-8 lying downstream of the earth are shown in Fig. 17, where they have been projected into a plane perpendicular to the tail axis. Also shown is a reference circle of radius 20 R_E, which would be the average position of the tail magnetopause for the case of cylindrical symmetry. The shaded region is that swept out by the estimated neutral sheet in its daily and seasonal motion during the period July through November. The lower end of each of the segments of orbits 6-8 is the inbound portion, and the large southerly latitude of those passes is clearly seen. It is significant that Explorer 33 was entering the magnetic tail on September 29-30, October 19-20, and November 7-8.

In an effort to understand the traversal data, the boundary positions were replotted in solar magnetospheric coordinates since the geomagnetic tail should

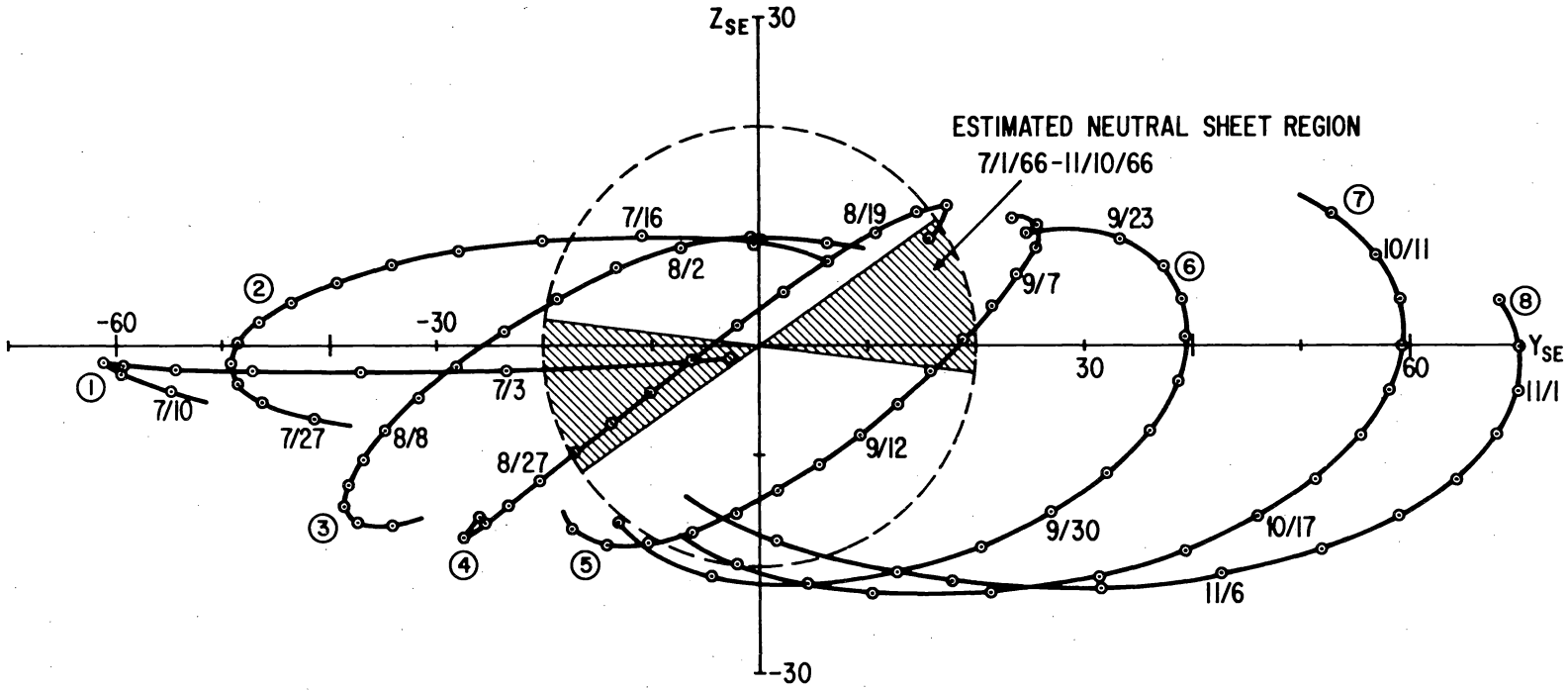

EXPLORER 33 TRAJECTORY Y_{SE}-Z_{SE} PLANE PROJECTION (X_{SE}<-15R_E)

Figure 17–View from the earth of the downstream segments of orbits 1-8 and the cross section of a cylindrical magnetic tail.

have the highest degree of symmetry in that frame of reference. Shown in Fig. 18, again looking down the tail, are cross-sectional views of boundary traversals for four different distance intervals down the tail. It is evident from this figure that the boundaries move in and out by as much as 10 R_E in response to solar wind variations. In two instances the magnetopause was compressed to within 15 R_E of the tail axis.

Ignoring those points representing large scale deformation of the tail during sudden commencement (SC) storms, the average magnetopause positions suggest a lack of cylindrical symmetry. They suggest that the tail cross-section is elongated in the direction perpendicular to the solar magnetospheric equatorial ($X_{SM} Y_{SM}$) plane. The distance from the tail axis to the magnetopause in that perpendicular direction is greater than the corresponding distance in the equatorial plane by a factor of roughly 3 to 2. Since the lines of force in the magnetic tail connect to the polar cap regions of the earth, it is not unreasonable to find that the tail is broadest in the direction parallel to the dipole axis. The shock traversal positions also suggest a lack of circular symmetry.

The average topology of the geomagnetic tail field during orbits 1-8 is shown in Fig. 19. Hourly averages were linearly computed from the 82 second sequence averages of the magnetic field components. The average solar magnetospheric components were used to plot the projection of the tail field vectors on the $X_{sm} Z_{sm}$ -plane. As many of the hourly vectors are shown as could be plotted without excessive overlapping.

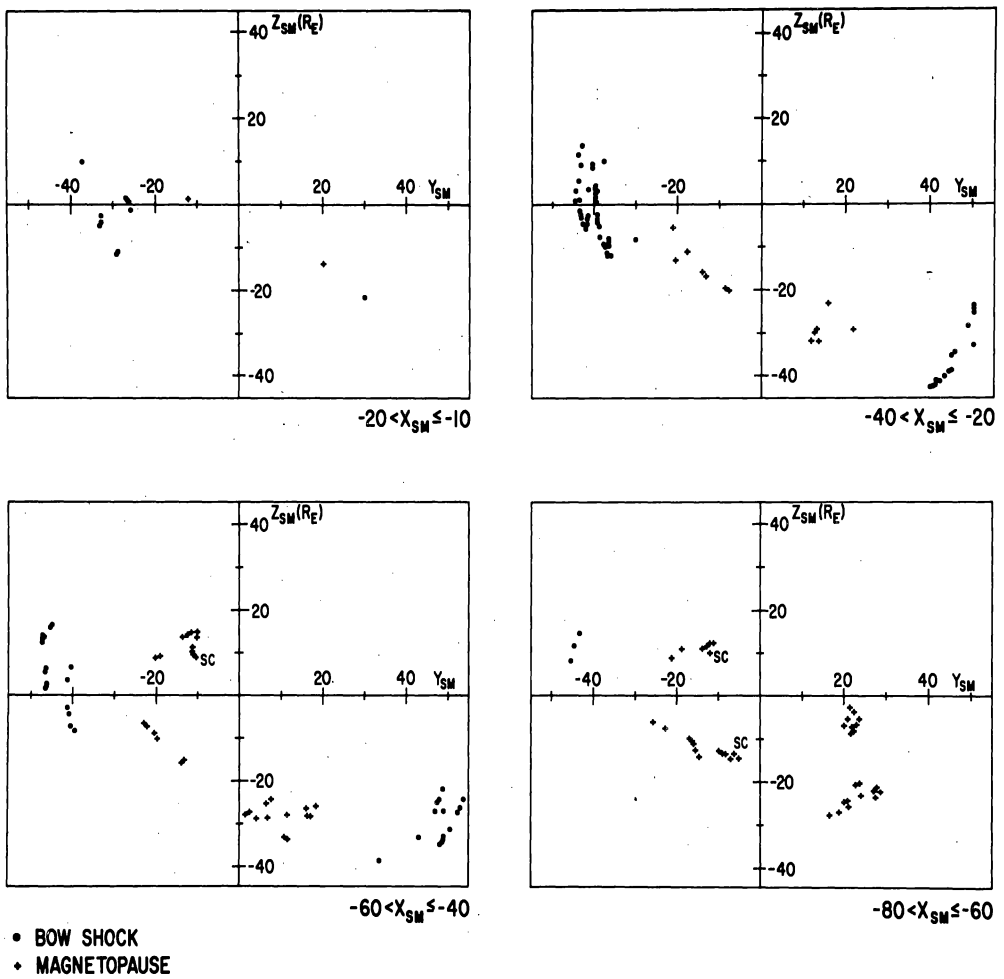

EXPLORER 33 BOUNDARY TRAVERSALS
JULY 2 - DEC. 9, 1966

Figure 18–Explorer 33 bow shock and magnetopause traversals in solar magnetospheric coordinates revealing the noncylindrical shape of the magnetic tail.

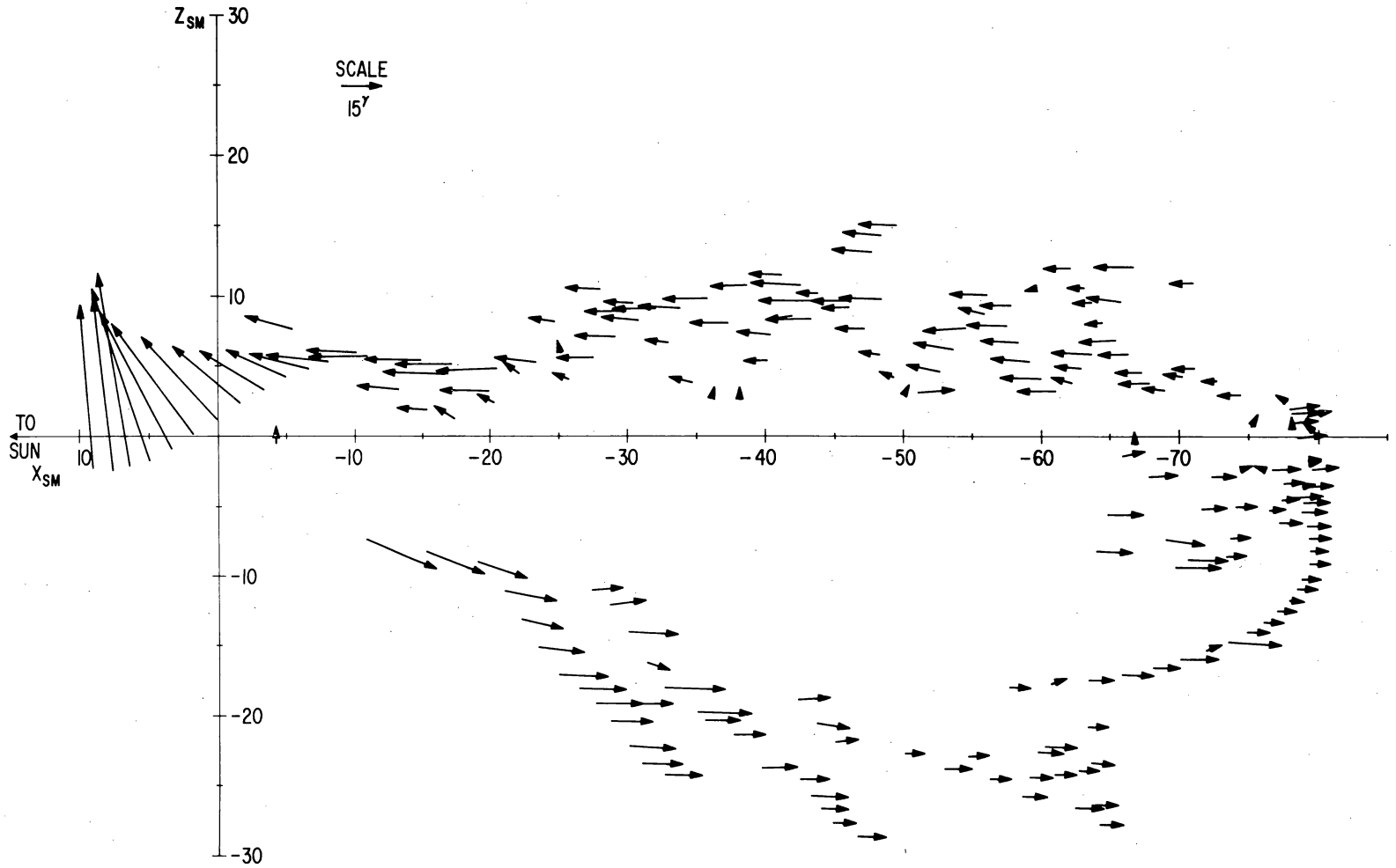

Figure 19–Average vector magnetic field topology in the geomagnetic tail during July-November 1966.

The constant antisolar orientation of the tail field below the neutral sheet with the opposite orientation above the sheet is clearly seen. The neutral sheet was generally found to lie approximately 3 R_E above the solar magnetospheric equatorial plane. Because the base of the neutral sheet lies near the geomagnetic equatorial plane (Speiser and Ness, 1967), the sheet would be expected to lie above the SM equatorial plane at the time of year that the neutral sheet was observed by Explorer 33 (August 18-26).

B. THE BOW SHOCK

The most distant bow shock traversals were observed on day 201 (July 21), when the shock surface swept past Explorer 33 a total of seven times. July 21 was classed as a magnetically disturbed day, with the planetary index K_p changing from 3- to 4- at 1800 UT (Lincoln, 1966). Fig. 20 shows one of the traversals of the shock on day 201 in detail. The spacecraft positions in solar ecliptic coordinates are given at the top. Again the two top panels are the solar ecliptic latitude and longitude angles of the 82 second sequence average field vector. $|\overline{F}| = F$ is again the linear average of the field magnitude over each telemetry sequence. In the bottom panel are plotted individual 5 second magnitudes for a time interval of approximately 8 minutes. The time interval of the other panels is approximately one hour.

In the case of this shock the magnitude jump is very sharp, going from 7.2 gammas to 15.0 gammas in 10.2 seconds. A very thin shock is suggested. The average total field vector undergoes changes of direction by approximately 16° in both θ_{SE} and ϕ_{SE} across the shock.

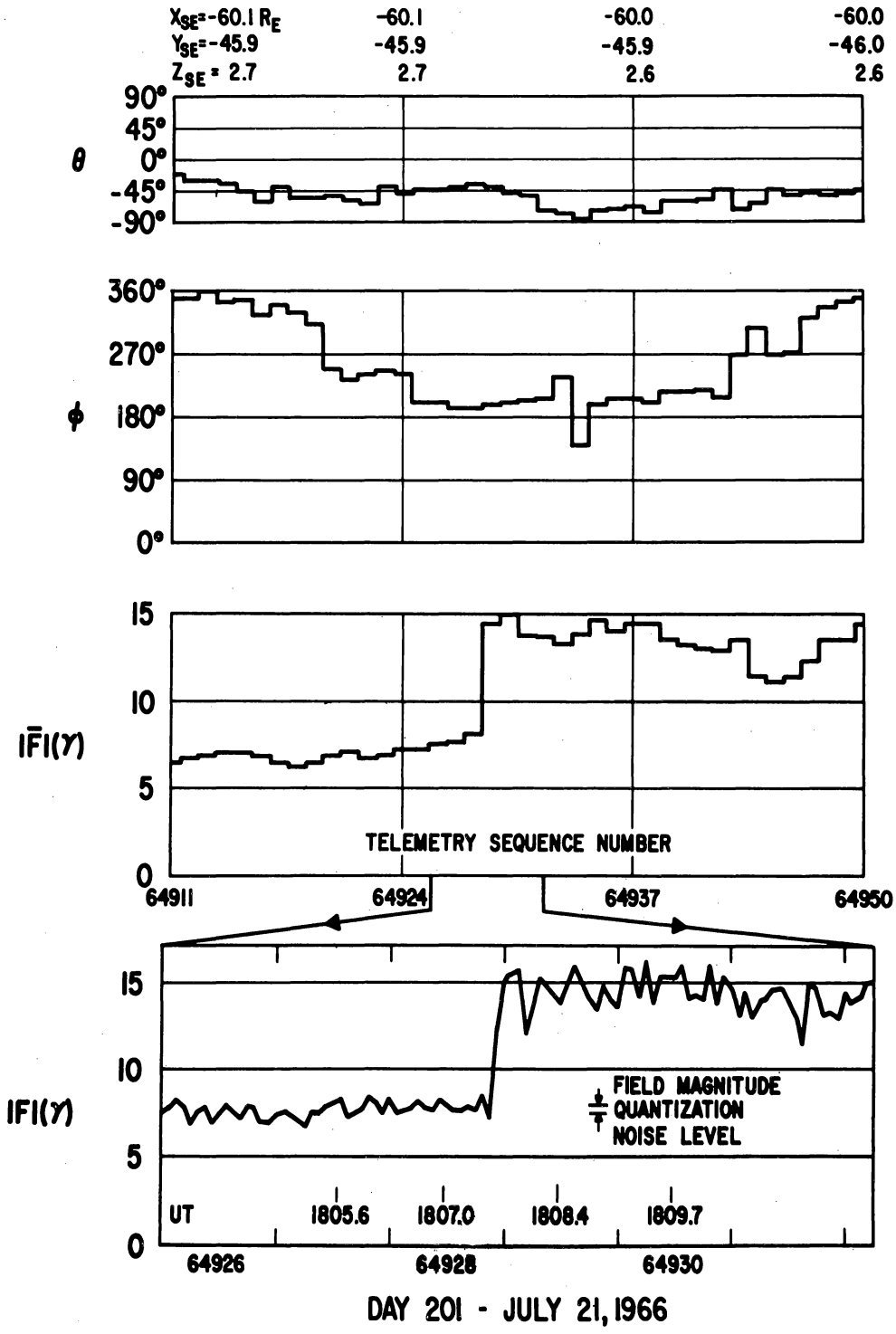

Figure 20—Detailed magnetic field data from July 21, 1966 illustrating a traversal of the bow shock at a geocentric distance of 75.7 R_E.

Changes in vector components were investigated using the shock model defined by the previously discussed coplanarity theorem. Assuming that the normal component of the magnetic field does not change as the shock is crossed and that the tangential component changes in magnitude but not in direction, then for $\vec{B}_1$ and $\vec{B}_2$ the field vectors on the two sides of the shock ($\vec{B}_2$ inside), the vectors $\vec{C} = \vec{B}_1 \times \vec{B}_2$ and $\vec{D} = \vec{B}_1 - \vec{B}_2$ are both in the shock surface. Then the normalized cross product

$$n = \frac{\vec{D} \times \vec{C}}{|\vec{D} \times \vec{C}|} \tag{1}$$

defines a unit vector normal to the shock.

Assuming that this model is valid for the bow shock, the average total field vector on each side of the shock surface can be used to compute the unit normal according to relation (1). Then the components parallel to the unit normal are given by

$$\vec{B}_{n1} = (\vec{B}_1 \cdot \vec{n})\vec{n}$$

$$\vec{B}_{n2} = (\vec{B}_2 \cdot \vec{n})\vec{n}$$

and the tangential components by

$$\vec{B}_{t1} = \vec{B}_1 - \vec{B}_{n1}$$

$$\vec{B}_{t2} = \vec{B}_2 - \vec{B}_{n2}.$$

For the shock on day 201 the tangential component was found to increase by a factor of 2.3 across the surface. The shock normal was found to be

$$\vec{n} = 0.55\,\vec{i} + 0.84\,\vec{j} - 0.05\,\vec{k} \text{ gamma}$$

in solar ecliptic coordinates. This is not in the direction expected from the orientation of the average shock shown in Fig. 16. This can be due to any or all of the following causes:

(1) the total vector field averages used did not appropriately describe the actual field vectors on each side of the discontinuity;

(2) the shock model used for computation did not accurately describe the observed shock;

(3) the shock surface was locally deformed due either to flapping or to surface waves.

This same type of shock surface analysis was applied to 40 more bow shock traversals, using total field vectors computed from components averaged over from 5 to 12 sequences. The number of sequences of data used in each case was determined by the duration of relatively steady sequence average fields on each side of the surface. The direction of the shock normal was sometimes found to be reasonably consistent with the average orientation expected for the surface. When the results were ordered according to the X_{SE} coordinate of the traversal, a relatively steady increase in the ratios

$$R_M = \frac{|\vec{B}_2|}{|\vec{B}_1|}$$

and

$$R_T = \frac{|\vec{B}_{t2}|}{|\vec{B}_{t1}|}$$

with increasing X_{SE} was found. A sample of the results typically found in this investigation are tabulated in Table 1.

Though some of the individual computed vector normals were roughly in the required direction for the expected orientation of the shock surface, many of them were not. The directions of shock normals computed for sets of multiple traversals were averaged, and in some cases this average direction was more than 30° from the required direction. Thus it is concluded that the classical "fast shock" model may not be valid for the earth's bow shock wave, although it is difficult to establish that this is so from magnetic field data alone.

It was previously stated that high frequency field fluctuations are always observed near the shock surface. A very high level of deviation was generally observed by Explorer 33 in only one telemetry sequence of data. This sequence contained the measurements made through the shock layer in each case. For 17 shock surface traversals on day 225, an average field magnitude of 11.6 gammas and an average magnitude RMS deviation of 5.16 gammas were observed

at the shock. Average values of FRATIO and CRATIO were 0.45 and 0.35, respectively. For 18 multiple traversals along the eastern flank on day 307, an average magnitude of 10.2 gammas and an average RMS of 2.88 were found. The corresponding average ratios for magnitude and components were 0.31 and 0.25, respectively. In the second case Explorer 33 was more than 30 R_E further downstream. It is seen that FRATIO > CRATIO in both cases, although they are of comparable magnitude.

TABLE 1

MAGNETIC FIELD CHARACTERISTICS AT THE BOW SHOCK

DAY	TIME	X_{SE}	Y_{SE}	Z_{SE}	R_M	R_T	n_x	n_y	n_z
201	1543	-60.3	-45.6	2.8	1.47	1.58	0.38	-0.92	-0.01
201	2300	-59.6	-46.5	2.3	1.63	2.69	0.18	-0.92	0.34
204	0701	-49.4	-49.1	- 2.2	2.04	2.12	0.99	-0.02	-0.13
205	1047	-41.1	-47.6	- 4.3	2.06	2.07	0.31	-0.94	-0.13
206	0802	-33.1	-44.9	- 5.8	2.42	2.84	0.32	-0.94	-0.13
206	1744	-28.8	-42.9	- 6.3	2.25	2.34	0.52	-0.16	-0.84
243	1246	-11.7	-22.6	-13.7	3.15	3.29	-0.51	0.80	0.31
225	0302	- 8.1	-25.9	-14.1	2.62	2.83	-0.41	0.79	0.46
225	0623	- 5.5	-24.2	-13.4	2.71	3.12	-0.68	0.62	0.40
225	0825	- 3.9	-23.1	-13.0	3.13	4.15	-0.58	0.82	-0.01
225	1020	- 2.4	-21.9	-12.5	3.90	4.40	-0.45	0.89	-0.02
193	0211	9.6	- 7.8	- 4.5	5.44	13.66	-0.83	0.23	-0.50

C. THE MAGNETOSHEATH

Magnetic measurements by Explorer 33 have shown that even far downstream the magnetosheath is characterized generally as a region of large amplitude low frequency magnetic fluctuations and small amplitude high frequency fluctuations. During magnetically quiet days (low Kp index), however, there are periods when the downstream magnetosheath is relatively quiet in terms of high frequency fluctuations. This is supported by observations of a very low level of magnitude RMS deviation for hours at a time. The magnitude ratio FRATIO is also found to be low at such times, of the order of between 0.05 and 0.08, whereas the component ratio CRATIO is often larger than FRATIO by a factor of from 2 to 4. This suggests that the high frequency fluctuations at such times are almost totally directional, and thus transverse and not longitudinal waves are present.

An example of the magnetosheath on a quiet day is shown in Fig. 21. Individual Kp indices ranged between 0 + and 1 on day 290 (October 18), with the daily sum equal to 8 (Lincoln, 1967b). The spacecraft was well downstream on the dusk side of the magnetosphere. Both the magnitude and the longitudinal angle are seen to be relatively steady throughout the day, with ϕ_{SE} roughly equal to the interplanetary negative sector azimuthal angle of 330°. θ_{SE} is seen to vary alternately between large positive and negative angles.

Fig. 22 shows the magnetosheath on a day when there was an intermediate level of magnetic activity. The spacecraft was nearer to the earth

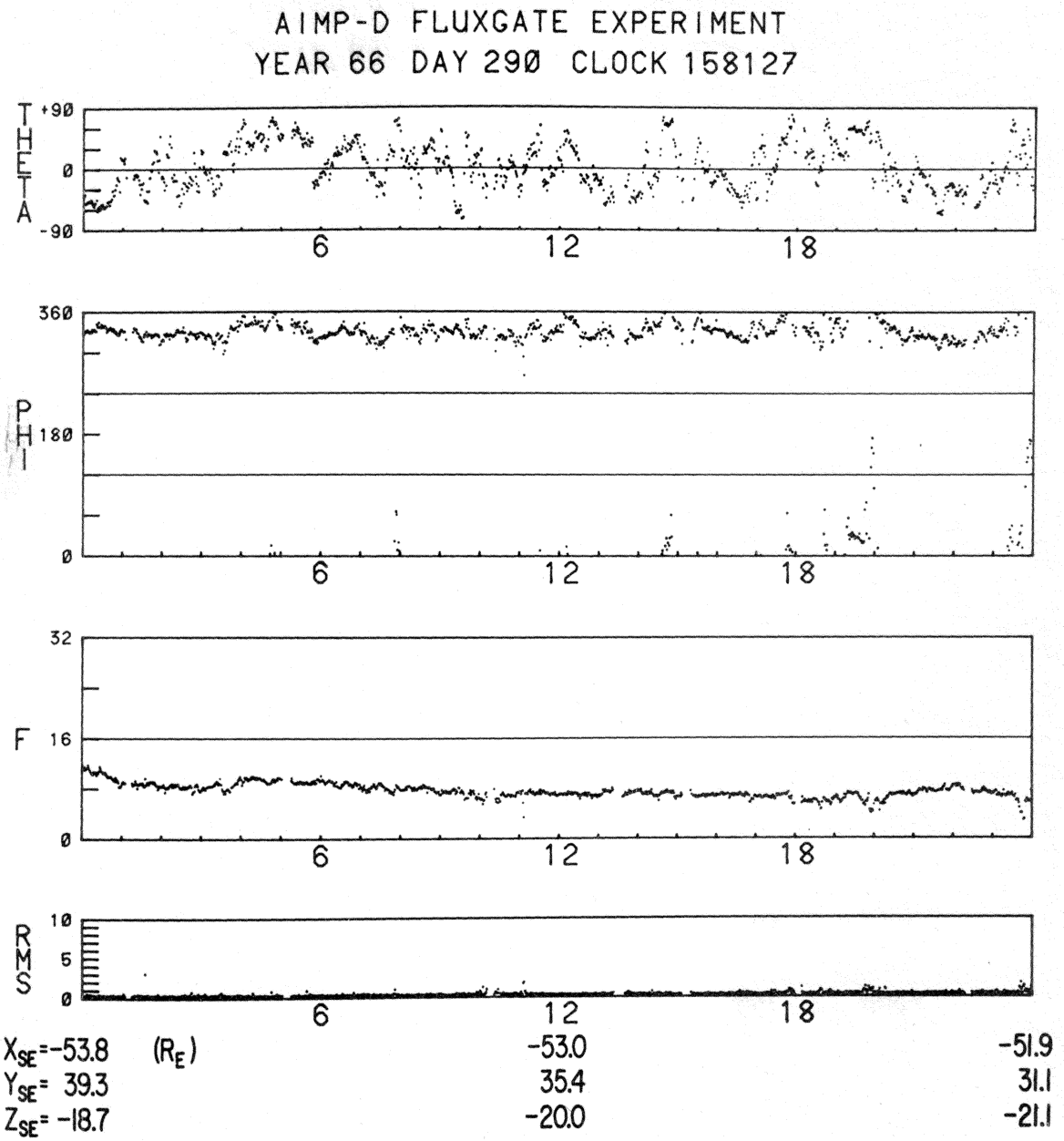

Figure 21–Magnetic field data from October 18, 1966 illustrating a quiet magnetosheath.

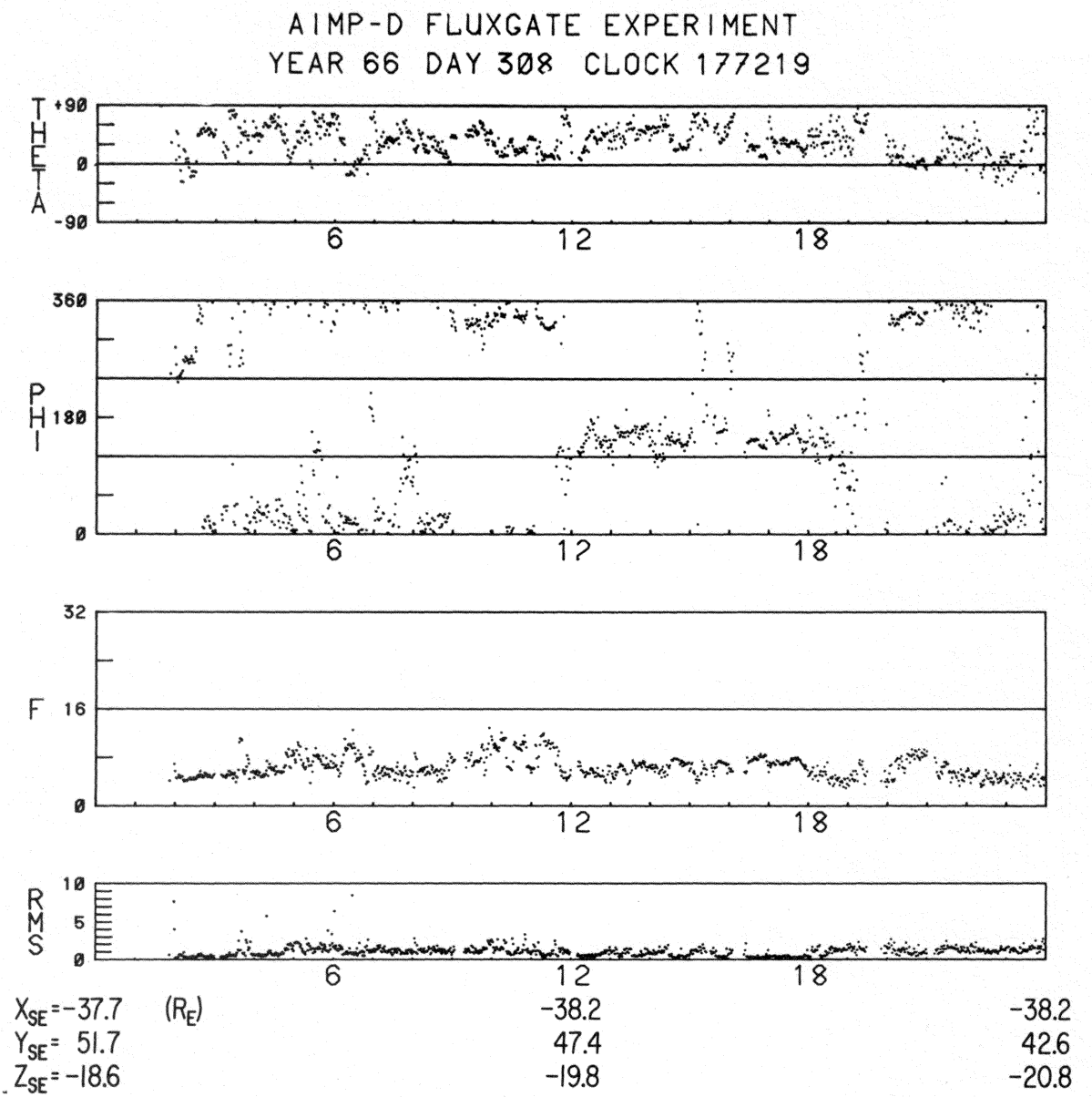

Figure 22–Magnetic field data from November 5, 1966 illustrating moderately disturbed magnetosheath.

but again on the dusk side and well below the ecliptic plane. On day 308 (November 5) the individual Kp values ranged from 1 to 3, with the daily sum equal to 17+ (Lincoln, 1967c), or more than double the sum for day 290. A moderate level of high frequency fluctuation is suggested by the magnitude RMS. From 1200 to 1800 the angle ϕ_{SE} is seen generally to lie in the positive sector direction of 150°. At other times it was along the spiral angle but toward the sun. θ_{SE} was generally large and negative throughout the day.

Fig. 23 shows data from the dawn side magnetosheath, closer to the bow, on day 277 (October 5). That day was classified as a disturbed day (Lincoln, 1967b). The Kp index ranged between 3 and 5+, with the daily sum up to 35-. This is once again double the previous value. Large amplitude fluctuations at both low and high frequencies are observed in this case. θ_{SE} is once again seen to alternate between large positive and negative values, each time remaining in one of the two directions for approximately two hours. This behavior is found to be characteristic of the downstream magnetosheath field orientation and suggests that the filamentary bundles of field lines being swept past the magnetosphere are alternately draped above and below the geomagnetic tail.

In Fig. 24 is shown the horizontal component of the geomagnetic field at the earth's surface as recorded at seven magnetic observatories on August 30 (day 241). At 1112 UT a sudden commencement magnetic storm began at the surface, and for the remainder of the day the surface field is seen to be highly disturbed. The Kp index increased from 3 to 5 for the 3-hour interval beginning at

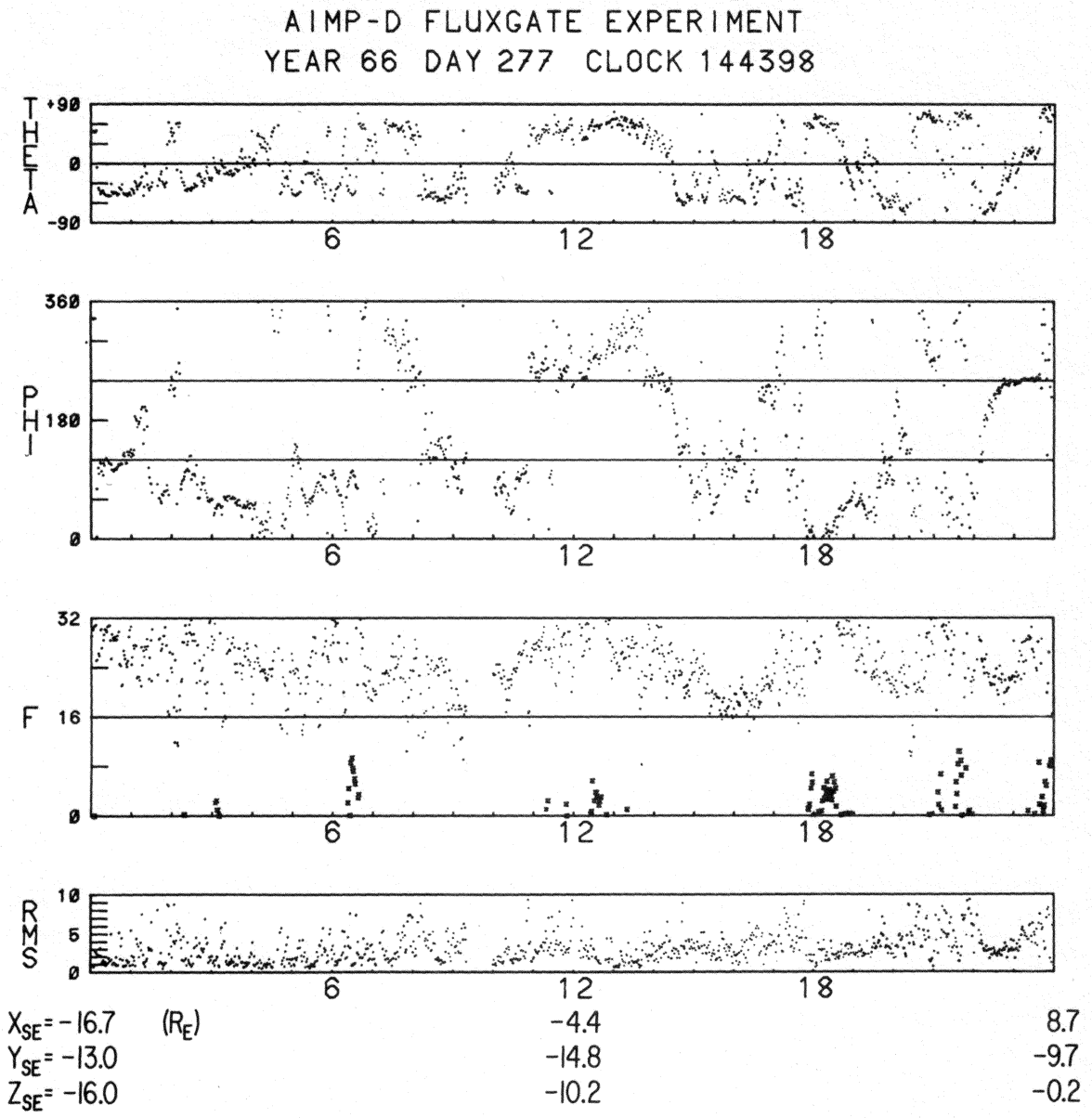

Figure 23–Magnetic field data from October 5, 1966 illustrating a highly disturbed magnetosheath.

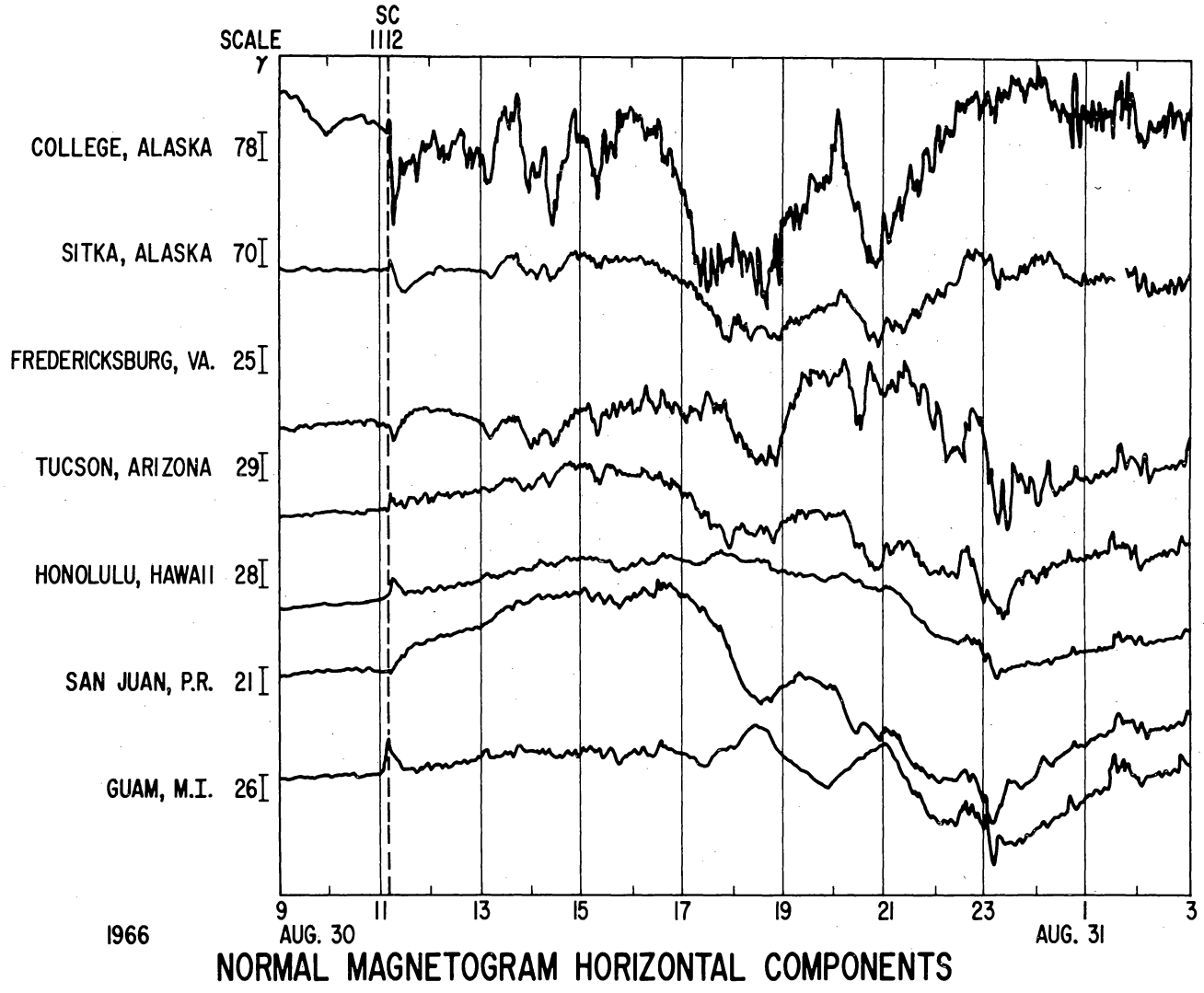

Figure 24–Regular-run magnetic observatory horizontal component magnetograms for August 30, 1966 sudden commencement storm period.

0900 and continued to increase to a maximum of 7+ during the last six hours of the day (Lincoln, 1967a). The daily sum was 45+.

The onset of that same magnetic storm in the magnetosheath is shown in Fig. 25. The field magnitude is seen to increase by approximately 28 gammas. The level of high frequency fluctuation is seen to increase with the onset of the disturbance, and large very low frequency variations are seen in the magnitude for the remainder of the day.

D. THE GEOMAGNETIC TAIL

The IMP 1 satellite established the permanent existence of the earth's magnetic tail as an important feature of the geomagnetic field (Ness, 1965). This conclusion has been substantiated by all spacecraft which have subsequently traversed the antisolar region of the distant magnetosphere. These results are supported and extended by the Explorer 33 measurements. During the first five months in orbit Explorer 33 observed a well-defined magnetic tail on each pass through that region of space, even at distances greater than the lunar orbital distance (Ness, et. al., 1967a). The average geomagnetic tail topology observed by Explorer 33 during that period was shown in Fig. 19.

During times when conditions are relatively quiet in the solar wind (as measured by Kp), the geomagnetic tail field is the steadiest magnetic field observed in space by Explorer 33. This is illustrated in Fig. 26. On day 293 (October 21) the magnetic activity index Kp ranged between 0 and 1, with a daily sum of 3- (Lincoln, 1967b). It is to be noted that the spacecraft traversed

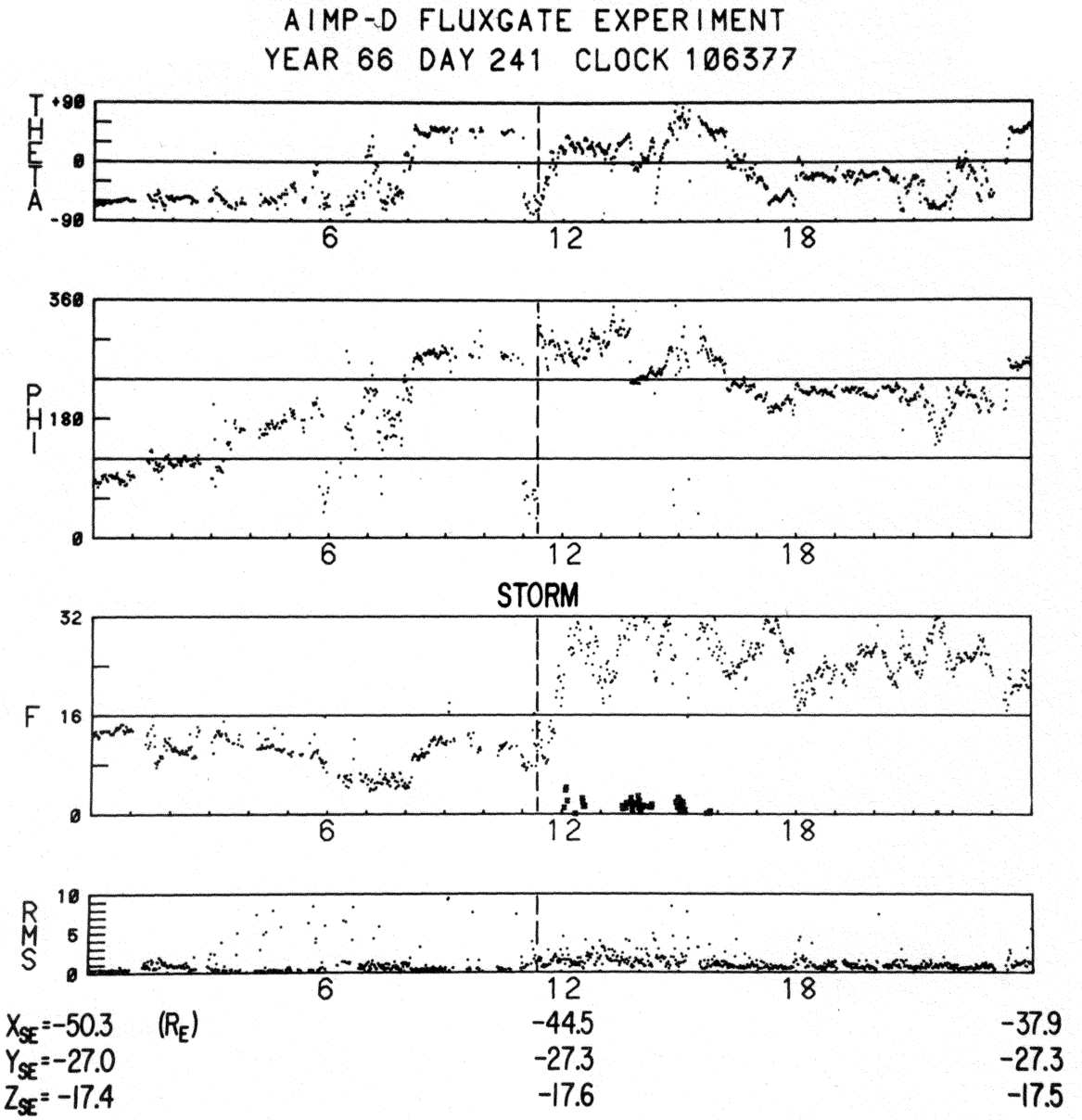

Figure 25–Magnetic field data illustrating commencement of August 30, 1966 magnetic storm in magnetosheath.

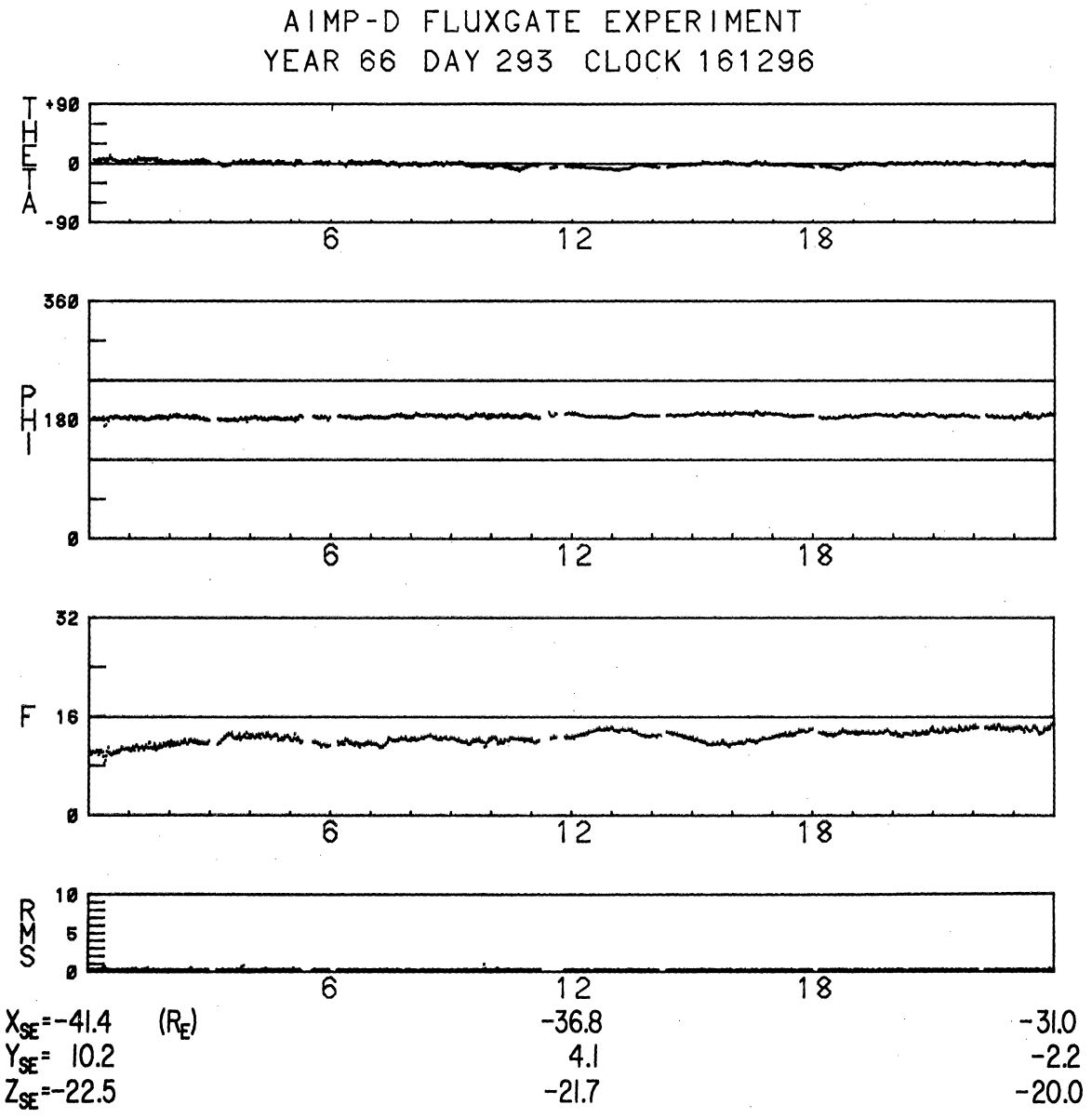

Figure 26–Magnetic field data from October 21, 1966 illustrating steady character of undisturbed magnetic tail field.

the midnight meridian plane on day 293 but remained at distances greater than 20 R_E below the ecliptic plane throughout the day.

The major types of variations observed in the geomagnetic tail field by Explorer 33 during five months in orbit were the following:

(1) temporal variations during magnetic disturbances;

(2) spatial variations associated with field reversal at the neutral sheet;

(3) a general decrease in the tail field magnitude with distance down the tail due to a magnitude gradient in the $-X_{SE}$ direction.

Each type of variations will be discussed and illustrated in turn.

Three magnetic storms occurred while Explorer 33 was in the earth's magnetic tail. These were all sudden commencement disturbances, beginning at 1500 UT on July 15, at 0003 UT on August 1, and at 1510 UT on September 14. In all cases there was a positive correlation between variations observed in the tail field magnitude and in the horizontal component of the field at the earth's surface during the compressional phase of the storms. A positive correlation was also found between the tail field magnitude and the Kp index in each case. These results are in agreement with the IMP 1 magnetic storm observations (Behannon and Ness, 1966).

The geomagnetic storm of September 14, as observed at the earth's surface, is shown in Fig. 27. Once again the horizontal component magnetogram traces from seven magnetic observatories are shown. The sudden commencement (SC) time of the disturbance onset at the surface was 1510 UT. This storm is of

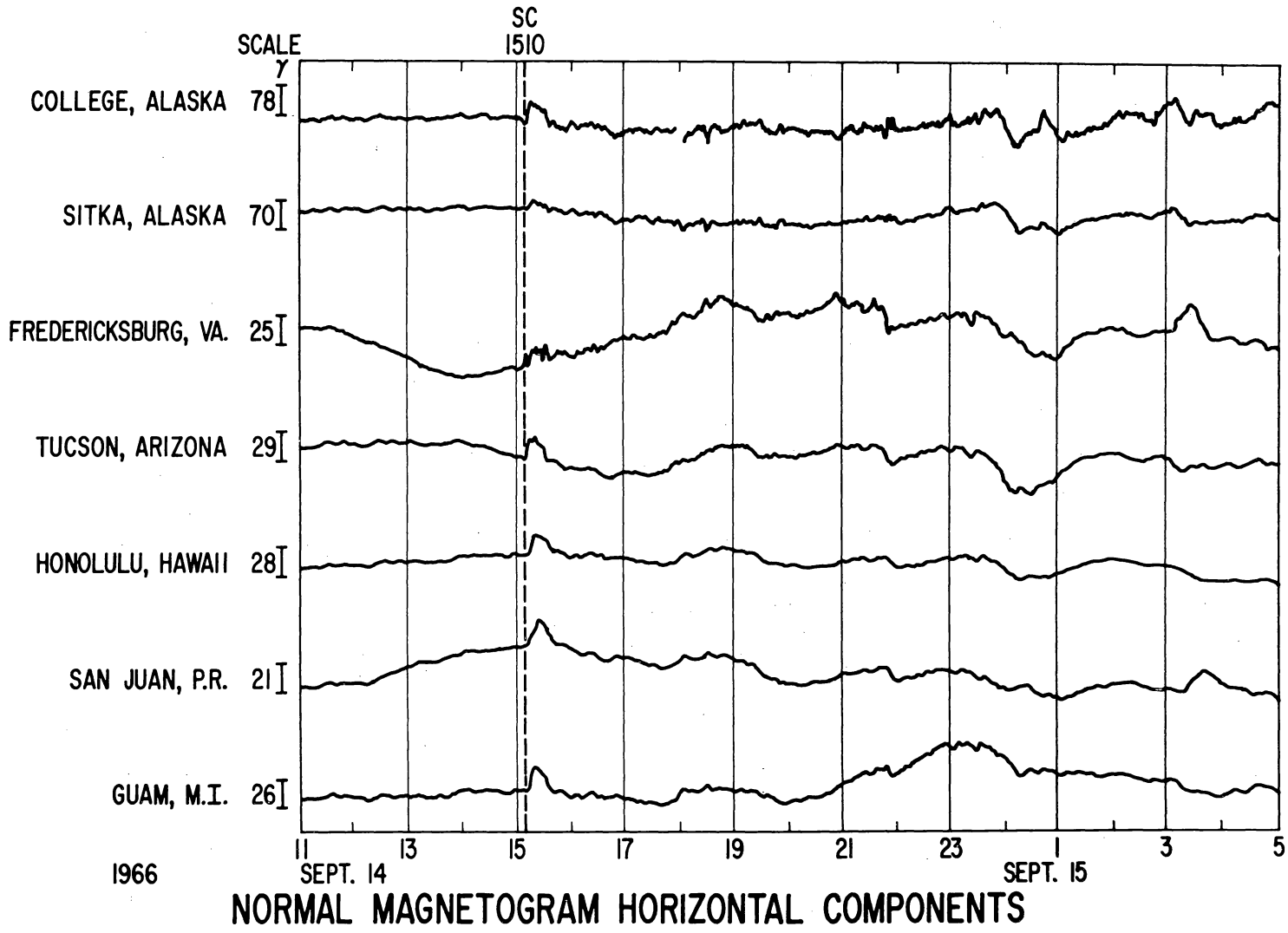

Figure 27—Regular-run magnetic observatory horizontal component magnetograms for September 14, 1966 sudden commencement storm period.

particular importance because of the unique position of Explorer 33 at the time of the storm. Figure 28 shows the projection of orbit 5 on both the noon-midnight meridian plane and the solar ecliptic plane. It can be seen that on September 14 the spacecraft traversed the midnight meridian plane at a geocentric distance down the magnetic tail of approximately 75 R_E and a distance below the ecliptic plane of approximately 14 R_E. Thus the satellite was in the magnetic tail, well beyond the lunar orbital distance of approximately 60 R_E, at the onset of this storm.

The satellite magnetic field data for September 14 (day 256) are shown in Fig. 29. The sudden commencement occurred at 1522 ± 2 UT at the spacecraft, giving a delay time of 12 ± 2 minutes. The satellite coordinates were X_{SE} = -73.8, Y_{SE} = -0.8 and Z_{SE} = -14.6. Thus the impulse propagation velocity parallel to the earth-sun line must have been 654 ± 109 km/sec. An increase of 10 gammas in the tail field magnitude occurred at the commencement of this storm. Note the magnitude fluctuations with a period of approximately 20 minutes following the SC at the satellite.

Large field variations were also observed by Explorer 33 prior to the storm sudden commencement. As can be seen in Fig. 29, the magnetic tail field was relatively steady and characteristically oriented parallel to the earth-sun line in the antisolar direction until 1009 UT. At that time a disturbance began which was characterized magnetically by angular excursions and steep magnitude decreases of between 4 and 8 gammas. The solar ecliptic coordinates

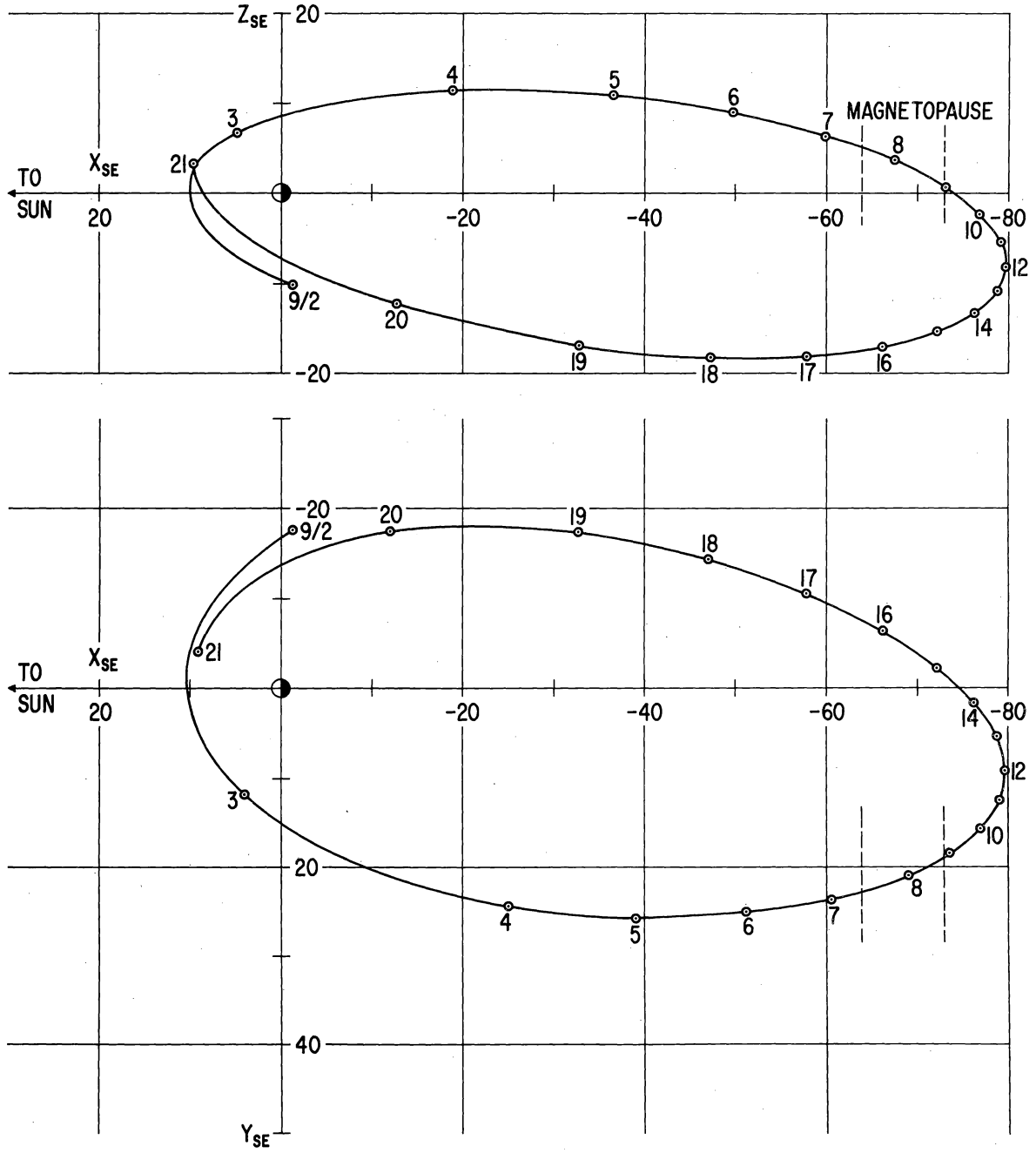

EXPLORER 33 ORBIT 5 SEPT. 1966

Figure 28—Solar ecliptic and midnight meridian plane views of orbit 5.

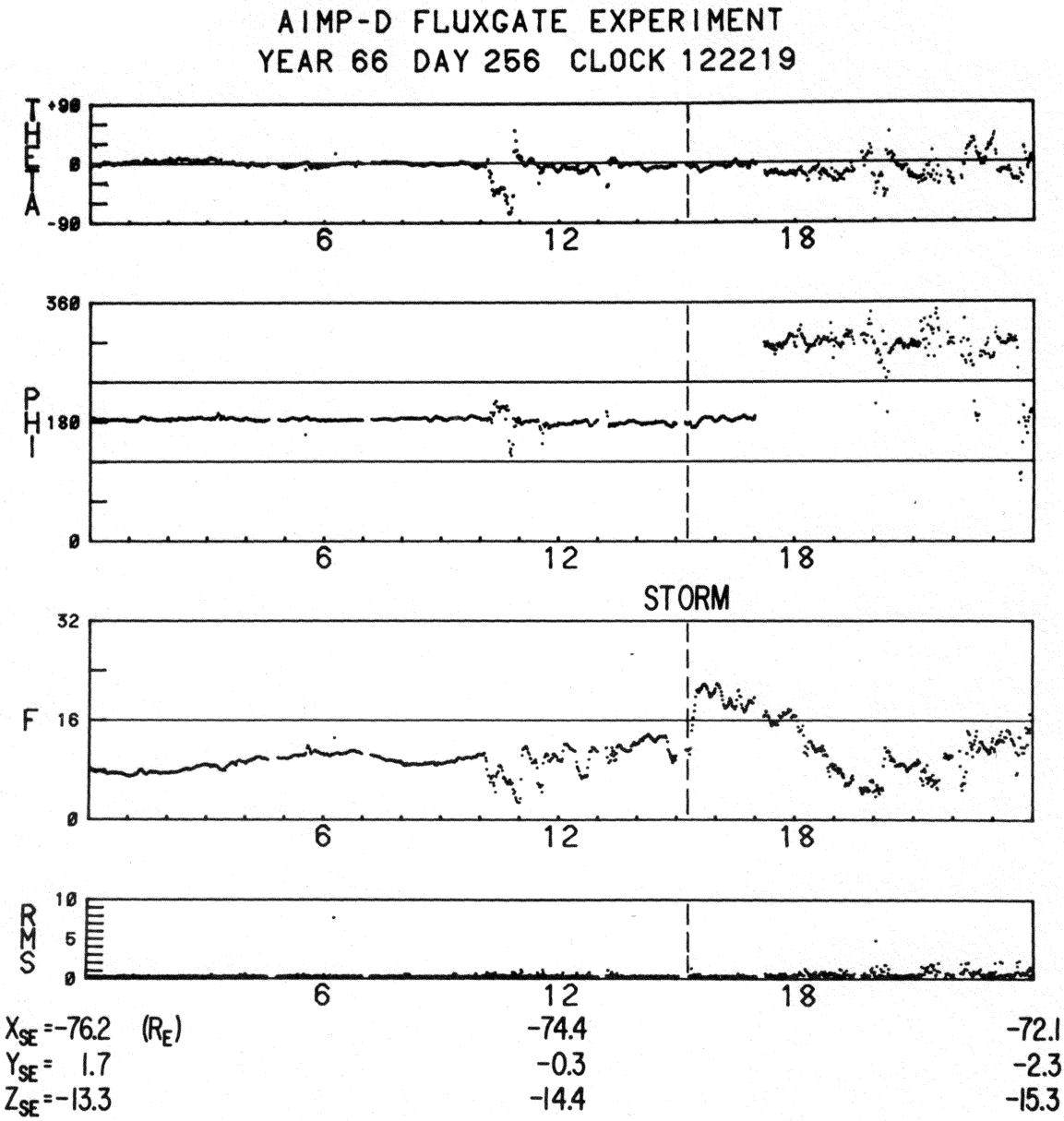

Figure 29—Magnetic field data from September 14, 1966 illustrating commencement of September 14, 1966 magnetic storm in the geomagnetic tail.

of the spacecraft at that time were $X_{SE} = -74.7$, $Y_{SE} = 0.0$ and $Z_{SE} = -14.2$. In addition the solar magnetospheric coordinates were $Y_{SM} = -8.1$ and $Z_{SM} = -11.7$. Thus Explorer 33 was in the midnight meridian plane but well below the solar magnetospheric equatorial plane, precluding any possible neutral sheet effects. However, the time at which the magnetic field variations began corresponds to the onset time of the detection of electrons by the MIT plasma detector (Bridge and Binsack, 1967).

The final magnetic field variation of interest on day 256, as shown in Fig. 29, occurred approximately two hours following the sudden commencement. At that time a sharp change in the direction of the field was observed. This event is interpreted as being a sudden traversal of the magnetopause. At that time the spacecraft had reached a point approximately 15 R_E from the axis of the magnetic tail. Thus the enhanced solar wind had compressed the tail boundary inward to that radius. The interpretation of the observed field variation as a magnetopause traversal is supported by the detection of magnetosheath plasma by the MIT detector (Bridge and Binsack, 1967) following the abrupt change in field direction. Also the magnitude RMS is seen to increase at that time.

The magnetopause was crossed a total of eight times during a period of approximately 12 hours before the field relaxed back to its undisturbed topology. The magnetic field data for day 257 is shown in Fig. 30. As can be seen, three shorter intervals of magnetosheath field orientation and magnitude were observed during the first six hours. Explorer 33 was inside the geomagnetic tail

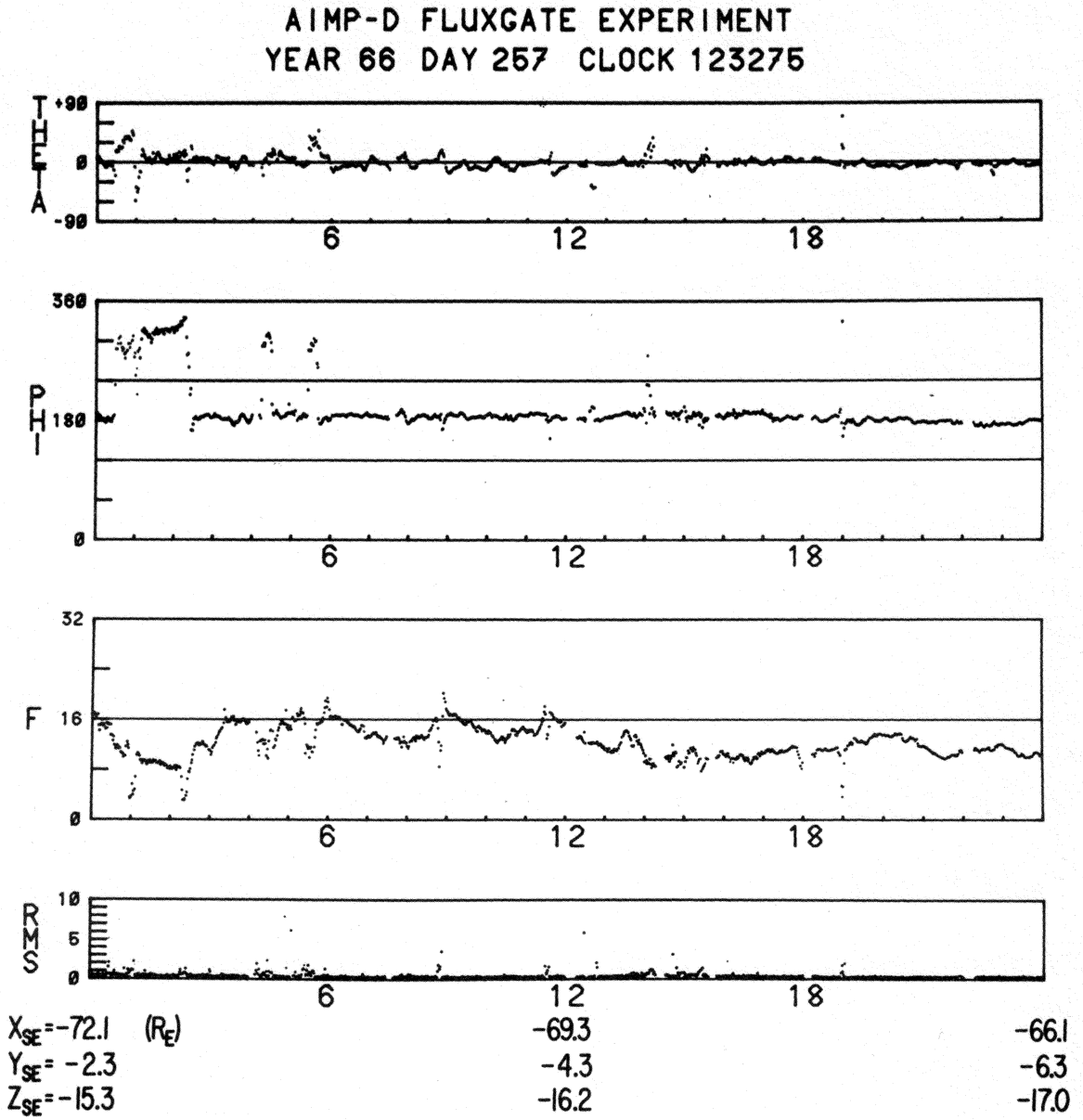

Figure 30—Magnetic field data from September 15, 1966 illustrating recovery phase in tail following geomagnetic storm.

for the remainder of the day. Throughout the day the field continued to show the effects of the disturbance. Higher levels of both high and low frequency fluctuations than are normally seen in the tail at large distances from the neutral sheet were observed.

The next class of geomagnetic tail field variation to be discussed is the spatial variation associated with field reversal at the neutral sheet. The neutral sheet has been defined as a region of abrupt directional change in the earth's magnetic tail field, where the magnitude decreases to a small value (Ness, 1965). Since the minimum of the field magnitude is not identically zero, the neutral sheet is not ideally "neutral"; however, since the field magnitude does decrease in the sheet, the field reversal region does not represent a purely rotational discontinuity in the magnetic field (Speiser and Ness, 1967).

It is not possible to uniquely determine the thickness of the neutral sheet for a particular traversal unless the relative velocity normal to the sheet between the spacecraft and the sheet is known. A lower limit of approximately 600 km was determined for the thickness from several traversals of the sheet by IMP 1 by neglecting the velocity of the sheet (Ness, 1965). The observed diurnal wobble of the sheet about its axis due to the daily 11.7° nutation of the earth's magnetic axis and the observations of multiple sheet traversals due to "flapping" of the sheet both establish that the sheet is always in motion. The results of an analysis of 42 IMP 1 neutral sheet traversals suggest that the sheet is probably less than 1 R_E thick, though evidence for an increase in thickness

toward the dawn magnetopause was found (Speiser and Ness, 1967). Thus the neutral sheet is a relatively thin region of field reversal embedded in a plasma sheet that is often 4-6 times as thick (Bame et. al., 1967).

The general flow pattern of current in the sheet deduced from the IMP 1 magnetic data is across the tail from dawn to dusk with a significant component down the tail for those sheet crossings near the earth and toward the dawn side (Speiser and Ness, 1967).

Figure 17 shows that the only times that Explorer 33 was in close proximity to the neutral sheet region were when outbound on orbit 1, during the orbit 4 pass through the tail, and during the first day of the orbit 5 pass through the tail. The orbit 1 outbound pass did not provide any complete traversals of the neutral sheet, nor is such a traversal clearly evident in the orbit 5 magnetic data.

A complete traversal of the neutral sheet by the spacecraft on orbit 4 beyond the lunar orbital distance has already been discussed in some detail (Ness et. al., 1967a). That traversal occurred on day 233 (August 22), and the sequence average magnetic field data for that day are shown in Fig. 31. Effects due to the flapping motion of the sheet are seen. Each time the spacecraft is immersed in the sheet the magnitude is seen to decrease, variations in the field orientation angles are observed with θ_{SE} generally increasing, and the RMS deviation of the magnitude is seen to increase.

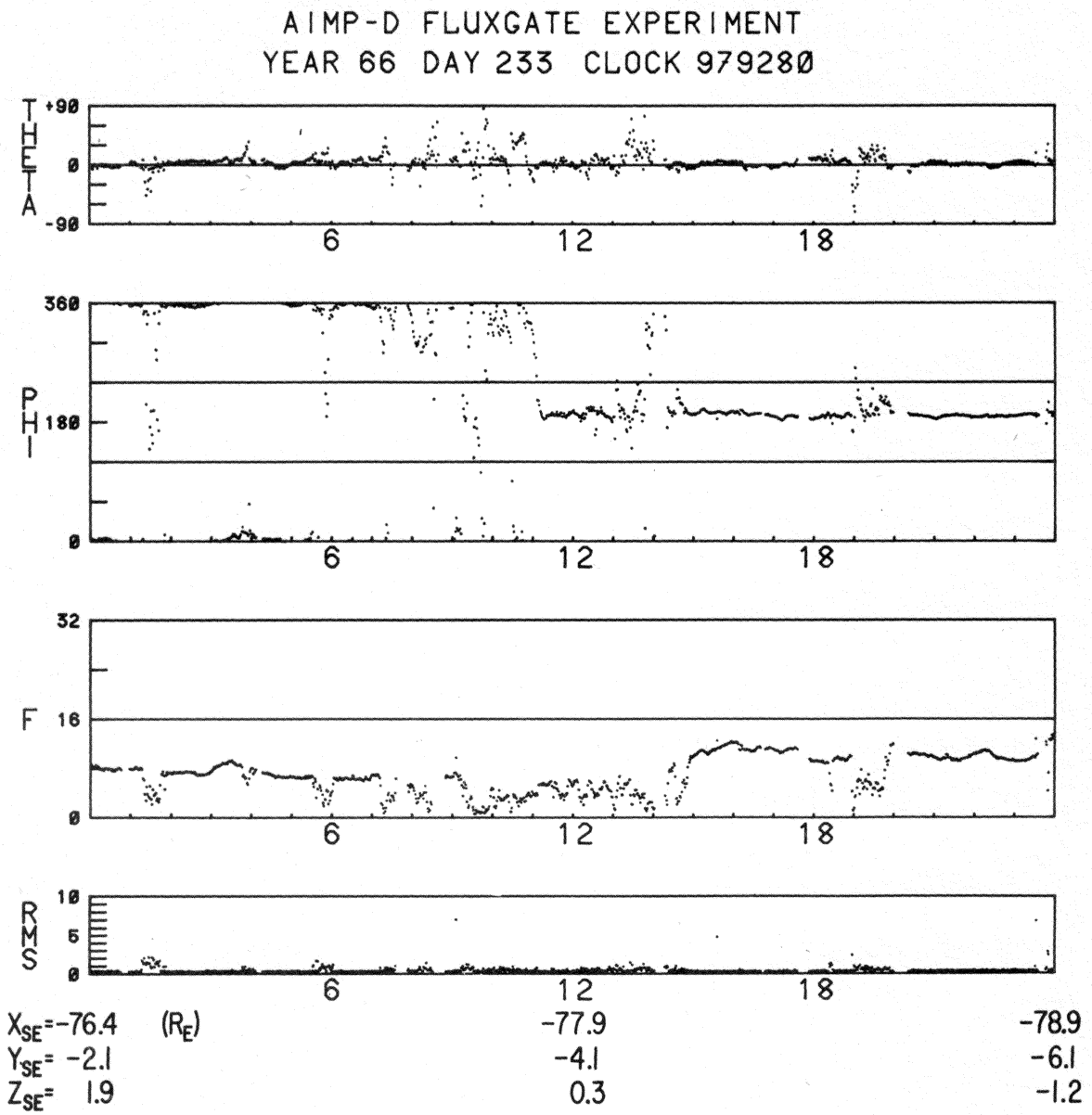

Figure 31–Magnetic field data from August 22, 1966 illustrating a traversal of the geomagnetic tail neutral sheet at 78.0 R_E.

Because of the motion of the sheet, other complete traversals for short periods of time were observed during the orbit 4 pass through the tail. One such sheet crossing by Explorer 33 is shown in detail in Fig. 32. Once again the top three panels are the sequence average field orientation and magnitude for approximately one hour. The lower panel shows the variation observed in the 5.11 second magnitude measurements during the traversal. This is an example of what might be called a "sharp" traversal, in which the magnitude drops sharply to near zero accompanied by a sharp change in the azimuthal angle ϕ_{SE}. The corresponding sequence average solar magnetospheric component data are shown in Fig. 33.

Fig. 34 illustrates a second type of neutral sheet traversal that was observed. In this case the field magnitude decrease is broad and shallow, with the 5.11 second magnitude data never falling below approximately 3 gammas. The fluctuating nature of the reversal of ϕ_{SE} suggests that the motion of the sheet past the spacecraft was not steady. The corresponding solar magnetospheric component variations are shown in Fig. 35. These show that when BX_{SM} was zero, BY_{SM} was also approximately zero but BZ_{SM} had a positive value of approximately 1 to 2 gammas. In the previous example all components were near zero simultaneously.

These results are consistent with the view that the neutral sheet was thicker in the second case, with a northward perpendicular component of several gammas observed throughout the reversal of the component of the field that is

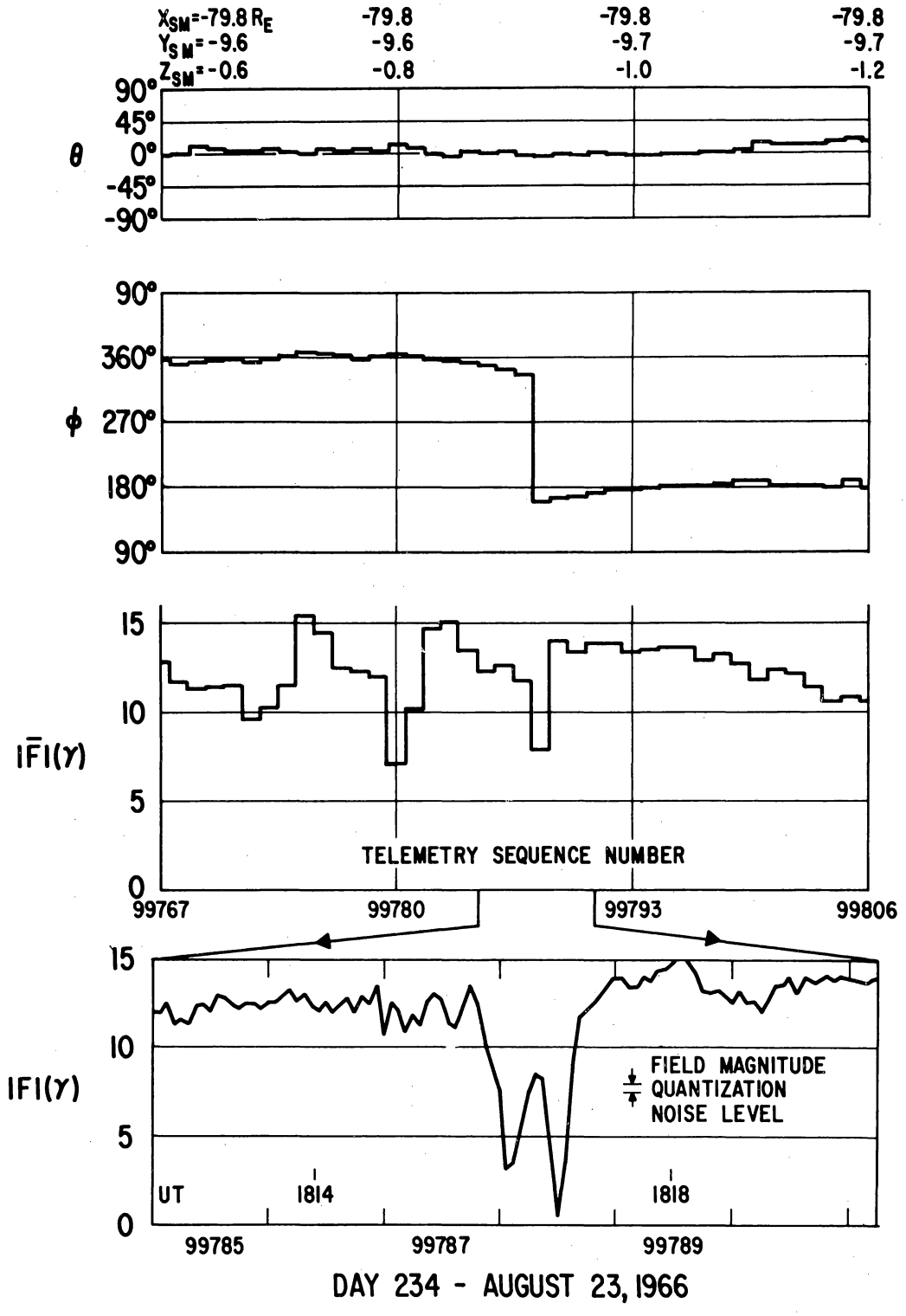

Figure 32–Detailed magnetic field data from August 23, 1966 illustrating a thin neutral sheet.

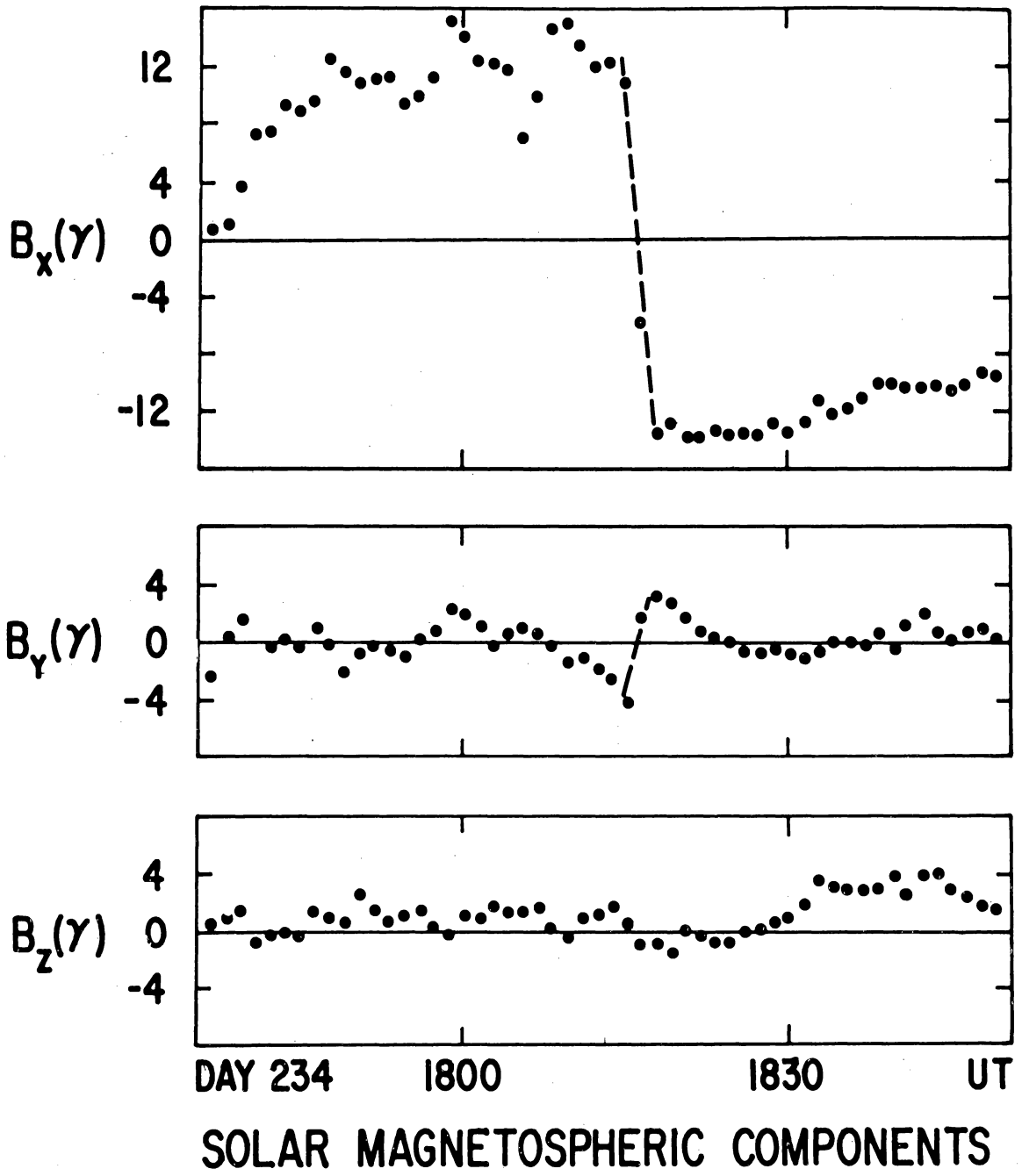

Figure 33–Magnetic field data illustrating the variations in SM field components during the August 23 neutral sheet traversal.

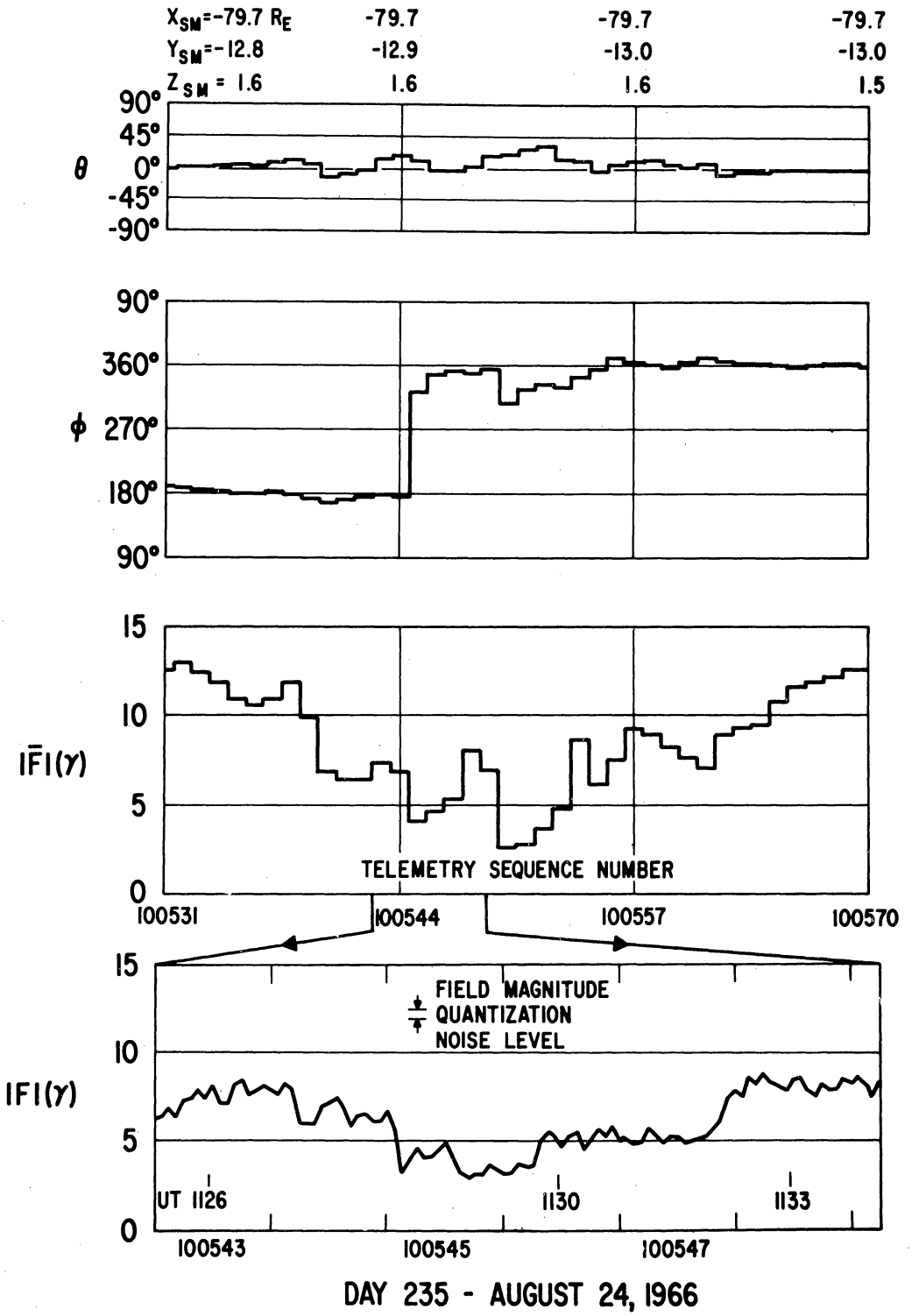

Figure 34–Detailed magnetic field data from August 24, 1966 illustrating an inflated neutral sheet.

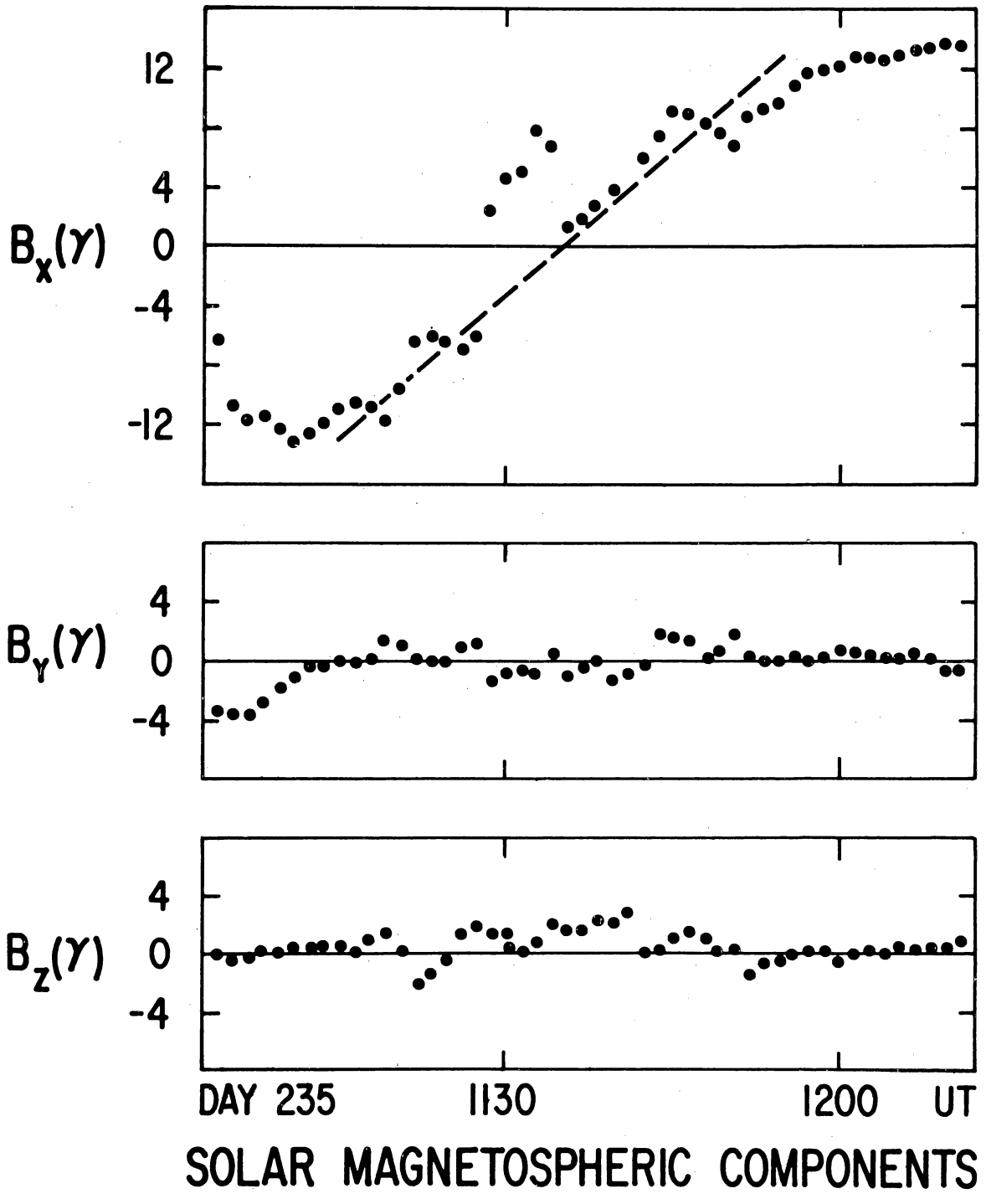

Figure 35–Magnetic field data illustrating the variations in SM field components during the August 24 neutral sheet traversal.

normally parallel to the tail axis. Thus the neutral sheet may undergo local variations in thickness. Whether these are spatial, temporal or both is still under investigation.

The simplest model of the neutral sheet that can be used for computational purposes assumes that the neutral sheet is two dimensional and stationary in time except for possible spatial motion. In terms of this model it can be argued that the resulting simplification of the expressions for the time rate of change of the field components, together with Ampere's law, lead to the following expressions for the components of the linear current density in the sheet (Speiser and Ness, 1967):

$$J_X = \frac{-1}{\mu_0} \Delta B_y \cdot (\text{sign of } \Delta B_x)$$

$$J_y = \frac{1}{\mu_0} |\Delta B_x|$$

$$J_z = 0.$$

Initial inspection of the Explorer 33 data revealed six really complete traversals that were suitable for computation of equivalent current density from the magnetic field component variations. The resulting linear current densities are tabulated in Table 2. Also listed are the changes in the field components that were used, the distance $X_{SM} = X_{SE}$ of the spacecraft down the tail, the distance Y_{SM} of the spacecraft from the tail axis at the time of the

TABLE 2

NEUTRAL SHEET EQUIVALENT CURRENT DENSITIES

DAY	TIME	X_{SM}	Y_{SM}	Z_{SM}	ΔB_X	ΔB_Y	J_X ($X10^{-2}$ amps/m)	J_y ($X10^{-2}$ amps/m)
229	0945	-50.6	17.0	3.1	19.6	3.6	0.3	1.6
	1003	-50.7	16.9	3.0	-23.2	1.2	-0.1	1.8
	1218	-51.8	16.5	3.2	28.2	2.8	0.2	2.2
234	0847	-79.4	- 7.5	1.9	32.0	1.2	0.1	2.5
	1817	-79.8	- 9.6	-0.9	26.0	7.5	-0.6	2.1
235	1129	-79.7	-12.8	1.6	26.0	0.0	0.0	2.1

traversal, and the distance Z_{SM} from the solar magnetospheric equatorial plane.

As stated by Speiser and Ness (1967), errors of ±10-20% in the determination of $\vec{J}$ result from the uncertainty involved in the straight line fitting of the component data to obtain the changes across the sheet. Also of course the validity of using the two dimensional model in a given case is limited by the magnitude of the observed perpendicular field component in the sheet.

The third major type of magnetic field variation observed by Explorer 33 in the geomagnetic tail is a general decrease in tail field magnitude with increasing geocentric distance down the tail. This magnitude decrease was evident in the summary plot of hourly average vectors in Fig. 19. Fig. 36 shows 256 hourly average field magnitudes as a function of distance along the earth-sun line down the tail. Only data corresponding to $Kp \leq 2$ (i.e., quiet data) and data

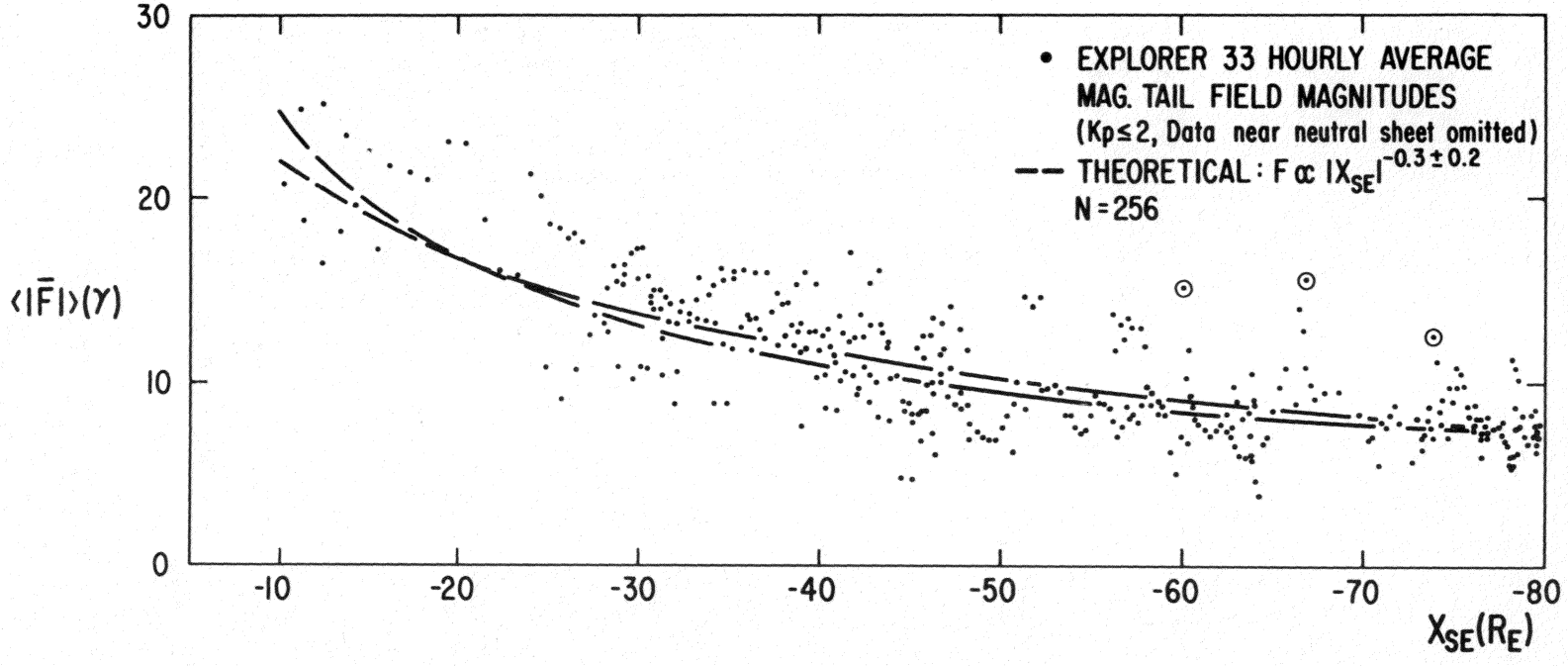

Figure 36–Distribution of undisturbed average magnetic tail field magnitudes as a function of geocentric distance down the tail.

for which the spacecraft was $\geq 2\ R_E$ away from the neutral sheet have been plotted.

Data from 740 hours during which Explorer 33 was clearly in the tail were subjected to a multiple correlation and regression analysis. The formulation used in this analysis has been described by Efroymson (1965). In this particular application the hourly average field magnitude was the dependent variable, while three independent variables were used. These were the earth-sun line distance X_{SE} of the spacecraft down the tail, the magnetic activity index K_P, and the perpendicular distance Z_{SM} of the satellite from the solar magnetospheric equatorial plane. The formulation is such that functions of the independent variables can also be correlated with the dependent variable. Various powers of the X_{SE} distance were tested, and the best correlation was obtained using $|X_{SE}|^{-0.3 \pm 0.2}$. The results of the analysis are tabulated in Table 3.

The expressions used to compute the multiple and partial correlation coefficients are listed in Appendix D. As can be seen in Table 3, the best correlation among the three independent variables used was between field magnitude and the inverse power of distance down the tail. The lack of a better correlation between magnitude and planetary index Kp is at least in part due to the lack of better resolution in Kp. The hourly average tail field magnitude can respond to the commencement of a magnetic disturbance before the 3-hour index Kp is effected by the disturbance. The data points that are circled in Fig. 36 are

TABLE 3

MULTIPLE CORRELATION AND REGRESSION COEFFICIENTS FOR MAGNETIC TAIL FIELD MAGNITUDE VARIATIONS

DEPENDENT VARIABLE = Magnetic Field Magnitude F

INDEPENDENT VARIABLE	PARTIAL CORRELATION COEFFICIENT	REGRESSION COEFFICIENT
$\lvert X_{SE} \rvert^{-0.3}$	$r_{FX \cdot KZ} = 0.66$	69.13 ± 2.88
kp	$r_{FK \cdot XZ} = 0.46$	1.30 ± 0.09
Z_{SM}	$r_{FZ \cdot XK} = 0.14$	0.07 ± 0.01
		Constant = -13.72
	MULTIPLE CORRELATION COEFFICIENT	
	$r_{F \cdot XKZ} = 0.69$	

examples of a large increase in field magnitude preceding a corresponding increase in Kp by one hour.

The lack of a good correlation between field magnitude and Z_{SM} was expected since the tail field magnitude is observed to be reduced by the neutral sheet only at points very close to (within 1 R_E) or within the sheet. In addition there is generally a nonzero difference between Z_{SM} and the actual perpendicular distance to the neutral sheet.

The regression coefficients obtained in the case of the "best" correlation provided a fit to 740 hourly average field magnitudes with a standard error of ±3.06 gammas. Limiting case best fits to the 256 data points shown in Fig. 36

were obtained from the regression equations for $|X_{SE}|^{-0.1}$ and $|X_{SE}|^{-0.5}$ and are represented by the dashed curves in Fig. 36. The curve that is highest at $X_{SE} = -10\ R_E$ illustrates the variation of F with $|X_{SE}|^{-0.5}$. The field magnitudes predicted by the regression curves in the interval between $-10\ R_E$ and $-30\ R_E$ are consistent with the median tail field magnitude of 16 gammas found by IMP 1 in that region (Behannon and Ness, 1966). From the 740 hours of Explorer 33 observations in the tail out to $80\ R_E$, a median magnitude of 10 gammas was found.

The observed field magnitude gradient in the tail can result either from an increase in the cross sectional area of the tail with distance down the tail or from reconnection of field lines across the neutral sheet or possibly from a combination of the two effects. If no magnetic field lines cross the neutral sheet, then the total number of tail field lines above the neutral sheet that pass through a cross section $A(x_1)$ is equal to the total number passing through $A(x_2)$, when there is a field magnitude decrease with distance, only if $A(x_2) > A(x_1)$.

In general the magnetic flux through a cross sectional area A is given by

$$\Phi = \int_A \vec{B} \cdot \vec{n}\ da,$$

where $\vec{n}$ is the unit vector normal to the area A. Consider for simplicity a general two dimensional model of the tail in the XZ-plane where the X-axis is the neutral plane and the tail boundary occurs at $Z = \pm Z'(x)$. The field is in general given by

$$\vec{B} = B_x\,(x,\ z)\,\vec{i} + B_z\,(x,\ z)\,\vec{j}$$

and therefore

$$\vec{B} \cdot \vec{n} = B_x\,(x,\ z).$$

Because of the oppositely directed fields in the two halves of the tail, the total flux through a cross section is

$$\Phi(x) = \int_{-Z'(x)}^{Z'(x)} B_x(x,\ z)\,dz = 0$$

Thus for purposes of investigating the field magnitude gradient, consider only the half of the tail lying above the neutral sheet. Then the flux through a cross section is given by

$$\Phi(x) = \int_{0}^{Z'(x)} B_x\,(x,\ z)\,dz.$$

In general the variation in flux with distance will be given by

$$\frac{d\Phi(x)}{dx} = \frac{dZ'(x)}{dx}\,B_x\,[x,\ Z'(x)] + \int_0^{Z'(x)} \frac{\partial B_x(x,\ z)}{\partial x}\,dz.$$

The component of the tail field normal to the cross section has not been observed to vary with distance from the neutral sheet. In this case $\partial B_x/\partial Z = 0$ and thus $B_x = B_x(x)$ only, and

$$\frac{d\Phi(x)}{dx} = \frac{dZ'(x)}{dx} B_x(x) + \frac{dB_x(x)}{dx} \int_0^{Z'(x)} dz$$

$$= \frac{dZ'(x)}{dx} B_x(x) + \frac{dB_x(x)}{dx} Z'(x),$$

or

$$\frac{dB_x(x)}{dx} = \frac{1}{Z'(x)} \left[\frac{d\Phi(x)}{dx} - B_x(x) \frac{dZ'(x)}{dx} \right].$$

Thus if

$$\frac{d\Phi(x)}{dx} = 0,$$

then

$$\frac{dB_x(x)}{dx} = -\frac{B_x(x)}{Z'(x)} \frac{dZ'(x)}{dx} \tag{2}$$

and hence the reduction in the normal (X) field component will simply be due to a change in the cross sectional area.

If on the other hand the area remains constant, i.e., $Z' \neq Z'(x)$, then

$$\frac{dZ'}{dx} = 0 \text{ and } \frac{dB_x(x)}{dx} = \frac{1}{Z'} \frac{d\Phi(x)}{dx}. \tag{3}$$

In this case there must be a decrease in flux with distance (through a cross section of constant area) to produce a decrease in the normal component. In case (2) since B_x does not vary with Z the field lines will remain parallel unless the total field $\vec{B}$ increases toward the boundary due to an increase toward the boundary in the component parallel to the Z-axis. Such a magnitude increase has not been observed in the earth's magnetic tail.

The rate of change in the cross sectional area at a given distance X can be computed from (2) if the field gradient and component magnitude in the X-direction and the area at that distance are known:

$$\frac{dA(x)}{dx} = -\frac{A(x)}{B_x(x)} \frac{dB_x(x)}{dx}$$

If the total field vector is in the X-direction, i.e.,

$$\vec{B} = B_x(x)\,\vec{i} = B(x)\,\vec{i},$$

then the total field magnitude gradient is the appropriate gradient to consider. This is the case to a good approximation in the earth's tail where in general $B_x >> B_z$

If the cross sectional area of the tail remains constant, then according to (3) the total number of field lines in the tail must diminish with distance to produce a magnitude gradient. This can occur if there is reconnection of field lines across the neutral sheet. Consider now the case where the tail boundary remains at a constant distance from the neutral sheet (no field lines cross a boundary at a constant distance). Then a simple consideration of conservation of flux through cross sections at $X_{SE} = -10\ R_E$ and at $X_{SE} = -80\ R_E$ and through the neutral sheet shows that an average 2 gamma field component perpendicular to the neutral sheet would account for the total decrease in field magnitude that occurs in that distance.

However, in the interval between -10 R_E and -30 R_E where the greatest part of the magnitude decrease occurs, an average 7 gamma component perpendicular to the neutral sheet would be required and nothing that large is seen on the average in that region. During the 230 hours of orbit 4 that Explorer 33 was near the neutral sheet an average northward component of 1 gamma was observed. However, it was northward in the sense of being in the direction of the positive Z_{SM} axis, and the real neutral sheet may not be coplanar with the solar magnetospheric equatorial plane. Thus it appears that both a small amount of increase in the tail cross section (as yet undetected) and a small amount of reconnection at the neutral sheet may combine to produce the observed magnitude gradient.

If one extends the computed regression curves shown in Fig. 36 beyond 80 R_E it is found that the tail field magnitude will have decreased to a value of 4 gammas at a geocentric distance between 125 and 175 R_E during times of low Kp. Although the magnetic field lines in the tail are probably stretched out much further than that (Ness et al., 1967b), the tail may be less well defined beyond some distance ≤ 200 R_E if the field magnitude decreases to the quiet time interplanetary level at that distance.

VI. SUMMARY OF RESULTS

During the first five months in orbit, the Explorer 33 satellite made detailed measurements at the earth's bow shock, in the magnetosheath and in the geomagnetic tail. This extensive survey has confirmed and substantially extended the results of previous investigations of those regions.

Explorer 33 has found that the earth's bow shock is a well-defined surface of discontinuity at geocentric distances as great as 75 R_E down the flanks. The average shock surface orientation computed using the classical "fast shock" model generally does not accurately describe the observed average orientation of the shock surface, although in some individual cases the model is in relatively good agreement with the expected orientation.

The magnetosheath is generally found to be a region of low frequency, large amplitude fluctuations and high frequency, small amplitude fluctuations, with the magnetosheath field magnitude generally decreasing with distance away from the bow region until the interplanetary field magnitude is reached. During times of low magnetic activity index Kp, the magnetosheath down the flanks is relatively steady in both magnitude and solar ecliptic azimuthal angle, with most of the fluctuations produced by transverse waves. However, as Kp increases, the levels of both low and high frequency fluctuations increase and a larger percentage of the fluctuation is found to occur in the longitudinal mode.

The magnetosheath fields along the flanks are generally characterized by a large component perpendicular to the ecliptic plane. This component is observed to be alternately positive and negative, suggesting that filaments are observed which are alternately draped above and below the magnetospheric tail.

Explorer 33 has generally observed a large discontinuity in magnetic field direction across the tail magnetopause. In addition, traversals of that boundary have shown that the geomagnetic tail is probably not cylindrical in shape. The cross section of the tail appears to be elongated in the direction perpendicular to the neutral sheet. The average bow shock also may not be circular in cross section. The shock and magnetopause boundaries move in and out by 10 R_E or more in response to solar wind variations. The tail magnetopause is compressed to within 15 R_E of the tail axis during magnetic storms.

Explorer 33 has shown that the geomagnetic tail is still well defined beyond the lunar orbital distance. During times of low Kp the magnetic field in the tail is the steadiest field observed in space by Explorer 33. At various distances down the tail out to 80 R_E the neutral sheet has been observed to be a relatively thin region which may undergo variations in thickness which are either spatial, temporal or both. Sudden commencement magnetic storm variations observed in the magnetic tail beyond the lunar orbital distance are similar in character to the storm variations observed in the tail nearer the earth.

A general decrease in tail field magnitude with distance down the tail has been found. The observed magnitude gradient is best described by an inverse

power of the geocentric distance along the earth-sun line. This magnitude decrease can be produced either by a gradual increase in the cross section of the tail with distance or by a reconnection of field lines across the neutral sheet. It may result from a combination of both mechanisms since there is no experimental evidence to support the view that either effect is sufficiently large to be solely responsible. If the tail field magnitude continues to decrease at the observed rate beyond a geocentric distance of 80 R_E, then the geomagnetic tail may be less well defined beyond a distance from the earth of several hundred earth radii.

VII. ACKNOWLEDGEMENTS

The author wishes to express his appreciation to Dr. Norman F. Ness of the Goddard Space Flight Center for his patient guidance and support throughout this work. He would also like to thank Mr. Herbert E. Haney for his substantial programming and data processing assistance and Dr. Donald H. Fairfield, Dr. Harold E. Taylor, Mr. Clell S. Scearce and Mr. William H. Mish for their contributions to the thesis in the form of many helpful discussions. In addition he would like to thank Dr. H. S. Bridge and Dr. J. H. Binsack of the Massachusetts Institute of Technology for a very profitable discussion of joint results.

VIII. BIBLIOGRAPHY

Allen, C. W., Relation between magnetic storms and solar activity, Mon. Not. Roy. Ast. Soc., 104, 13-21, 1944.

Anderson, K. A., Energetic electron fluxes in the tail of the geomagnetic field, J. Geophys. Res., 70, 4741-4763, 1965.

Anderson, K. A., H. K. Harris, and R. J. Paoli, Energetic electron fluxes in and beyond the earth's outer magnetosphere, J. Geophys. Res., 70, 1039-1050, 1965.

Anderson, K. A. and N. F. Ness, Correlations of magnetic fields and energetic electrons on the IMP 1 satellite, J. Geophys. Res., 71, 3705-3727, 1966.

Auer, P. L., H. Hurwitz and R. W. Kilb, Low mach number magnetic compression waves in a collision-free plasma, Phys. Fluids, 4, 1105-1121, 1961.

Auer, P. L., H. Hurwitz and R. W. Kilb, Large amplitude magnetic compression of a collision-free plasma, 2; Development of a thermalized plasma, Phys. Fluids, 5, 298-316, 1962.

Axford, W. I., The interaction between the solar wind and the earth's magnetosphere, J. Geophys. Res., 67, 3791-3796, 1962.

Axford, W. I., Viscous interaction between the solar wind and the earth's magnetosphere, Planet. Space Sci., 12, 45-54, 1964.

Axford, W. I., Solar wind interaction with the magnetosphere, fluid dynamic aspects, The Solar Wind, ed. R. J. Mackin, Jr. and M. Neugebauer, 231-242, Pergamon Press, New York, 1966.

Axford, W. I. and C. O. Hines, A unifying theory of high-latitude geophysical phenomena and geomagnetic storms, Can. J. Phys., 39, 1433-1464, 1961.

Axford, W. I., H. E. Petschek and G. L. Siscoe, The tail of the magnetosphere, J. Geophys. Res., 70, 1231-1236, 1965.

Bame, S. J., J. R. Asbridge, H. E. Felthauser, R. A. Olson, and I. B. Strong, Electron angular, spatial, and energy distributions, measured near 17 R_E with an electrostatic analyzer, Trans. Am. Geophys. Union, 45, 624, 1964.

Bame, S. J., J. R. Asbridge, H. E. Felthauser, R. A. Olson, and I. B. Strong, Electrons in the plasma sheet of the earth's magnetic tail, Phys. Rev. Letters, 16, 138-142, 1966.

Bame, S. J., J. R. Asbridge, H. E. Felthauser, E. W. Hones, and I. B. Strong, Characteristics of the plasma sheet in the earth's magnetic tail, J. Geophys. Res., 72, 113-129, 1967.

Bartels, J., Terrestrial magnetic activity and its relations to solar phenomena, Terr. Magnetism and Atmos. Elec., 37, 1-52, 1932.

Beard, D. B., The interaction of the terrestrial magnetic field with the solar corpuscular radiation, J. Geophys. Res., 65, 3559-3568, 1960a.

Beard, D. B., Interaction of the solar plasma with the earth's magnetic field, Phys. Rev. Letters, 5, 89-91, 1960b.

Beard, D. B., Interaction of the terrestrial magnetic field with the solar corpuscular radiation: 2. Second-order approximation, J. Geophys. Res., 67, 477-484, 1962.

Beard, D. B., The solar wind geomagnetic field boundary, Rev. Geophys., 2, 335-365, 1964.

Behannon, K. W. and N. F. Ness, Magnetic storms in the earth's magnetic tail, J. Geophys. Res., 71, 2327-2351, 1966.

Bernstein, W., R. W. Fredericks, and F. L. Scarf, A model for a broad disordered transition between the solar wind and the magnetosphere, J. Geophys. Res., 69, 1201-1210, 1964.

Biermann, L., Kometenschweife und solare korpuscular strahlung, Z. Astrophys., 29, 274-286, 1951.

Bonetti, A., H. S. Bridge, A. J. Lazarus, B. Rossi, and F. Scherb, Explorer 10 plasma measurements, J. Geophys. Res., 68, 4017-4063, 1963.

Bridge, H. S. and J. H. Binsack, personal communication, 1967.

Bridge, H., S. Egidi, A. Lazarus, E. Lyon and L. Jacobson, Preliminary results of plasma measurements on IMP-A, Space Research V, 969-978, 1965.

Cahill, L. J., The geomagnetic field, Chapter 9, Space Physics, ed. D. P. LeGalley and A. Rosen, John Wiley and Sons, 1964.

Cahill, L. J., Inflation of the magnetosphere near 8 earth radii in the dark hemisphere, Space Research VI, 662-678, 1966.

Cahill, L. J. and P. J. Amazeen, The boundary of the geomagnetic field, J. Geophys. Res., 68, 1835-1844, 1963.

Cahill, L. J. and D. H. Bailey, Distortion of the magnetosphere during a magnetic storm on September 30, 1961, J. Geophys. Res., 72, 159-169, 1967.

Chapman, S. and V.C.A. Ferraro, A new theory of magnetic storms, Terr. Mag. Atmos. Elec., 36, 77-97, 171-186, 1931; 37, 147-156, 421-429, 1932.

Coleman, P. J. Jr., Characteristics of the region of interaction between the interplanetary plasma and the geomagnetic field-Pioneer 5, J. Geophys. Res., 69, 3051-3076, 1964.

Coleman, P. J. Jr., C. P. Sonett, D. L. Judge and E. J. Smith, Some preliminary results of the Pioneer 5 magnetometer experiment, J. Geophys. Res., 65, 1856-1857, 1960.

Coon, J., Vela satellite measurements of particles in the solar wind and the distant geomagnetosphere, Radiation Trapped in the Earth's Magnetic Field, ed. B. M. McCormac, D. Reidel, Dordrecht, Holland, 1966.

Corday, J. G., On the structure of the collision-free bow shock wave, J. Geophys. Res., 70, 1278-1280, 1965.

De Hoffman, F. and E. Teller, Magneto-hydrodynamic shocks, Phys. Rev., 80, 692-703, 1950.

Dessler, A. J., Length of the magnetospheric tail, J. Geophys. Res., 69, 3913-3918, 1964.

Dessler, A. J. and R. D. Juday, Configuration of auroral radiation in space, Planet. Space Sci., 13, 63-72, 1965.

Dessler, A. J. and J. A. Fejer, Interpretation of Kp index and M-region geomagnetic storms, Planet. Space Sci., 11, 505-511, 1963.

Dessler, A. J. and G. K. Walters, Hydromagnetic coupling between the solar wind and the magnetosphere, Planet. Space Sci., 12, 227-234, 1964.

Dungey, J. W., Interplanetary magnetic field and the auroral zones, Phys. Rev. Letters, 6, 47-48, 1961.

Dungey, J. W. Interactions of solar plasma with the geomagnetic field, Planet. Space Sci., 10, 233-237, 1963.

Dungey, J. W., The length of the magnetospheric tail, J. Geophys. Res., 70, 1753, 1965.

Efroymson, M. A., Multiple regression analysis, Mathematical Methods for Digital Computers, ed A. Ralston and H. S. Wilf, John Wiley and Sons, New York, 1965.

Fairfield, D. H., The ordered magnetic field of the magnetosheath, NASA-GSFC preprint X-612-67-174, April, 1967.

Fairfield, D. H. and N. F. Ness, Magnetic field measurements with the IMP 2 satellite, NASA-GSFC preprint X-612-66-530, November, 1966.

Fan, C. Y., G. Gloeckler, and J. A. Simpson, Acceleration of electrons near the earth's bow shock and beyond, J. Geophys. Res., 71, 1837-1856, 1966.

Fishman, F. J., A. R. Kantrowitz, and H. E. Petschek, Magnetohydrodynamic shock wave in a collision-free plasma, Rev. Mod. Phys., 32, 959-966, 1960.

Frank, L. A., A survey of electrons E > 40 kev beyond 5 earth radii with Explorer 14, J. Geophys. Res., 70, 1593-1626, 1965.

Fredricks, R. W., F. L. Scarf, and W. Bernstein, Numerical estimates of superthermal electron production by ion acoustic waves in the transition region, J. Geophys. Res., 70, 21-28, 1965.

Freeman, J. W., The morphology of the electron distribution in the outer radiation zone and near the magnetospheric boundary as observed by Explorer 12, J. Geophys. Res., 69, 1691-1723, 1964.

Freeman, J. W., J. A. Van Allen and L. J. Cahill, Explorer 12 observations of the magnetospheric boundary and the associated solar plasma on September 13, 1961, J. Geophys. Res., 68, 2121-2130, 1963.

Gold, T., Magnetic storms, Space Sci. Rev., 1, 100-114, 1962.

Gosling, J. T., J. R. Asbridge, S. J. Bame and I. B. Strong, Vela 2 measurements of the magnetopause and bow shock positions, J. Geophys. Res., 72, 101-112, 1967.

Gringaus, K. I., V. G. Kurt, V. I. Moroz, and I. S. Shklovsky, Results of observations of charged particles observed out to 100,000 km with the aid of charged particle traps on Soviet space probes, Astron. Zh., 37-4, 716-735, 1960.

Harris, C. A., AIMP-D prototype (01) and flight (02) spacecraft final deperm and AMR pre-launch mapping, NASA-GSFC Memorandum Report No. 665-022, Dec. 7, 1966.

Heppner, J. P., Recent measurement of the magnetic field in the outer magnetosphere and boundary regions, NASA-GSFC preprint X-612-65-490, November, 1965.

Heppner, J. P., M. Campbell, T. L. Skillman, and B. G. Ledley, Preliminary report on EGO magnetic field measurements, Amer. Geophys. Union Annual Meeting, April, 1965.

Heppner, J. P., N. F. Ness, T. L. Skillman and C. S. Scearce, Explorer 10 magnetic field measurements, J. Geophys. Res., 68, 1-46, 1963.

Holtzer, R. E., M. G. McLeod, and E. J. Smith, Preliminary results from the OGO 1 search coil magnetometer: boundary positions and magnetic noise spectra, J. Geophys. Res., 71, 1481-1486, 1966.

Kaufmann, R. L., Shock observations with the Explorer 12 magnetometer, Univ. of New Hampshire Dept. of Physics pub. UNH-66-3, Durham, New Hampshire, 1966.

Kellogg, P. J., Flow of plasma around the earth, J. Geophys. Res., 67, 3805-3811, 1962.

Kenney, J. F. and E. S. Keeping, Mathematics of statistics, Van Nostrand, New York, 1951.

Landau, L. D. and E. M. Lifshitz, Electrodynamics of Continuous Media, Pergamon Press, New York, 1960.

Levy, R. H., H. E. Petschek and G. L. Siscoe, Aerodynamic aspects of the magnetospheric flow, AIAA Journal, 2, 2065-2076, 1964.

Lincoln, J. V., Geomagnetic and solar data, J. Geophys. Res., 71, 5784, 1966.

Lincoln, J. V., Geomagnetic and solar data, J. Geophys. Res., 72, 453, 1967a.

Lincoln, J. V., Geomagnetic and solar data, J. Geophys. Res., 72, 1660, 1967b.

Lincoln, J. V., Geomagnetic and solar data, J. Geophys. Res., 72, 2050, 1967c.

McDiarmid, I. B., and J. R. Burrows, Electron fluxes at 1000 kilometers associated with the tail of the magnetosphere, J. Geophys. Res., 70, 3031-3044, 1965.

Mead, G. D. and L. J. Cahill, Jr., Explorer 12 measurements of the distortion of the geomagnetic field by the solar wind, NASA-GSFC preprint X-640-66-527, November, 1966.

M.I.T. Electrical Engineering Staff, Magnetic Circuits and Transformers, John Wiley and Sons, New York, 1943.

Montgomery, M. D., S. Singer, J. P. Conner, and E. E. Stogsdill, Spatial distribution, energy spectra, and time variations of energetic electrons (E > 50 kev) at 17.7 earth radii, Phys. Rev. Letters, 14, 209-213, 1965.

Morawetz, C. S., Magnetohydrodynamic shock structure without collisions, Phys. Fluids, 4, 988-1006, 1961.

Morawetz, C. S., Modification for magnetohydrodynamic shock structure without collisions, Phys. Fluids, 5, 1447-1450, 1962.

Mustel, E., Quasi-stationary emission of gases from the sun, Space Science Revs., 139-231, 1964.

Ness, N. F., The earth's magnetic tail, J. Geophys. Res., 70, 2989-3005, 1965.

Ness, N. F., Observations of the solar wind interaction with the geomagnetic field: conditions quiet, NASA-GSFC preprint X-612-66-381, August, 1966a; to be published in Proceedings of Belgrade Solar Terrestrial Relationships Interunion Meeting, 1966.

Ness, N. F., A proposal for magnetic field experiment for IMPs H and J, NASA-GSFC preprint X-612-66-461, September, 1966b.

Ness, N. F., K. W. Behannon, S. C. Cantarano and C. S. Scearce, Observations of the earth's magnetic tail and neutral sheet at 510,000 kilometers by Explorer 33, J. Geophys. Res., 72, 927-933, 1967a.

Ness, N. F., C. S. Scearce and J. B. Seek, Initial results of the IMP 1 magnetic field experiment, J. Geophys. Res., 69, 3531-3570, 1964.

Ness, N. F., C. S. Scearce, J. B. Seek and J. M. Wilcox, Summary of results from the IMP 1 magnetic field experiment, Space Research VI, 581-628, 1966a.

Ness, N. F., C. S. Scearce and S. Cantarano, Preliminary results from the Pioneer 6 magnetic field experiment, J. Geophys. Res., 71, 3305-3313, 1966b.

Ness, N. F., C. S. Scearce and S. Cantarano, Probable observation of the geomagnetic tail at 6×10^6 kilometers by Pioneer 7, NASA-GSFC preprint X-612-67-183, April, 1967b.

Ness, N. F. and D. J. Williams, Correlated magnetic tail and radiation belt observations, J. Geophys. Res., 71, 322-325, 1966.

Noerdlinger, P. D., Wave generation near the outer boundary of the magnetosphere, J. Geophys. Res., 69, 369-375, 1964.

Parker, E. N., Interaction of the solar wind with the geomagnetic field, Phys. Fluids, 1, 171-187, 1958.

Petschek, H. E., Collision-free plasmas, Suppl. Nuovo Cimento, 22-10, 448-458, 1961.

Piddington, J. H., Geomagnetic storm theory, J. Geophys. Res., 65, 93-106, 1960.

Piddington, J. H., The geomagnetic tail and magnetic storm theory, Planet. Space Sci., 13, 281-284, 1965.

Rossi, B., Interplanetary plasma, Space Research III, 529-539, 1963.

Saemundssen, Th., Statistics of geomagnetic storms and solar activity, Mon. Not. Roy. Ast. Soc., 123, 299-316, 1962.

Scarf, F. L., W. Bernstein and R. W. Fredricks, Electron acceleration and plasma instabilities in the transition region, J. Geophys. Res., 70, 9-20, 1965.

Serbu, G. P., Results from the IMP 1 retarding potential analyzer, Space Research V, 564-574, 1965.

Serbu, G. P. and E. J. R. Maier, Low energy electrons measured on IMP 2, J. Geophys. Res., 71, 3755-3766, 1966.

Siscoe, G. L., L. Davis, Jr., E. J. Smith, P. J. Coleman, Jr., and D. E. Jones, Magnetic fluctuations in the magnetosheath: Mariner 4, J. Geophys. Res., 72, 1-18, 1967.

Singer, S., J. P. Conner, W. D. Evans, M. D. Montgomery and E. E. Stogsdill, Plasma observations at 10^5 km, Space Research V, 546-563, 1965.

Smith, E. J. and C. P. Sonett, Satellite observations of the distant field during magnetic storms: Explorer 6, Proc. Interm. Conf. Cosmic Rays Earth Storm, Kyoto, Sept. 1961, J. Phys. Soc. Japan, 17, 17, 1962.

Smith, E. J., C. P. Sonett, and J. W. Dungey, Satellite observations of the geomagnetic field during magnetic storms, J. Geophys. Res., 69, 2669-2688, 1964.

Sonett, C. P., Coupling of the solar wind and the exosphere, Phys. Rev. Letters, 5, 46-48, 1960.

Sonett, C. P., D. L. Judge, A. R. Sims and J. M. Kelso, A radial rocket survey of the distant geomagnetic field, J. Geophys. Res., 65, 55-68, 1960a.

Sonett, C. P., E. J. Smith, D. L. Judge and P. J. Coleman, Current systems in the vestigial geomagnetic field: Explorer 6, Phys. Rev. Letters, 4, 161-163, 1960b.

Sonnerup, B. U. O. and L. J. Cahill, Jr., Magnetopause structure and attitude from Explorer 12 observations, J. Geophys. Res., 72, 171-184, 1967.

Speiser, T. W. and N. F. Ness, The neutral sheet in the geomagnetic tail: its motion, equivalent currents, and field line connection through it, J. Geophys. Res., 72, 131-142, 1967.

Spreiter, J. R. and W. P. Jones, On the effect of a weak interplanetary magnetic field on the interaction between the solar wind and the geomagnetic field, J. Geophys. Res., 68, 3555-3564, 1963.

Tidman, D. A., Turbulent shock waves in plasmas, submitted to Phys. Fluids, 1967a.

Tidman, D. A., The earth's bow shock wave, J. Geophys. Res., 72, 1799-1808, 1967b.

Van Allen, J. A., Absence of 40-kev electrons in the earth's magnetospheric tail at 3300 earth radii, J. Geophys. Res., 70, 4731-4739, 1965.

Walters, G. K., Effect of oblique interplanetary magnetic field on shape and behavior of the magnetosphere, J. Geophys. Res., 69, 1769-1783, 1964.

Wilcox, J. M. and N. F. Ness, Quasi-stationary co-rotating structure in the interplanetary medium, J. Geophys. Res., 70, 5793-5805, 1965.

Wilson, E. B., Jr., An Introduction to Scientific Research, McGraw-Hill, New York, 1952.

Wilson, T. A., Structure of collision-free magnetohydrodynamic waves, Phys. Fluids, 5, 1451-1455, 1962.

Wolfe, J. H., R. W. Silva, and M. A. Myers, Observations of the solar wind during the flight of IMP 1, J. Geophys. Res., 71, 1319-1340, 1966.

Zhigulev, V. N., On the phenomenon of magnetic detachment of the flow of a conducting medium, Soviet Physics, Doklady, 4, 514-516, 1959.

The vita has been removed from the scanned document

APPENDIX A – LEAST SQUARES FIT ROUTINE

The output of an equatorial plane sensor is spin modulated about some base level of counts (DC level), which must be the zero level of the sensor. The ith sample of the output of the sensor in a given telemetry sequence may be expressed by

$$Y_i = A \cos(\omega t - \Psi) + DC.$$

The error is

$$E = \sum_{i=1}^{N} e_i^2 = \sum_{i=1}^{N} (Y_0 - Y_i)^2 = \sum_{i=1}^{N} [Y_0 - (A \cos(\omega t_i - \Psi) + DC)]^2.$$

To minimize the deviations set

$$\frac{\delta E}{\delta A} = -2 \sum_{i=1}^{N} [Y_i - A \cos(\omega t_i - \Psi) - DC] \cos(\omega t_i - \Psi) = 0,$$

and

$$\frac{\delta E}{\delta DC} = -2 \sum_{i=1}^{N} [Y_i - A \cos(\omega t_i - \Psi) - DC] = 0.$$

These expressions can be rewritten

$$DC \cos(\omega t_i - \Psi) + A \sum_{i=1}^{N} \cos^2(\omega t_i - \Psi) = \sum_{i=1}^{N} Y_i \cos(\omega t_i - \Psi) \quad (1)$$

$$N(DC) + A \sum_{i=1}^{N} \cos(\omega t_i - \Psi) = \sum_{i=1}^{N} Y_i . \quad (2)$$

Given Ψ_k at 4° intervals from 0° to 360° (91 values) as well as ω, t_i and Y_i, (1) and (2) can be solved for A_k and DC_k for each Ψ_k. In each case E_k is computed from

$$E_k = \sum_{i=1}^{N} [Y_i - A_k \cos(\omega t_i - \Psi) + DC_k]^2 .$$

The "best" values of A, DC and Ψ will be those corresponding to minimum E_k. Hence because the output from a sensor is linear in A and DC, then assuming ω is known tables (DC_k, A_k and E_k, k = 1, 91) can be constructed from table (Ψ_k, k = 1, 91) and arrays of times and corresponding sensor outputs. The E_k can be scanned for a minimum value, E_k (min.). Then for each sensor the corresponding amplitude A, DC level, and phase angle Ψ will be the best choice for a cosine wave fit to the output for the given sequence. The root-mean-square error of the "best fit" will be

$$RMSE = \sqrt{\frac{E_k\,(min)}{N}} .$$

APPENDIX B – DATA TRANSFORMATIONS

The transformation from the triaxial sensor frame of reference to the frame which rotates with the spacecraft but is stationary with respect to sensor reorientation is given, for sensor outputs (D_1, D_2, D_3), by

$$\begin{bmatrix} BX \\ BY \\ BZ \end{bmatrix}_A = \begin{bmatrix} 0 & -1 & 0 \\ +1 & 0 & 0 \\ 0 & 0 & +1 \end{bmatrix} \begin{bmatrix} D_1 \\ D_2 \\ D_3 \end{bmatrix}$$

if the sensors are in the normal position, and by

$$\begin{bmatrix} BX \\ BY \\ BZ \end{bmatrix}_A = \begin{bmatrix} 0 & -1 & 0 \\ 0 & 0 & -1 \\ +1 & 0 & 0 \end{bmatrix} \begin{bmatrix} D_1 \\ D_2 \\ D_3 \end{bmatrix}$$

if the sensors are in the "flipped" position (see Fig. 11).

The transformation from $(X, Y, Z)_A$ to the fixed payload $(X, Y, Z)_p$ coordinates is given by

$$\begin{bmatrix} BX \\ BY \\ BZ \end{bmatrix}_p = \begin{bmatrix} \cos \text{DELTA} & -\sin \text{DELTA} & 0 \\ \sin \text{DELTA} & \cos \text{DELTA} & 0 \\ 0 & 0 & 1 \end{bmatrix} \begin{bmatrix} BX \\ BY \\ BZ \end{bmatrix}_A$$

where for the kth field measurement in a telemetry sequence

$$\text{DELTA} = \frac{2\pi}{T_{spin}} [t_s(k) - t_{0A}] + \text{SA} - \text{PSHFT}.$$

Here t_s and t_{0A} are sample time and time that the optical aspect (OA) sensor on the spacecraft sees the sun, respectively. SA is the angle from the OA sensor axis to the GSFC magnetometer boom in the direction of satellite rotation, and PSHFT is the instrumental phaseshift defined in Section IV. It has been determined experimentally that for 2 sec. $\leq T_{spin} \leq$ 3 sec. The phaseshift for all three sensors is given to within ±1° by

$$\text{PSHFT} = 5^\circ + 1.5\,(2 - T_{spin}).$$

The transformation to solar ecliptic (SE) coordinates is accomplished by rotating the X_p axis through an angle A into the X_{SE} axis and then rotating the Z_p axis through an angle D into the Z_{SE} axis. Sin A, cos A, sin D and cos D may be expressed in terms of the SE coordinates of a unit spin axis. These coordinates can be computed from the right ascension RASE and declination DECSE of the spin axis in SE coordinates, which are provided on the Explorer 33 trajectory tape, using

$$SAXE = \cos RASE \cos DECSE$$

$$SAYE = \sin RASE \cos DECSE$$

$$SAZE = \sin DECSE.$$

Then

$$\cos A = \sqrt{SAYE^2 + SAZE^2}$$

$$\sin A = SAXE$$

$$\cos D = SAZE/\cos A$$

$$\sin D = SAYE/\cos A.$$

By combining the A and D rotations in the transformation, the SE field components can then be computed from the payload components using

$$\begin{bmatrix} BY \\ BY \\ BZ \end{bmatrix}_{SE} = \begin{bmatrix} \cos A & 0 & \sin A \\ -\sin A \sin D & \cos D & \cos A \sin D \\ -\sin A \cos D & -\sin D & \cos A \cos D \end{bmatrix} \begin{bmatrix} BX \\ BY \\ BZ \end{bmatrix}_{p}$$

The transformation to solar magnetospheric (SM) coordinates is accomplished at the same time as the transformation to SE coordinates. Since by definition $X_{SM} = X_{SE}$, the only difference in transforming from payload to the SM reference frame from transforming to the SE frame is rotation through a different angle in the YZ-plane. Using the right ascension RASM and declination DECSM of the

spin axis in solar magnetospheric coordinates, which are also provided on the Explorer 33 trajectory tape, and making use of the already computed cos A and sin A, the procedure is analogous to what is done in the SE computations.

Computing

$$\text{SAYSM} = \sin \text{RASM} \cos \text{DECSM}$$

$$\text{SAZSM} = \sin \text{DECSM}$$

$$\cos \text{DM} = \text{SAZSM}/\cos \text{A}$$

$$\sin \text{DM} = \text{SAYSM}/\cos \text{A},$$

then

$$\begin{bmatrix} \overline{BY} \\ \\ \underline{BZ} \end{bmatrix}_{SM} = \begin{bmatrix} -\sin A \sin DM & \cos DM & \cos A \sin \overline{DM} \\ & & \\ -\sin A \cos DM & -\sin DM & \cos A \cos \underline{DM} \end{bmatrix} \begin{bmatrix} \overline{BX} \\ BY \\ \underline{BZ} \end{bmatrix}_p .$$

APPENDIX C – ERROR ANALYSIS

(1) Error in magnitude:

The magnetic field magnitude is computed from

$$F = \sqrt{BX_A^2 + BY_A^2 + BZ_A^2}\,.$$

The A subscript will be dropped for simplification of notation. Small variations dB_i in the components B_i will change F by the amount

$$dF = \sum_i \frac{\partial F}{\partial B_i}\, dB_i$$

$$= \frac{BX}{F}\, dBX + \frac{BY}{F}\, dBY + \frac{BZ}{F}\, dBZ.$$

Letting the error in the ith quantity be represented by s_i, squaring the error gives

$$s_F = \sqrt{\frac{1}{F^2}\,[BX^2 s_x^3 + BY^2 s_y^2 + BZ^2 s_z^2 + 2(BX \cdot BY s_x s_y + BX \cdot BZ s_x s_z + BY \cdot BZ s_y s_z)]}$$

In this case assuming that $s_x = \pm 0.25$ gamma, $s_y = \pm 0.25$ gamma and $s_z = \pm 0.25$ gamma, then $s_x^2 = s_y^2 = s_z^2 = (0.25)^2$ gamma^2 and

$$s_F = \sqrt{\frac{F^2}{F^2}(0.25)^2 + \frac{2(BX \cdot BY s_x s_y + BX \cdot BZ s_x s_z + BY \cdot BZ s_y s_z)}{F^2}}.$$

This error has its largest value when the signs of the components and component errors combine so as to make all of the cross product terms positive:

$$s_F = \sqrt{(0.25)^2 + \left(\frac{BX \cdot BY + BX \cdot BZ + BY \cdot BZ}{F^2}\right)(0.25)^2 \text{ gamma}}.$$

It has its smallest value when all of the cross product terms are negative:

$$s_F = \sqrt{(0.25)^2 - \left(\frac{BX \cdot BY + BX \cdot BZ + BY \cdot BZ}{F^2}\right)(0.25)^2 \text{ gamma}}.$$

On the average, assuming a component error is as likely to the negative as positive,

$$s_F = \sqrt{(0.25)^2} = 0.25 \text{ gamma}.$$

Thus on the average the error in the total field is equal to the error in each components.

In general, according to Wilson (1952), if the variations $dx_1, \ldots, dx_n = s_1 \ldots, s_n$ can be assumed to be independently distributed and symmetrical with respect to positive and negative values, then $s_i s_j$ $(i \neq j)$ will vanish on the average, so that for $y = f(x_1, x_2, \ldots, x_n)$,

$$s^2 = \sum_{i=1}^{n} \left(\frac{\partial f}{\partial x_i}\right)^2 s_i^2 .$$

This general formulation will be used to determine errors throughout this analysis. As shown above, application to magnitude F yields $S_F^2 = 0.0625 \text{ gamma}^2$.

(2) Error in rotation angle:

$$\Psi = \frac{2\pi}{T_{spin}} (t_s - t_{OA}) + SA + PSHFT.$$

Hence

$$s_\Psi^2 = \left(\frac{2\pi}{T_{spin}}\right)^2 \left[s_s^2 + s_{OA}^2 + \left(\frac{t_s - t_{OA}}{T_{spin}}\right)^2 s_T^2 + \left(\frac{T_{spin}}{2\pi}\right)^2 (s_{SA}^2 + s_p^2)\right]$$

where s_s, s_{OA}, s_T, s_{SA} and s_p are the errors in sample time, OA time, spin period, OA sensor-boom angle, and phaseshift, respectively. If

$$s_s = s_{OA} = \pm 0.001 \text{ seconds}$$

$$s_T = \pm 0.00001 \text{ seconds}$$

$$s_{SA} = \pm 0.1^\circ$$

and

$$s_p = \pm 1.0^\circ$$

then typically $s_\Psi = \pm 0.245^\circ = \pm 0.00436$ radians.

(3) Errors in payload components:

$$BX_p = BX \cos \Psi - BY \sin \Psi$$

$$BY_p = BX \sin \Psi + BY \cos \Psi$$

$$BZ_p = BZ$$

Hence

$$s^2_{BXP} = \cos^2\Psi s_x^2 + \sin^2\Psi s_y^2 + (BX^2 \sin^2\Psi + BY^2 \cos^2\Psi + 2BX \cdot BY \sin\Psi \cos\Psi) s^2_\Psi$$

or, since

$$s_x^2 = s_y^2 = s_z^2 = (0.25)^2 \text{ gamma}^2,$$

$$s^2_{BXP} = (0.25)^2 \text{ gamma}^2 + (BX^2 \sin^2\Psi + BY^2 \cos^2\Psi + 2BX \cdot BY \sin\Psi \cos\Psi) s^2_\Psi.$$

Similarly,

$$s^2_{BYP} = (0.25)^2 \text{ gamma}^2 + (BX^2 \cos^2\Psi + BY^2 \sin^2\Psi - 2BX \cdot BY \sin\Psi \cos\Psi) s^2_\Psi.$$

Because the Z component is not effected by the payload transformation,

$$s^2_{BZP} = (0.25)^2 \text{ gamma}^2 \text{ (assuming } s_z = \pm 0.25 \text{ gamma)}.$$

Using the value found in (2) for s_Ψ, then s_{BXP} and s_{BYP} typically range from ±0.25 gamma to ±0.40 gamma for component magnitudes ranging from 0 to 64 gammas.

(4) Errors in solar ecliptic components:

$$BX_{SE} = CA \cdot BX_p + SA \cdot BZ_p$$

$$BY_{SE} = - SA \cdot SD \cdot BX_p + CD \cdot BY_p + CA \cdot SD \cdot BZ_p$$

$$BZ_{SE} = - SA \cdot CD \cdot BX_p - SD \cdot BY_p + CA \cdot CD \cdot BZ_p ,$$

where

$$SA = EPX$$

$$CA = \sqrt{EPY^2 + EPZ^2}$$

$$SD = EPY/CA$$

$$CD = EPZ/CA,$$

and

$$EPX = \cos RASE \cos DECSE$$

$$EPY = \sin RASE \cos DECSE$$

$$EPZ = \sin DECSE.$$

Then

$$s_{SA}^2 = s_{EPX}^2 = \sin^2 RASE \cos^2 DECSE\, s_{RASE}^2 + \cos^2 RASE \sin^2 DECSE\, s_{DECSE}^2$$

$$s_{DPY}^2 = \cos^2 RASE \cos^2 DECSE\, s_{RASE}^2 + \sin^2 RASE \sin^2 DECSE\, s_{DECSE}^2$$

$$s_{EPZ}^2 = \cos^2 DECSE\, s_{DECSE}^2 ,$$

and

$$s_{CA}^2 = \frac{EPY^2\, s_{EPY}^2 + EPZ^2\, s_{EPZ}^2}{EPY^2 + EPZ^2}$$

$$s_{CD}^2 = \frac{s_{EPZ}^2}{CA^2} + \left(\frac{EPZ}{CA^2}\right)^2 s_{CA}^2$$

$$s_{SD}^2 = \frac{s_{EPY}^2}{CA^2} + \left(\frac{EPY}{CA^2}\right)^2 s_{CA}^2 .$$

In terms of all of these individual errors the total errors in the solar ecliptic components are given by

$$s_{BXE}^2 = BX_p^2\, s_{CA}^2 + CA^2\, s_{BXP}^2 + BZ_p^2\, s_{SA}^2 + SA^2\, s_{BZP}^2$$

$$s_{BYE}^2 = (SA \cdot BX_p)^2 s_{SA}^2 + (SD \cdot BX_p)^2 s_{SA}^2 + (SA \cdot SD)^2 s_{BXP}^2 + CD^2 s_{BYP}^2 + BY_p^2 s_{CD}^2$$

$$+ (SD \cdot BZ_p)^2 s_{CA}^2 + (CA \cdot BZ_p)^2 s_{SD}^2 + (CA \cdot SD)^2 s_{BZP}^2$$

$$s_{BZE}^2 = (SA \cdot BX_p)^2 s_{SA}^2 + (CD \cdot BX_p)^2 s_{SA}^2 + (SA \cdot CD)^2 s_{BXP}^2 + SD^2 s_{BYP}^2 + BY_p^2 s_{SP}^2$$

$$+ (CD \cdot BZ_p)^2 s_{CA}^2 + (CA \cdot BZ_p)^2 s_{CD}^2 + (CA \cdot CD)^2 s_{BZP}^2 .$$

The errors in the solar ecliptic field orientation angles ϕ_{SE} and θ_{SE} can then be computed also.

Since $\phi_{SE} = \tan^{-1}\left(\frac{BY_{SE}}{BX_{SE}}\right)$ and $\theta_{SE} = \tan^{-1}\left(\frac{BZ_{SE}}{\sqrt{BX_{SE}^2 + BY_{SE}^2}}\right)$,

then

$$s_{\phi}^2 = \left(\frac{BX_{SE}}{BX_{SE}^2 + BY_{SE}^2}\right)^2 s_{BYE}^2 + \left(\frac{BY_{SE}}{BX_{SE}^2 + BY_{SE}^2}\right)^2 s_{BXE}^2$$

and

$$s_{\theta}^2 = \frac{1}{(BX_{SE}^2 + BY_{SE}^2 + BZ_{SE}^2)} \left[\frac{BZ_{SE}^2}{BX_{SE}^2 + BY_{SE}^2} (BX_{SE}^2 s_{BXE}^2 + BY_{SE}^2 s_{BYE}^2) + (BX_{SE}^2 + BY_{SE}^2) s_{BZE}^2\right].$$

If $s_{RASE} = s_{DECSE} = \pm 0.1°$ and the payload component uncertainties range from ± 0.25 gamma to ± 0.40 gamma, then the solar ecliptic component uncertainties typically range from ± 0.26 gamma to ± 0.43 gamma and the angular uncertainties from $\pm 1°$ to $\pm 2°$. Hence for small uncertainties in spin axis orientation, there is only a slight additional increase in magnetic field component uncertainty when the data are transformed to the solar ecliptic frame of reference. Because of its similarity to the solar ecliptic transformation, the errors produced by the rotation from payload to solar magnetospheric coordinates are of the same magnitude as those produced by the solar ecliptic transformation.

APPENDIX D –
MULTIPLE AND PARTIAL CORRELATION COEFFICIENTS

The simple correlation coefficient between the variables F and X is given by

$$r_{FX} = \frac{\sum_i (F_i - \bar{F})(X_i - \bar{X})}{\sqrt{\sum_i (F_i - \bar{F})^2 \sum_i (X_i - \bar{X})^2}} .$$

In terms of simple correlation coefficients, the multiple correlation coefficient between the dependent variable F and the independent variables $X_1, X_2, \ldots, X_n$ is given by

$$r_{F \cdot X_1 X_2 \ldots X_n} = \left(1 - \frac{R}{R_{11}}\right)^{1/2} ,$$

where R is the determinant of the simple correlation coefficients r_{ij} and R_{11} is the cofactor of the element r_{11} (Kenney and Keeping, 1951).

The partial correlation between the variables F and X, independent of the effect on F of a third variable Z, is expressed by

$$r_{FX \cdot Z} = \frac{r_{FX} - r_{FZ}\, r_{XZ}}{\sqrt{(1 - r_{FZ}^2)(1 - r_{XZ}^2)}} ,$$

where r_{FX} is the simple correlation coefficent between F and X. If F is a function of three variables X, F and Z, then the partial correlation between F

and X, independent of the effects on F of the variables K and Z, is expressed by

$$r_{FX \cdot KZ} = \frac{r_{FX \cdot Z} - r_{FK \cdot Z}\, r_{XK \cdot Z}}{\sqrt{(1 - r^2_{FK \cdot Z})\,(1 - r^2_{XK \cdot Z})}}$$

where $r_{FX \cdot Z}$ is the previously defined partial correlation coefficient for two independent variables. This formulation can be extended to higher levels for any number n of independent variables. However, in each case this requires computations of n - 1 levels of partial correlation coefficients.

INITIAL MAPPING OF THE EARTH'S BOW SHOCK, MAGNETOSHEATH AND MAGNETIC TAIL BY EXPLORER 33*

by

Kenneth Wayne Behannon

ABSTRACT

The Explorer 33 satellite was launched July 1, 1966 and was injected into a highly elliptical earth orbit. The Goddard Space Flight Center magnetic field experiment on board the spacecraft consists of a triaxial fluxgate sensor with a maximum dynamic range of ±64 gammas and a sensitivity of ±0.25 gammas along each axis. Because of the initial apogee-earth-sun angle of 118° west of the sun, the first 8 orbits of Explorer 33 (July-November 11, 1966) mapped the earth's magnetosheath and magnetic tail from the western flank of the bow shock to the eastern flank. This mapping of the geomagnetic tail out to 80 earth radii established that the tail extends beyond the lunar orbital distance. Explorer 33 has also found that the earth's bow shock is still a detectable boundary between the interplanetary magnetic field and the downstream magnetosheath at a geocentric distance of 75.7 earth radii. This spacecraft has further revealed that the cross section of the geomagnetic tail is probably not cylindrical, and that the magnetic field magnitude in the tail decreases with distance down the tail from the earth. This magnitude decrease can be due both to a gradual expansion of the tail with distance and to a reconnection of magnetic field lines across the tail neutral sheet.